MINISTÉRIO DA CIÊNCIA, TECNOLOGIA E INOVAÇÃO
INSTITUTO NACIONAL DE PESQUISAS ESPACIAIS

sid.inpe.br/mtc-m21d/2023/06.20.14.44-TDI

A PAST-PRESENT-FUTURE PERSPECTIVE OF CLIMATE CHANGES AND TERRESTRIAL ECOSYSTEM RESPONSES IN SOUTH AMERICA: INSIGHTS FROM MODEL SIMULATIONS AND PALEOCLIMATE RECONSTRUCTIONS

Jelena Maksic

Doctorate Thesis of the Graduate Course in Earth System Science, guided by Drs. Gilvan Sampaio de Oliveira, and Francisco William da Cruz Júnior, approved in June 14, 2023.

URL of the original document:
<http://urlib.net/8JMKD3MGP3W34T/49ATFRE>

INPE
São José dos Campos
2023

PUBLISHED BY:

Instituto Nacional de Pesquisas Espaciais - INPE
Coordenação de Ensino, Pesquisa e Extensão (COEPE)
Divisão de Biblioteca (DIBIB)
CEP 12.227-010
São José dos Campos - SP - Brasil
Tel.:(012) 3208-6923/7348
E-mail: pubtc@inpe.br

MINISTÉRIO DA CIÊNCIA, TECNOLOGIA E INOVAÇÃO
INSTITUTO NACIONAL DE PESQUISAS ESPACIAIS

sid.inpe.br/mtc-m21d/2023/06.20.14.44-TDI

A PAST-PRESENT-FUTURE PERSPECTIVE OF CLIMATE CHANGES AND TERRESTRIAL ECOSYSTEM RESPONSES IN SOUTH AMERICA: INSIGHTS FROM MODEL SIMULATIONS AND PALEOCLIMATE RECONSTRUCTIONS

Jelena Maksic

Doctorate Thesis of the Graduate Course in Earth System Science, guided by Drs. Gilvan Sampaio de Oliveira, and Francisco William da Cruz Júnior, approved in June 14, 2023.

URL of the original document:
<http://urlib.net/8JMKD3MGP3W34T/49ATFRE>

INPE
São José dos Campos
2023

Cataloging in Publication Data

Maksic, Jelena.

M289p A past-present-future perspective of climate changes and terrestrial ecosystem responses in South America: Insights from model simulations and paleoclimate reconstructions / Jelena Maksic. – São José dos Campos : INPE, 2023.

xix + 136 p. ; (sid.inpe.br/mtc-m21d/2023/06.20.14.44-TDI)

Thesis (Doctorate in Earth System Science) – Instituto Nacional de Pesquisas Espaciais, São José dos Campos, 2023.

Guiding : Drs. Gilvan Sampaio de Oliveira, and Francisco William da Cruz Júnior.

1. Last glacial maximum. 2. Simulation. 3. Biomes. 4. Future scenario. 5. Paleo records. I.Title.

CDU 551.583(8)

MINISTÉRIO DA CIÊNCIA, TECNOLOGIA E INOVAÇÃO

INSTITUTO NACIONAL DE PESQUISAS ESPACIAIS

DEFESA FINAL DE TESE JELENA MAKSIC
BANCA Nº 168/2023, REGISTRO 41981/2019

No dia 14 de junho de 2023, as 10h, presencialmente, o(a) aluno(a) mencionado(a) acima defendeu seu trabalho final (apresentação oral seguida de arguição) perante uma Banca Examinadora, cujos membros estão listados abaixo. O(A) aluno(a) foi APROVADO(A) pela Banca Examinadora, por unanimidade, em cumprimento ao requisito exigido para obtenção do Título de Doutora em Ciência do Sistema Terrestre, com a exigência de que o trabalho final a ser publicado deverá incorporar as correções sugeridas pela Banca Examinadora, com revisão pelo(s) orientador(es).

Título: "A past-present-future perspective of climate changes and terrestrial ecosystem responses in South America: Insights from model simulations and paleoclimate reconstructions".

Observações da banca:
As observações são restritas a formatação e melhorias no texto. Os membros da banca irão enviar para o aluno o documento com suas considerações e o Dr. Gilvan Sampaio de Oliveira (Orientador) ficará responsável pela aprovação final do documento a partir da inclusão dos comentários dos membros da banca.

Membros da Banca:

Dr. Lincoln Muniz Alves – Presidente – INPE
Dr. Gilvan Sampaio de Oliveira – Orientador (a) – INPE
Dr. Francisco William da Cruz – Orientador (a) – USP
Dra. Marília Harumi Shimizu– Membro Externo – UFF
Dr. Nicolás Misailidis Stríkis – Membro Externo – UFF

Documento assinado eletronicamente por **Francisco William da Cruz Junior (E)**, **Usuário Externo**, em 20/06/2023, às 08:01 (horário oficial de Brasília), com fundamento no § 3º do art. 4º do Decreto nº 10.543, de 13 de novembro de 2020.

Documento assinado eletronicamente por **Marilia harumi shimizu (E)**, **Usuário Externo**, em 20/06/2023, às 08:25 (horário oficial de Brasília), com fundamento no § 3º do art. 4º do Decreto nº 10.543, de 13 de novembro de 2020.

Documento assinado eletronicamente por **Lincoln Muniz Alves**, **Pesquisador**, em 20/06/2023, às 13:56 (horário oficial de Brasília), com fundamento no § 3º do art. 4º do Decreto nº 10.543, de 13 de novembro de 2020.

Documento assinado eletronicamente por **Gilvan Sampaio de Oliveira**, **Coordenador-Geral de Ciências da Terra**, em 20/06/2023, às 13:59 (horário oficial de Brasília), com fundamento no § 3º do art. 4º do Decreto nº 10.543, de 13 de novembro de 2020.

Documento assinado eletronicamente por **nICOLÁS MISAILIDIS sTRIKIS (E)**, **Usuário Externo**, em 22/06/2023, às 11:49 (horário oficial de Brasília), com fundamento no § 3º do art. 4º do Decreto nº 10.543, de 13 de novembro de 2020.

A autenticidade deste documento pode ser conferida no site https://sei.mcti.gov.br/verifica.html, informando o código verificador **11135404** e o código CRC **91AA2872**.

Referência: Processo nº 01340.004980/2023-26 SEI nº 11135404

ABSTRACT

The main objective of the thesis is to provide a past-present-future perspective of climate changes and terrestrial ecosystem responses in South America. The first part investigates the vegetation response to a temperature increase from the Last Glacial Maximum (LGM) to the pre-industrial era. In order to verify the most affected biomes and explore how they might react to future warming it was employed the Center for Weather Forecasting and Climate Studies Potential Vegetation Model version 2 model (CPTEC PVM2). In addition, to determine the influence of each climate parameter on biome distribution, sensitivity experiments for both LGM and future scenario were run, considering the anomalies of CO_2, precipitation and temperature separately. The results for the LGM indicate grassland expansion in southern Brazilian highlands and the persistence of the Amazon rainforest under colder and drier conditions. The western and central Amazon forest remained due to negative temperature anomalies, while a decrease in precipitation led to changes in the eastern portion. The reliability of computed precipitation anomalies and simulated potential vegetation for LGM is validated with compilation of 149 published vegetation and hydroclimate records. Results reaffirmed paleo studies that claim that changes in monsoon intensity cannot be used as the main driver for vegetational changes/stability across the Amazon biome, and that lower temperatures in combination with substantially lower CO_2 are important controlling factors during the LGM. In contrast, for the future +4°C warming scenario, biome shifts will be driven by changes in precipitation. Savanna/Cerrado is projected to expand, while the Amazon forest, Tropical seasonal forest, and Caatinga may decrease. In the future warming scenario increasing temperatures with reduction in precipitation neutralize the potential gain in biomass from the positive effect of CO_2 fertilization. The thesis also investigates the Atlantic Multidecadal Oscillation (AMO) as a potential main driver of warming/cooling scenarios and changes in precipitation in South America during the last millennium. This study evaluates AMO influence on atmospheric dynamics, precipitation and consequently $\delta^{18}O$ of precipitation in South America using the water isotope-enabled version of the Community Earth System Model version 1.2 (iCESM1.2) forced with cold and warm AMO phase sea surface temperature fields. The model-derived AMO signal for the region under the influence of the Atlantic ITCZ aligns with proxy reconstructions, indicating changes in ITCZ during the Little Ice Age (LIA). One implication of these findings is that a change in the core strength of the ITCZ, caused by a persistent cold AMO, might have contributed to dry conditions over the northernmost part of South America and increased precipitation along the coastal area of northeastern Brazil during the LIA. Hydroclimatic spatiotemporal patterns during last millennium in other regions of South America remain puzzling. The study also warns that caution should be exercised when interpreting records reflecting annual means, as they may actually record signals of seasonal variability rather than ITCZ shifts. This thesis contributes to our understanding of past and future climate changes and terrestrial ecosystem

responses in South America, highlighting the importance of considering both simulations and paleo records as neither available paleorecords nor state-of-the-art models alone are conclusive, especially under extremely heterogeneous and complex environmental conditions.

Keywords: Last Glacial Maximum. Simulation. Biomes. Future scenario. Paleo Records. Last millennium. Atlantic Multidecadal Oscillation. Isotope-enabled model. $\delta^{18}O$.

UMA PERSPECTIVA PASSADO-PRESENTE-FUTURO DAS MUDANÇAS CLIMÁTICAS E RESPOSTAS DO ECOSSISTEMA TERRESTRE NA AMÉRICA DO SUL: CONHECIMENTOS DE SIMULAÇÕES DE MODELOS E RECONSTRUÇÕES PALEOCLIMÁTICAS

RESUMO

O objetivo principal da tese é fornecer uma perspectiva passado-presente-futuro das mudanças climáticas e respostas dos ecossistemas terrestres na América do Sul. A primeira parte investiga a resposta da vegetação ao aumento da temperatura desde o Último Máximo Glacial (UMG) até a era pré-industrial. Para verificar os biomas mais afetados e explorar como eles podem reagir ao aquecimento futuro, foi utilizado o modelo do Potencial Vegetacional do Centro de Previsão de Tempo e Estudos Climáticos (CPTEC PVM2). Além disso, foram realizados experimentos de sensibilidade para determinar a influência de cada parâmetro climático na distribuição dos biomas, tanto para o LGM quanto para cenários futuros. Os resultados para o LGM indicam expansão de campos no planalto sul brasileiro e a persistência da Floresta Amazônica sob condições mais frias e secas. A Floresta Amazônica ocidental e central permaneceram devido a anomalias negativas de temperatura, enquanto uma redução na precipitação causou alterações na porção leste. Os resultados reafirmaram os estudos paleo que afirmam que as mudanças na intensidade das monções não podem ser usadas como o principal fator para mudanças/estabilidade da vegetação em todo o bioma Amazônia, e que temperaturas mais baixas em combinação com CO_2 substancialmente mais baixo são fatores de controle importantes durante o LGM. A confiabilidade das anomalias de precipitação calculadas e da vegetação potencial simulada para o LGM é validada com a compilação de 149 registros de vegetação e hidroclima. Por outro lado, para o cenário futuro de aquecimento de +4°C, as mudanças nos biomas serão impulsionadas por alterações na precipitação. A savana/Cerrado é projetada para expandir, enquanto a Floresta Amazônica, Floresta Tropical sazonal e Caatinga podem diminuir. No cenário de aquecimento futuro, o aumento das temperaturas com a redução da precipitação neutraliza o ganho potencial de biomassa pelo efeito positivo da fertilização de CO_2. A tese também investiga a Oscilação Multidecenal do Atlântico (AMO) como um possível motor principal de cenários de aquecimento/resfriamento e mudanças na precipitação na América do Sul durante o Último milênio. Este estudo avalia a influência da AMO usando a versão habilitada para isótopos do Modelo de Sistema Terrestre da Comunidade, versão 1.2 (iCESM1.2). O sinal de AMO derivado do modelo para a região sob a influência da Zona de Convergência Intertropical do Atlântico (ITCZ) coincide com reconstruções de proxy, indicando mudanças na ITCZ durante a Pequena Idade do Gelo (PIG). Uma implicação dessas descobertas é que uma mudança na força central da ITCZ, causada por uma AMO fria persistente, pode ter contribuído para condições secas na parte mais ao norte da América do Sul e aumento da precipitação ao longo da área costeira do nordeste do Brasil durante a LIA. Os padrões espácio-temporais hidroclimáticos durante o último milênio em outras regiões da América do Sul ainda são enigmáticos. Esta tese contribui para nossa compreensão das mudanças climáticas passadas e futuras e respostas dos ecossistemas terrestres na América do Sul, destacando a importância de considerar tanto simulações quanto registros paleo, já que nem os paleoregistros disponíveis nem

os modelos por si só são conclusivos. Insights em escalas e estados climáticos devem contribuir para uma compreensão mais profunda das projeções climáticas futuras.

Palavras-chave: Último Máximo Glacial, Simulação, Biomas, Cenário futuro, Registros paleo, Último milênio, Oscilação Multidecenal do Atlântico, Modelo habilitado para isótopos, δ18O.

ACKNOWLEDGEMENTS

First and foremost I am extremely grateful to my supervisor Dr. Gilvan Sampaio de Oliveira for his support, advice and continuous encouragement.

I am also immensely grateful to Dr. Marília Harumi Shimizu for her ideas and efforts with the analysis. Thank you very much for always being patient and supportive with all my many questions.

I am also very grateful to Prof. Cristiano Chiessi for his ideas and for always being patient and supportive.

I would also like to thank Dr. Francisco William da Cruz Júnior for sharing his time and constructive comments.

I would like to thank FAPESP for the financial support (grant 2018/23522-6) that allowed me to conduct this thesis.

Many thanks to CAPES for the opportunity to study at INPE.

Getting through my dissertation required more than academic support, and I have many, many people to thank for listening to me and, at times, having to tolerate me over the past four years. I was fortunate enough to be surrounded by a great group of people who really supported me and helped me – Weriton, Leticia, Marcia, Viviane, Igor, Mabel. Thank you all!

This thesis would not have been written without the understanding and support from my husband. Thank you Dragan!

Lastly, my deepest gratitude goes to my parents and my sister for support and belief in me.

LIST OF FIGURES

Pág.

LIST OF TABLES

Pág.

LIST OF ACRONYMS

AMO	The Atlantic Multidecadal Oscillation
iCAM5.3	The isotope-enabled Community Atmosphere Model version 5
iCESM1.2	The Community Earth System Model version 1.2
ITCZ	The Intertropical Convergence Zone
LIA	Little Ice Age
LM	The Last Millennium
LGM	Last Glacial Maximum
MCA	Medieval Climate Anomaly
SAMS	The South American Monsoon System
SACZ	The South Atlantic Convergence Zone
SALLJ	The South American low-level jet
SST	Sea-surface Temperatures

LIST OF SYMBOLS

$\delta^{18}O$	measure of the ratio of stable isotopes oxygen-18 (^{18}O) and oxygen-16 (^{16}O)

SUMMARY

Pág.

1 INTRODUCTION

South America presents unique ecosystems with enormous biodiversity and differing vulnerability to future climate change (IPCC, 2021). South America has distinct rainy season from November to March, and dry season from May to September. The main driver of this difference in precipitation between winter dry and summer wet season is South America Monsoon System (SAMS) (VERA et al., 2006; GARREAUD et al., 2009). Global warming is expected to alter precipitation regime, by changing the timing or duration of the wet season, the frequency and magnitude of extreme events in different regions of South America (PASCALE et al., 2015; DUFFY et al., 2015; HOEGH-GULDBERG et al., 2018; KONAPALA et al., 2020). Projected changes in hydroclimate, together with increases in global temperature and carbon dioxide concentrations, will certainly affect vegetation distribution and structure, by implying significant and varied shifts in phenology (CLELAND et al., 2007), possibly disrupting ecosystem services and decreasing biodiversity (ROOT et al., 2003; GONZÁLEZ-OROZCO et al., 2016; AGUIRRE-GUTIÉRREZ et al., 2020). In the case of the Amazon, a potential replacement of the forest by other types of drought-resilient vegetation (i.e., tropical savanna) has been previously hypothesized (NOBRE et al., 1991; OYAMA; NOBRE et al., 2004; TRISOS et al., 2020). Besides the risk of biome replacement, there is considerable amount of evidences that show the risk of transforming some parts of the Amazon Forest from a carbon sink into a carbon source (AGUIAR et al., 2016; QIN et al., 2021; GATTI et al., 2021; LAPOLA et al., 2023). The consequences of one such biome change would not only have a negative effect on biodiversity, but would also affect the climate of other South American regions, potentially affecting global climate (LENTON et al., 2008; LOVEJOY; NOBRE, 2018). Recent study also shows that CO_2 physiological effect can cause rainfall decrease as strong as large-scale deforestation in the Amazon (SAMPAIO et al., 2022). Besides the Amazon forest, the Caatinga biome has been also identified as particularly vulnerable to climate change (SEDDON et al., 2016). If these predictions were to occur in the future, it would likely put pressure on existing water resources

and threaten agricultural and ecological security, with further implications on biosphere and humans.

Literature confirms that is “extremely likely” that since the start of the industrial era (about 1850 Common Era (CE)), the main cause of global warming is increased emissions of greenhouse gasses (IPCC, 2021), which by far exceeds the natural range of the last 650 kyr (SIEGENTHALER et al., 2005). While shortness of instrumental records hinders direct attributions of observed changes in hydrological variability and extremes to this anthropogenic forcing, palaeoclimate and palaeoecological proxies (e.g. ice cores, speleothems, tree-ring width and density, boreholes, charcoal records, lake sediments) provide valuable insights into hydrological variability and environmental responses in the past (BUSH et al., 2020). The most widely reported climate proxies with high temporal resolution and precisely dated time series are records of speleothem oxygen isotope composition (δ18O). These climate proxies are a valuable source of information about magnitudes of extremes in the past and thus could place recent hydrological extremes and projected changes for the end-of-century into context. This rainfall-sensitive paleoclimate records inform us about decadal to centennial or even longer-scale variations in magnitude and frequency of hydroclimate, as well as exceptionality of observed extremes (STRÍKIS et al., 2015; STEIGER et al., 2021; COOK et al., 2022). Nevertheless, proxies provide evidence-based insights into timing of precipitation or temperature changes, but identification of the underlying spatial patterns of those changes, as well as factors behind climate shifts, is hardly possible without model simulations.

Climate models are constantly improved (FLATO et al., 2011). When we evaluate them, we actually evaluate their accuracy in simulating a particular point in history, by comparing simulations with the instrumental climate record of the last 100–150 years. However, even when models reproduce the general features of observed climate; this is not guarantee for an accurate simulation of a different climate state. This is mostly because climate models are parameterized and calibrated to reproduce the instrumental record (HOURDIN et al., 2017). Climate reconstructions from the so-called pre-instrumental period

can thus serve for out-of-sample evaluation of climate models (HARRISON; BARTLEIN, 2012). Therefore, simulations of the periods with wide range of variations in climate forcings and responses, give us valuable clues of models' performance in reproducing climate across different scales and climate states (BRACONNOT et al., 2012; NOLAN et al., 2018). If models are able to simulate both historical period and past climate changes, then we gain more confidence in projections for the end of the twenty-first century.

In the last decades, the Coupled Model Intercomparison Project (CMIP) coordinated a series of past climate experiments in order to evaluate the ability of climate models to simulate past scenarios and to test a model's response to forcings. Since the beginning of CMIP, the Last Glacial Maximum (LGM) has been considered an important period for understanding Earth's systems (MEEHL et al., 2005). The LGM is the most recent global cold extreme period, placed between 26 500 and 19 000 years before present (CLARK et al., 2009). It has a clear longterm global signature, for which radiative forcings, boundary conditions and climate responses are relatively well known. The most important characteristic of the LGM is global cooling under relatively small change in orbital forcing (BERGER, 1978). Due to global cooling ice sheets in the Northern Hemisphere reached their maximum in extent and volume (ca 3000 m over North America), but there is currently no consensus about the form of the LGM ice sheets (ABE-OUCHI et al., 2015). Simultaneously, the $\sim$ 120 m lower global sea level (KHAN et al., 2019) characterized LGM. Greenhouse gas concentrations were also lower: 350 ppb for CH_4, 200 ppb for N_2O and 180 ppm for CO_2, and additionally contributed to the cooling (SIEGENTHALER et al., 2005).

Proxy based data of global LGM cooling give us wide range of estimates, from −1.7 °C to −8.0°C (SCHNEIDER VON DEIMLING et al., 2006; SCHMITTNER et al., 2011; ANNAN; HARGREAVES, 2013; TIERNEY et al., 2020). Models compiled in the Palaeoclimate Modeling Intercomparison Project phase 3 / Coupled Model Intercomparison Project phase 5 (PMIP3/CMIP5) (TAYLOR et al., 2012) in general agree about the sign and magnitude of temperature change for the LGM. The PMIP3/CMIP5 models simulate a LGM cooling of -5.9

to -3.1 °C (ARIAS et al., 2021). The most recent study (KAGEYAMA et al., 2021) showed that the simulations from the PMIP4/CMIP6 (KAGEYAMA et al., 2017) span larger range, but, the multi-model global cooling average is similar for the PMIP4 and PMIP3 ensembles (KAGEYAMA et al., 2017).

In contrast to temperature, PMIP3 models show large discrepancies in precipitation patterns for the LGM (HARRISON et al., 2015). This lack of consensus about the LGM precipitation persisted in the most recent PMIP4 simulations (KAGEYAMA et al., 2021). Discrepancies between models came mostly from systematic differences (in special physical parametrizations and vertical and horizontal resolution) and the complexity in simulating precipitation (YIN et al., 2013).

Although the climate was very different from the present one, the estimated global mean warming since the LGM to the present time is of a similar magnitude to the upper range of CMIP5 projections for the end of the twenty-first century (COLLINS et al., 2013). Thus, the LGM provides the rare opportunity to test the vegetation response to a temperature increase from the LGM to the present, and then use this knowledge to project and to explore the consequences of potential future warming. However, much uncertainty still exists about the precipitation in the LGM. It is worth bearing in mind that precipitation biases in models inflict bias in vegetation modeling. Distinct precipitation projections lead to distinct vegetation responses in models. Therefore, the assessment of paleovegetation based on outputs from one climate model (e.g. LEITE et al., 2016; COSTA et al., 2018) can lead to false estimation of vegetation distribution. Thus, prior to discussing the vegetation simulations for the LGM and further future warming, especially under extremely heterogeneous and complex environmental conditions like in South America, it is first necessary to validate the climate simulations using paleoclimate proxies.

On the other hand, the multiple climatic variables influenced each archive and proxy. Although powerful resource for the precipitation reconstruction, the relationship between precipitation and cave drip water $\delta^{18}O$ is complex and influenced by several factors, such as temperature of condensation,

atmospheric humidity, precipitation amount and dominant moisture source region (DANSGAARD, 1964; LACHNIET et al., 2009). Besides complex spatio-temporal interactions of all these factors, speleothem oxygen isotopes are strongly shaped by dynamics (changes in winds) and thus signals are not always regionally coherent (BAKER et al., 2019). Although the number of available speleothem records from South America significantly increased in the last two decades, climate reconstruction for South America is still difficult, mostly due to the sparseness of the available proxy data (COMAS-BRU et al., 2020). That is why the estimates of hydrological conditions in the LGM in South America come mostly from fossil pollen observations and vegetation reconstructions. Nevertheless, when we evaluate the regional precipitation of the LGM based on the vegetation reconstructions we must take into account the effect of low CO_2 on water-use efficiency (COWLING; SYKES, 1999; PRENTICE; HARRISON, 2009; SCHEFF et al., 2017). That is, estimates based on vegetation reconstructions are potentially dry biased by low CO_2 levels due to neglecting the negative effect of low CO_2 on water use efficiency (PRENTICE et al, 2022). However, isolating the direct impact of each parameter (i.e. temperature, precipitation and CO_2) is not easy, as none of these factors can be considered in isolation. Thus, to generate continuous maps of precipitation over South America for LGM is currently not possible using a strictly proxy-driven approach. This indicates that neither available paleorecords nor state-of-the-art models alone are conclusive, and that it is crucial to employ both while reconstructing past biomes.

Studies also explore the change of central feature of tropical rainfall, a narrow band known as the intertropical convergence zone (ITCZ). Arbuszewski et al., (2013) suggest that ITZC migrated about 7° southward of their present position during the LGM. On the other hand, Mcgee et al., (2014) found only slight shift of likely <1°. The most recent study (WANG et al., 2023) shows that LGM ITCZ significantly shifted southward, narrowed, and weakened both at global and regional scales relative to the preindustrial period.

According to Haug et al., (2001) the ITCZ underwent another southward shift during the period known as the Last Millennium (LM), which spans from 850 CE

to 1849 CE and is characterized by stable CO_2 levels at approximately 280 ppm (JONES; MANN, 2004). Notably, the LM period is distinguished by two prolonged intervals of anomaloustemperatures: the Medieval Climate Anomaly (MCA) from around 950 to 1250 CE, characterized by warmer global temperatures, and the subsequent Little Ice Age (LIA) spanning approximately 1450 to 1850 CE, characterized by cooler global temperatures. The definitions of these periods were provided by the Intergovernmental Panel on Climate Change (IPCC) in 2013, but the exact timing of the MCA and LIA remains a topic of ongoing debate among researchers.

Studies suggest that although temperatures did not fluctuate uniformly, the MCA in some regions might be as warm as much of the twentieth century (PAGES 2K CONSORTIUM, 2013). By contrast, the LIA was the last cold event recorded worldwide and referred to as mini glaciation (WANNER et al., 2011). The cooling was likely caused by several factors, including clusters of volcanic eruptions, weak solar activity during specific periods, and interactions within the climate system. These processes and feedbacks contributed to the abrupt cooling (TOOHEY; SIGL, 2017; OWENS et al., 2017; SMIRNOV et al., 2017; BREHM et al., 2021; BRÖNNIMANN et al., 2019; HEGERL et al., 2011; MILLER et al., 2012; SCHLEUSSNER; FEULNER, 2013; SLAWINSKA; ROBOCK, 2018; SUN et al., 2022). However, the recent study by Lapointe and Bradeley (2021) offers an explanatory hypothesis that the LIA was preceded and potentially triggered by an exceptional intrusion of warm Atlantic water into the Nordic Seas in the late 1300s that allowed the large volume of ice to be exported into the North Atlantic.

Signals of these two temperature anomalies are well-recognized and extensively documented in records from the mid-to-high latitudes of the Northern Hemisphere (GROVE, 2001; MANN, JONES, 2003; MANN et al., 2009; WANNER et al., 2022). The most remarkable implication of LIA cooling was that glaciers in most of the highest mountains worldwide reached their greatest volumes over the last 10 000 years (BRADLEY; JONES, 1993; WANNER et al., 2022). Although these anomalies varied on small scales, both spatially and temporally, focusing more narrowly on the LM is of particular

relevance to future assessments of climate, as this shift in the climate system occurred right before anthropogenic forcing became the significant factor in shaping climate.

Over the past two decades, numerous studies (APAÉSTEGUI et al., 2014; AZEVEDO et al., 2019; BIRD et al., 2011; LÜNING et al., 2019; NEUKOM et al., 2011; NOVELLO et al., 2012; NOVELLO et al., 2018; REUTER et al., 2009; VUILLE et al., 2012; UTIDA et al., 2019) have presented increasing evidence for the existence of both the Medieval Climate Anomaly (MCA) and the Little Ice Age (LIA) in South America. Climate variability over the LM and the relative contributions of internal climate variability and externally forced changes have been studied using outputs from fully coupled global climate models (SCHMIDT et al., 2011; JUNGCLAUS et al., 2017; OTTO-BLIESNER et al., 2016; BRADY et al., 2019). Simulations, however, do not show very strong temperature anomalies over these two specific periods in South America, nor clear precipitation anomalies (ROJAS et al., 2016). Due to relatively scarce proxy data, climatic spatiotemporal patterns of the MCA and LIA in South America remain puzzling.

Sediment, pollen analyses and speleothems reconstructions (FLANTUA et al., 2015; CAMPOS et al., 2019; ORRISON et al., 2022) suggest regionally contrasting patterns of hydrological changes in South America. Previous research has established that in regions under monsoon influence an anomalously drier climate prevailed during the MCA, in contrast to anomalously wetter conditions during the LIA (CAMPOS, et al., 2019). Proxy evidence also suggests a more southerly position of the monsoon convective axis during the LIA (NOVELLO et al., 2018). Reconstructions from the Northeast Brazil region show that MCA was characterized by an abrupt transition from wet to dry conditions that persisted until the onset of the LIA (UTIDA et al., 2019). The results inferred from the sedimentary concentrations of titanium (HAUG et al., 2001), show widespread aridity during LIA in the northern regions of South America and drought conditions in the Cariaco Basin. According to Peterson and Haug, (2006) these conditions are best explained by the meridional shift of the ITCZ. SACHS et al. (2009) suggested that the southward ITCZ shift during

the LIA was approximately 5°. Previous simulation indeed showed that minor changes in SST could influence ITCZ position. The SST change of ca. 0.2 - 0.3°C drive southward (northward) shift in the austral summer (winter), induced seasonal changes in precipitation over Western Amazon and Northeast Brazil, but minor change in the annual mean position of the precipitation band (MAKSIC et al., 2019; SHIMIZU et al., 2020). It is worthwhile mentioning that speleothem records are not able to capture changes on seasonal scales (e.g. CRUZ et al., 2009; PRADO et al., 2013; STRÍKIS et al., 2011; WANG et al., 2004) and indicate only southward displacement of the ITCZ for the mid-Holocene, but no evidence of seasonal variation.

The meridional shift of ITCZ has also been suggested as a mechanism through which the Atlantic Multidecadal Oscillation (AMO) influences precipitation in present time (KNIGHT et al., 2006, TING et al., 2011, LEVINE et al., 2018). Indeed, Lapointe et al., (2020) highlights the period of LIA as the longest and most persistent period with a cold anomaly in the North Atlantic. This supports the hypothesis of ITCZ shifting during LIA to a more southerly position of present-day mean (HAUG et al., 2001; BIRD et al., 2011; ZHANG et al., 2019). The observational data of $\delta^{18}O$ of precipitation in the International Atomic Energy Agency-Global Network of Isotopes in Precipitation (IAEA-GNIP) database are unfortunately short (initiates in 1960), discontinuous, and spatially scarce to allow unraveling the relationship of isotope signals and modern decadal/centennial modes (LACHNIET, 2009; BAKER et al., 2019). Although the scientific literature frequently explains the changes in $\delta^{18}O$ signals in speleothem records from LM in the context of zonally uniform northward and southward shifts of the mean position of the ITCZ in consequence of interhemispheric balance of energy inputs to the atmosphere, this is by no means assured (ROBERTS; VALDES, 2017; BIASUTTI; VOIGT, 2020; MAMALAKIS et al., 2021). This hypothesis has recently also been challenged by synthesis of paleoclimate records from Central America which show significant spatial variability in hydroclimate during LIA. Steinman et al. (2022) and Asmerom et al. (2020) argue that ITCZ shift cannot be the main driver of inferred precipitation patterns. Despite the relative consensus in the literature

that ITCZ shift controled precipitation over the LM, existing paleoclimate data suggest much more complex evolution of hydroclimate within South America (ORRISON et al., 2022; MEDINA et al., 2023) that goes beyond changes in mean position of the ITCZ.

To better understand the AMO and whether the signals in paleo records could be influenced by AMO, that is, how AMO is reflected on $\delta^{18}O$ of precipitation requires use of isotope-enabled models.

As previously discussed, insights across scales and climate states should contribute to a deeper understanding of future climate projections. Therefore, the main objective of this thesis is to provide a past-present-future perspective of climate changes and terrestrial ecosystem responses in South America, analyzing both simulations and records-based reconstructions. Thus, this thesis intends to:

1. Test the vegetation response to a temperature increase of approximately 4°C from the Last Glacial Maximum to the pre-industrial period, and then use this knowledge to project vegetation response on an additional 4°C of potential future warming.
2. Establish the relationship between specific forcings and observed responses in both past and future projections.
3. Investigate scenarios of warming/cooling in the period right before the anthropogenic warming of the 20th century and the Atlantic Multidecadal Oscillation as potential major driver of precipitation changes in South America.

This thesis is composed of three themed chapters (chapters 2, 3, and 4). Chapter Two evaluates vegetation response to a temperature increase of approximately 4°C from the LGM to the pre-industrial, and to an additional 4°C of potential future warming. Three analyzes the influence of the AMO on South American atmosphere, dynamics and precipitation. Four analyzes the results of simulated isotopic fingerprint of AMO and paleoclimate reconstructions of the LM. Thesis chapters Two and Three are amended versions of published

papers. The published papers are in the appendix. Finally, chapter Five presents the general conclusions of the research.

2 BRAZILIAN BIOMES DISTRIBUTION: PAST AND FUTURE

2.1 Introduction

During the LGM global climate was significantly different from modern (i.e., pre-industrial) climate. Since the LGM, the atmosphere warmed and given climate models projections, warming will certainly continue in the coming decades. The global mean warming since the LGM is of a similar magnitude to the upper range of Coupled Model Intercomparison Project phase 5 (CMIP5) projections for the end of the twenty-first century (COLLINS et al., 2013). This provides the rare opportunity to test the vegetation response to a temperature increase of approximately 4°C from the LGM to the pre-industrial, and then use this knowledge to project vegetation response on an additional 4°C of potential future warming. Hereafter, the LGM will also be referred to as the "-4°C" scenario and the end-of-century scenario will also be referred to as "+4°C". In this study, the potential vegetation of Brazil is simulated for both scenarios in order to verify the most affected biomes and explore the extent of biome changes with temperature increase in each scenario. With the aim to determine the main drivers behind vegetation changes sensitivity experiments were conducted. By isolating each factor (CO_2, precipitation and surface temperature), the sensitivity experiments allowed us exploring the influence of each factor over vegetation for both scenarios. In addition, biome projections for the past are compared with a compilation of 149 published reconstructions of climate and vegetation within Brazil and adjacent areas.

2.2 Data and methods

In the chapter that follows, I present a description of the model data selected for the temperature and precipitation analyses, as well as the methods used for vegetation projections and compilation of proxy data from paleoclimate archives used for model validation.

2.2.1 Past and future climate simulations

With the aim of analyzing the maximum number of models compiled in the Coupled Model Intercomparison Project phase 5 (CMIP5) / Palaeoclimate

Modeling Intercomparison Project phase 3 (PMIP3) (TAYLOR et al., 2012), we used all the models that were available at the moment of analysis at the British Atmospheric Data Centre (BADC) and had both past and future scenario outputs. Climate scenarios for both past and future were extracted from the following models: CCSM4, CNRM-CM5, FGOALS-g2, GISS-E2-R, IPSL-CM5A-LR, MIROC-ESM, MPI-ESM-P, and MRI-CGCM3. Models references are given in the Table 2.1.

Table 2.1 - CMIP5 Earth system models analyzed in this study, with the atmospheric resolution (lat x lon grid; number of vertical levels), references and experiments.

Model	References	Grid	Experiments
CCSM4	Gent et al. 2011	1.25º x 0.9º; 27	Historical, LGM, RCP8.5
CNRM-CM5	Voldoire et al. 2013	~1.4º x 1.4º; 31	Historical, LGM, RCP8.5
FGOALS-g2	Li et al., 2013	2.8º x 2.8º	Historical, LGM
GISS-E2-R	Schmidt et al. 2014	2º x 2.5º ; 40	Historical, LGM
IPSL-CM5A-LR	Dufresne et al. 2013	1.9º x 3.75º; 39	Historical, LGM, RCP8.5
MIROC-ESM	Watanabe et al. 2011	2.8º x 2.8º; 80	Historical, LGM
MIROC5	Watanabe et al. 2010	0.79° × 1.41°	Historical, RCP8.5
MPI-ESM-P	Giorgetta et al. 2013	~1.9º x 1.9º; 47	Historical, LGM
MPI-ESM-LR	Giorgetta et al. 2013	~1.9º x 1.9º; 47	Historical, RCP8.5
MRI-CGCM3	Yukimoto et al. 2012	~0.9º x 0.9º; 48	Historical, LGM, RCP8.5

Here are analyzed the results of eight CMIP5 Earth system models for the past, present and future climates obtained from the British Atmospheric Data Centre (BADC). The parameters for these climate simulations were defined by the protocol established by the Coupled Model Intercomparison Project phase 5 (CMIP5; TAYLOR et al. 2012), which is a series of coordinated experiments to evaluate the ability of climate models to simulate past scenarios and assess the sensibility of the climate to changes in atmospheric composition and biosphere. Here are analyzed the results from the Historical, LGM and RCP8.5 CMIP5 experiments, which are briefly described below.

The Historical experiment covers the period between 1850 and at least 2005, and it aims to evaluate the model performance against the present climate and observed climate change. External forcings include observed greenhouse

gases concentration, solar forcing, volcanic activity, ozone, and aerosols. The LGM experiment is a climate simulation for 21,000 year ago (21ka), with imposing conditions consistent with the Paleoclimate Modeling Intercomparison Project phase 3 (PMIP3) specifications (BRACONNOT et al. 2012). Excluding global mean insolation, the LGM external forcings are significantly different from the Historical ones: global ice was at its maximum, atmospheric dust was very high, greenhouse gas concentrations were low, and sea level was at its minimum (~ 120m lower). The RCP8.5 simulation (RIAHI et al. 2011) provides estimates of future anthropogenic climate change for future scenario of increasing radiative forcing until ~8.5 W m-2 near ~2100. The LGM and RCP8.5 CMIP5/PMIP3 experiments are used as nearly opposite scenarios.

As models differ in type, configuration, parameterization and resolution, projections for some regions differ significantly among them (KNUTTI; SEDLÁČEK, 2013). In order to diminish those differences, the model data were converted to the same spatial resolution, and the multi-model ensemble mean was calculated. The surface air temperature and precipitation, both single model and multi-model ensemble mean, are evaluated and analyzed in comparison with the Historical experiment. The LGM experiment was used for the -4°C scenario and the 30-year average monthly mean for temperature and precipitation were calculated. The RCP8.5 experiment is used for the +4°C scenario. The + 4°C period for each model is determined separately, where the +4°C period is defined as the time when the global mean temperature reaches +4°C compared to the Historical run (1850-2005) (as in VAUTARD et al., 2014). This method was adopted to reduce uncertainty originating from the different climate sensitivity of a model and analyze +4°C warmer global climate in terms of temperature and precipitation distribution, independently of the period of the century when it could occur.

2.2.2 Past and future biomes distribution

The outputs of the climate simulations described in the previous section were used to force the Center for Weather Forecasting and Climate Studies Potential Vegetation Model version 2 (CPTEC-PVM2; LAPOLA et al., 2009) and produce

equilibrium vegetation projections. This model can reproduce the main South American biomes like tropical forests over Amazonia and the Atlantic coastal region, savannas over central Brazil (‘cerrado’), dry shrublands (‘caatinga’) over northeastern Brazil and the Chaco region, grasslands over the Pampas, and semi-desert vegetation over Patagonia (OLSON et al., 2001). Model resolution in this study is 1° lat × 1° lon. To perform the potential vegetation simulations for the -4°C and +4°C scenarios as well as sensitivity experiments for each scenario, the climatology from CMIP5 models described in the previous section have been used. To filter out the effect of the systematic errors from the different models (MUELLER; SENEVIRATNE, 2014), the CPTEC-PVM2 model was initialized with the 1961–1990 observed climatology (WILLMOTT; MATSUURA, 2001) and then were added the anomalies (i.e., experiment minus present) for each scenario, following the anomaly coupling procedure (KUTZBACH et al., 1998). Both single model and multi-model ensemble mean climatologies are considered, but as the multi-model ensemble means of present-day climate agrees better with observations than any single model (TEBALDI; KNUTTI, 2007), and in order to decrease the range of climate models uncertainty, final analyses of biome projections were based on runs with the multi-model ensemble mean anomalies input. Regarding the concentration of CO_2, the -4°C and the +4°C scenarios used 180 ppm and 900 ppm, respectively (KAGEYAMA et al., 2017) (Table 2.2).

To perform the potential vegetation simulations for Present scenario the CPTEC-PVM2 model was initialized and calibrated with the 1961–1990 observed monthly climatology Willmott and Matsuura, 2001(WM), that is: (precWM+tempWM) with CO_2=350ppm. To perform the potential vegetation simulations for the -4°C and +4°C scenarios the CPTEC-PVM2 model was initialized with the observed monthly climatology plus the monthly fields of multi-model ensemble mean anomalies (MME) for each scenario: (precWM + MME-4)+(tempWM + MME-4) with CO_2 = 180ppm for the LGM or (precWM + MME+4)+(tempWM + MME+4) with CO_2 = 900ppm for the future.

Table 2.2 - Inputs used for the Center for Weather Forecasting and Climate Studies Potential Vegetation Model version 2 (CPTEC-PVM2) experiments.

Experiment	CO_2 (ppm)	Precipitation	Temperature
Present	350	Willmott and Matsuura, 2001; (WM)	Willmott and Matsuura, 2001; (WM)
- 4 °C (LGM)	180	WM + MME anomalies from scenario - 4 °C	WM + MME anomalies from scenario - 4 °C
+4°C (Future)	900	WM + MME anomalies from scenario + 4 °C	WM + MME anomalies from scenario + 4 °C

Note: For the Present experiment the model was forced with surface temperature and precipitation from the Willmott and Matsuura (2001)(WM) data set. For the - 4 °C scenario (representing the Last Glacial Maximum (LGM)) and the +4 °C scenario (representing +4 °C Future) with added anomalies from the multi-model ensemble mean (MME).

In the case of sensitivity experiments, only one parameter has been changed. For example, in performing sensitivity simulations for the LGM precipitation the setup was (precWM + MME-4) + (tempWM) with CO_2=350ppm; or, in performing sensitivity simulations for the LGM CO_2 the setup was (precWM+ tempWM) with CO_2 = 180ppm.

To determine the influence of each climate parameter on biome distribution, sensitivity experiments for both -4°C and +4°C scenarios were run, considering the anomalies of CO_2, precipitation and temperature separately. How biome projections and sensitivity experiments were performed in each case is depicted in the Table 2.3.

Table 2.3 - Description of sensitivity experiments performed with the Center for Weather Forecasting and Climate Studies Potential Vegetation Model version 2 (CPTEC-PVM2).

Sensitivity experiment	CO_2 180 ppm	CO_2 350 ppm	CO_2 900 ppm	PREC from WM	TEMP from WM	PREC WM +MME (-4°C)	TEMP WM +MME (-4°C)	PREC WM +MME (+4°C)	TEMP WM +MME (+4°C)
-4°C (LGM) CO_2									
-4°C (LGM) PREC									
-4°C (LGM) TEMP									
Present									
+4°C (Future) CO_2									
+4°C (Future) PREC									
+4°C (Future) TEMP									

2.2.3 Compilation of proxy data from paleoclimate archives

For this study the compilation of 107 published hydroclimate records from tropical South America made by Zhang et al. (2016) was updated. All their records that cover the LGM were considered and new ones, published since then, that showed vegetation, hydroclimate and environmental reconstructions were added. Compilation of 149 published vegetation and hydroclimate records (MAKSIC et al., 2021) with their respective references can be found in Table A.1 or at https://doi.org/10.1594/PANGAEA.927527. Original chronologies of all paleorecords were used. To evaluate the dating quality of the compiled records, I applied a chronological reliability index. The Chronological reliability index (CRI) is based on age model properties and sampling resolution of each record, where higher CRI values indicate more reliable paleorecords (PRADO et al., 2013; ZHANG et al., 2016). CRI is a semiquantitative approach that simply involves the computation of an arithmetic mean, where the same weight is given to the calibration, sampling resolution and the sample age model. This index, established by Prado et al. 2013, simply involves the computation of an

arithmetic mean, where the same weight is given to calibration (C), sampling resolution of each record (R) and dating (D):

$$CRI = (C + R + D)/3 \quad (2.1)$$

where C equals 1 if ages are calibrated, or 0 if they are not calibrated; D (dating) is the number of age control points within LGM(19-23ka), divided by 10; R (resolution) refers to the mean number of total samples per entire core length ratio, as given:

R ={ 0.1 for ratio between 0.01 and 0.1

0.2 for ratio between 0.11 and 0.2

…

…

11.0 for ratio between 10.01and 11.00}.

The temporal proximity of the LGM to two Heinrich Stadials (namely Heinrich Stadial 2 and Heinrich Stadial 1) make the CRI particularly necessary, since Heinrich Stadials are thought to have substantially altered the distribution of Brazilian biomes (e.g., WANG et al., 2004; BOUIMETARHAN et al., 2018; PINAYA et al., 2019).

In order to compare the results from the compilation with model simulations, categories for precipitation and vegetation (biome) changes based on the original interpretations of the authors have been defined. In the case of precipitation, anomalies are expressed as the difference between LGM and present time, and the categories are “drier”, “wetter” and “unclear”. Also for vegetation anomalies are expressed as the difference between LGM and present time, and the categories are “change”, “no change” and “unclear”. Although this approach has been used in other studies, this simplification can result in an agreement between the proxy record and the model scenario even in case when they show opposite signals, so description of change and change evidence is specified in the compilation.

2.3 Results

2.3.1 Validation of the climate simulations for the -4°C scenario using paleoclimate proxies

To validate multi-models ensemble mean for the -4°C scenario, it is compared with the proxy compilation (see Proxy Compilation Table https://doi.org/10.1594/PANGAEA.927527). Figure 2.1 shows multi-models ensembles mean and single model anomalies of annual precipitation (mm/month) calculated for the -4°C in comparison with the Historical multi-model ensemble. As can be seen from the Figure 2.1 fully coupled models still show a large spread on the anomalies. The calculated multi-model ensemble mean (Figure 2.1a) diminishes those differences. However, even the calculated multi-model ensemble mean precipitation anomaly shows some discrepancy in paleo precipitation reconstructions. Higher precipitation simulated along the Andes is consistent with lake and ice core records. The simulated anomaly over equatorial South America corroborates the findings from 39 records between 10°N and 10°S that suggest a drier LGM. Over the SAMS region, simulated precipitation increase is in agreement with 4 high-resolution speleothem-based records. However, 10 other reconstructions, mostly estimations from biological proxies between 10°S and 20°S, appear to contradict the increased activity of the SAMS. Still, the comparison with 20 paleorecords south of 20°S shows high consistency and indicates a reduction in precipitation (for full details about proxies see Proxy Compilation).

Figure 2.1 - Difference between scenario -4°C and Historical multi-models ensembles mean of annual precipitation (mm/month) calculated from models: (b-i) CCSM4, CNRM-CM5, FGOALS-g2, GISS-E2-R, IPSL-CM5A-LR, MIROC-ESM, MPI-ESM-P, MRI-CGCM3; Shaded areas correspond to drier (wetter) conditions; Proxies (MAKSIC et al., 2021) are marked with the red (blue) dots representing drier (wetter) conditions, grey color of dots represent neutral conditions; Dots size represent chronological reliability index (CRI<1●, 1<CRI<3 □, CRI>3●).

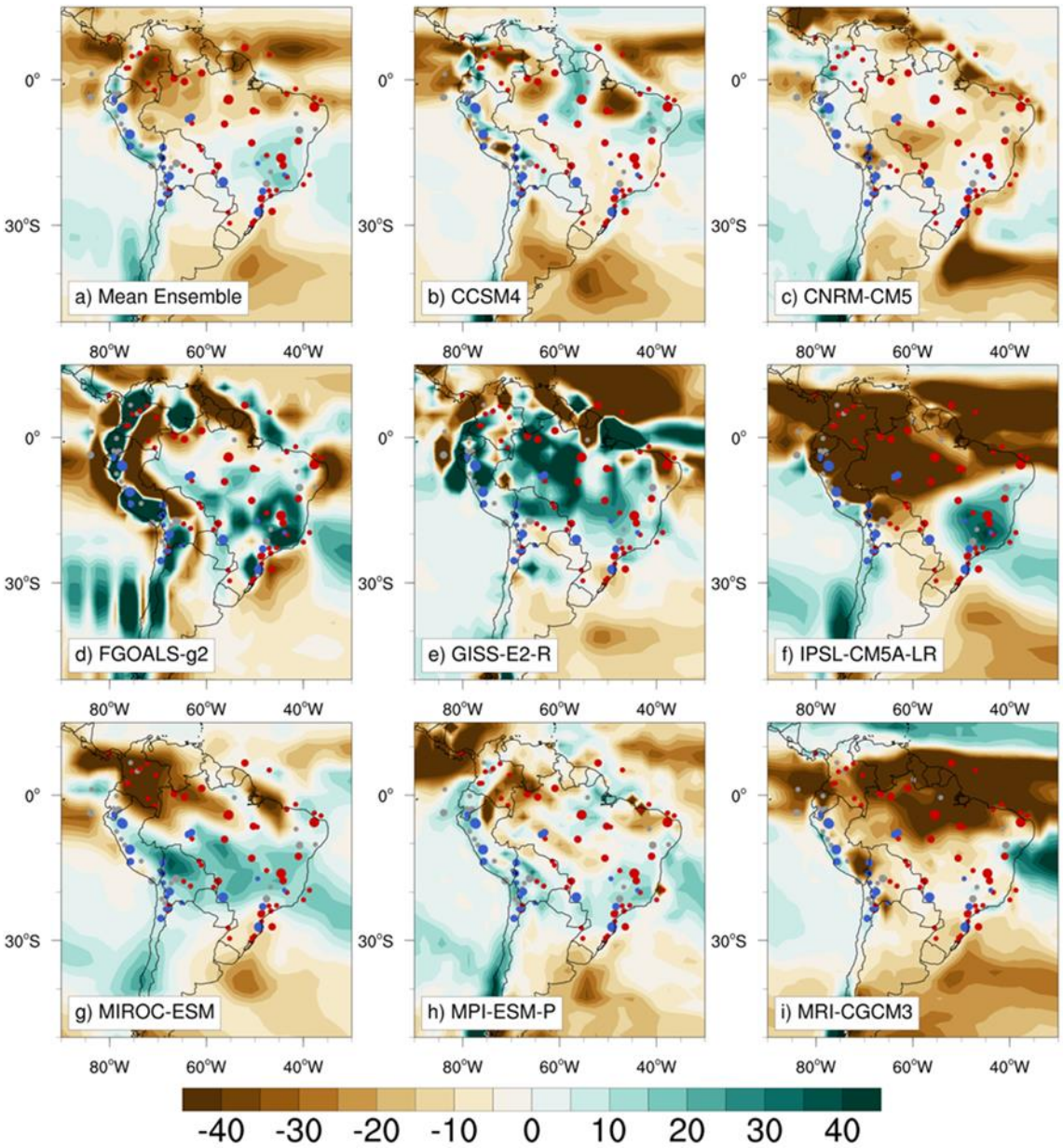

2.3.2 Climate simulations

From the Figure 2.2 it is apparent that model-to-model differences in the forced response are present in +4°C scenario as well. It can be seen that projections for some regions differ significantly. In order to diminish those differences and decrease the range of climate models uncertainty, analyses and further biome simulations are based on the calculated multi-model ensemble mean (Figure 2.3).

Figure 2.2 - Annual precipitation (mm/month) and temperature (°C) differences between the RCP 8.5(+4°C) and Historical scenarios from models (a-f) CCSM4, CNRM-CM5, IPSL-CM5A-LR,MIROC-ESM, MPI-ESM-P, MRI-CGCM3.

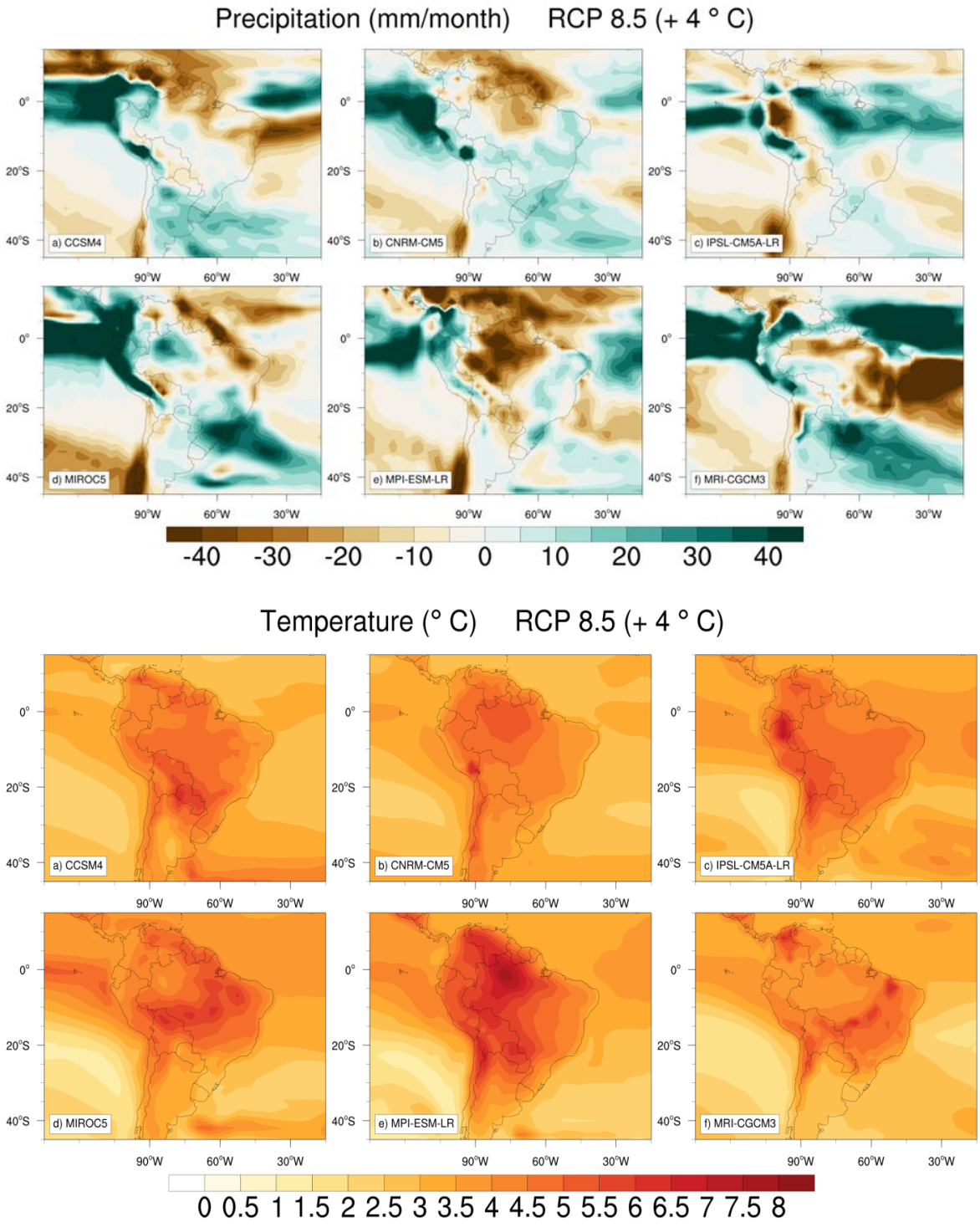

Figure 2.3 shows the annual mean precipitation and temperature anomaly fields from the multi-model ensemble calculated for the -4°C and the +4°C scenarios in comparison with the Historical multi-model ensemble mean. A comparison reveals that for the -4°C scenario there is a negative precipitation anomaly over the tropical region (0°-10°S) (Figure 2.3a). The highest precipitation reduction of more than 14 mm/month has been projected for the northwestern sector of Amazonia. Multi-model ensemble mean anomaly also suggests increased precipitation, higher than 10 mm/month, over the southeastern portion of the South American Monsoon System region (50°W–40°W, 10°S–28°S) (Figure 2.3a). For the +4°C scenario a precipitation decrease of ~14 mm/month is projected for the eastern equatorial Brazil (i.e., the region around the Marajó island). Central Brazil shows a weak positive anomaly of 2 to 4 mm/month, while precipitation increase (~20 mm/month) is the highest over southern Brazil, below 20°S (Figure 2.3b). Temperature projections for both scenarios are more uniform, with more than 70% of agreement among models over the entire Brazil (Figure 2.3c, d). Temperature anomalies show generally higher values inland than in the coastal regions, with regional variations of approximately 2°C.

Figure 2.3 - Annual mean precipitation (mm/month) (a-b) and temperature (°C) (c-d) fields from the multi-model ensemble mean differences calculated between the -4°C scenario (a, c) and the +4°C scenario (b, d) in comparison with Historical simulations. Stippling represents areas where at least 70% of the models agree with the sign of the difference.

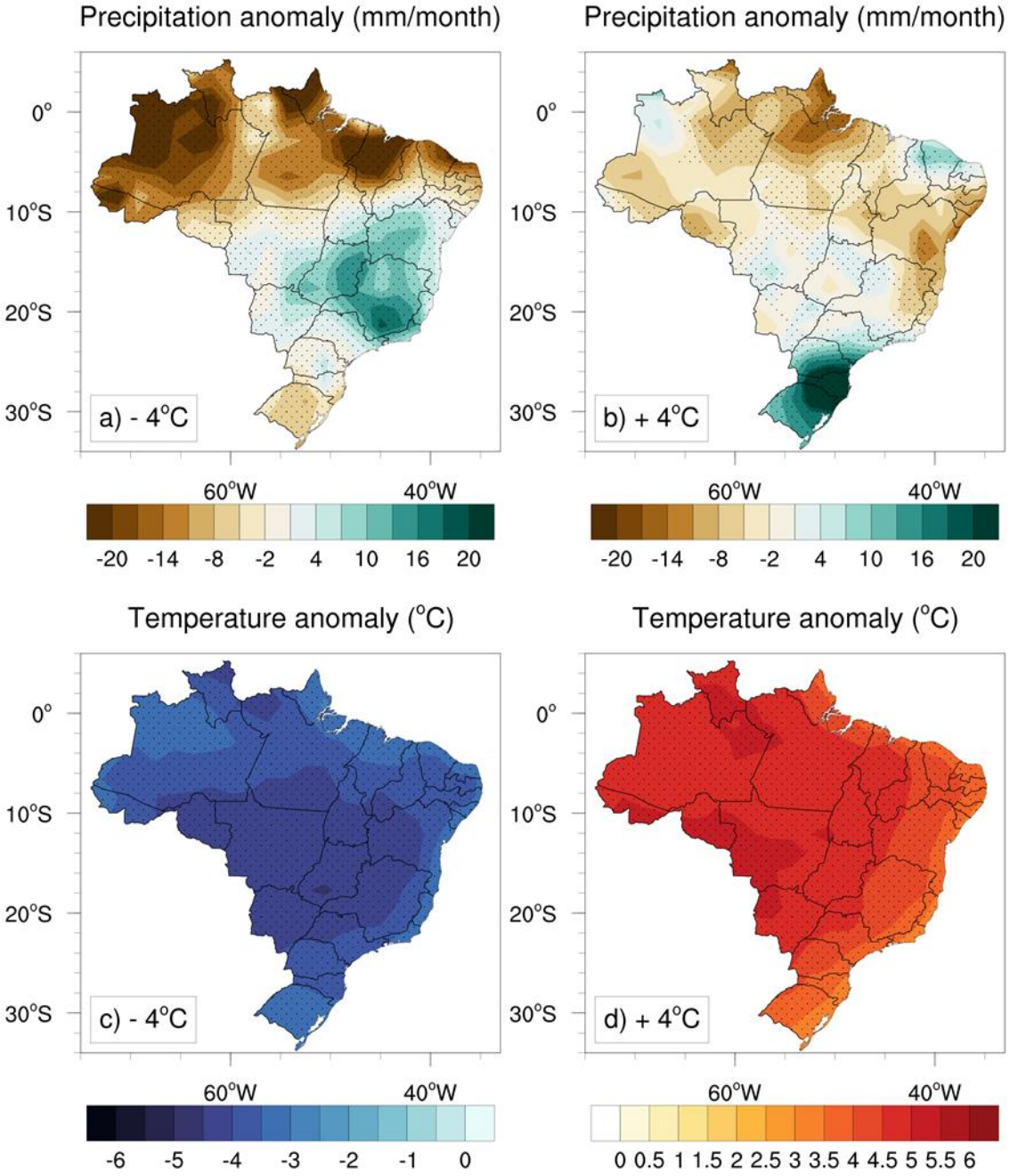

2.3.3 Simulated biome changes for -4°C and +4°C scenarios

Figure 2.4 shows CPTEC-PVM2 vegetation equilibrium solutions based on long-term mean monthly climate variables for the -4°C scenario, Present (1961–

1990) climate, and the +4°C scenario. The simulation of the -4°C scenario indicates a distinct difference in southern Brazil (60°W–40°W, 20°S–35°S) in comparison with the Present simulation (Figure 2.4a, b) suggesting grassland expansion. In northeastern Brazil, Open shrubland/Caatinga is rearranged and its central part is transformed in semi-desert (Figure 2.4a). While western Amazonia persisted as a tropical forest with no substantial changes, eastern Amazonia was transformed into tropical seasonal forest. Tropical seasonal forests with savanna patches are also simulated in northern Amazonia (65°W–55°W, 5°N–0°). The simulation of the +4°C scenario shows an expansion of Savanna/Cerrado, replacing most of the open shrubland/caatinga simulated from the Present conditions (Figure 2.4b, c). The eastern part of the tropical evergreen forest of Amazonia is replaced with patches of savanna that reach 55°W, while the +4°C scenario conditions favor tropical evergreen forest expansion over southern Brazil.

Figure 2.4 - Distribution of Brazilian biomes projected by the Center for Weather Forecasting and Climate Studies Potential Vegetation Model version 2 (CPTEC-PVM2) for a) the -4°C scenario (representing the Last Glacial Maximum), b) Present (1961–1990) climate, and c) the +4°C scenario (representing RCP8.5 experiment period when the 30-year average global mean temperature reaches +4°C compared to the Historical run). The color scale displays different biomes.

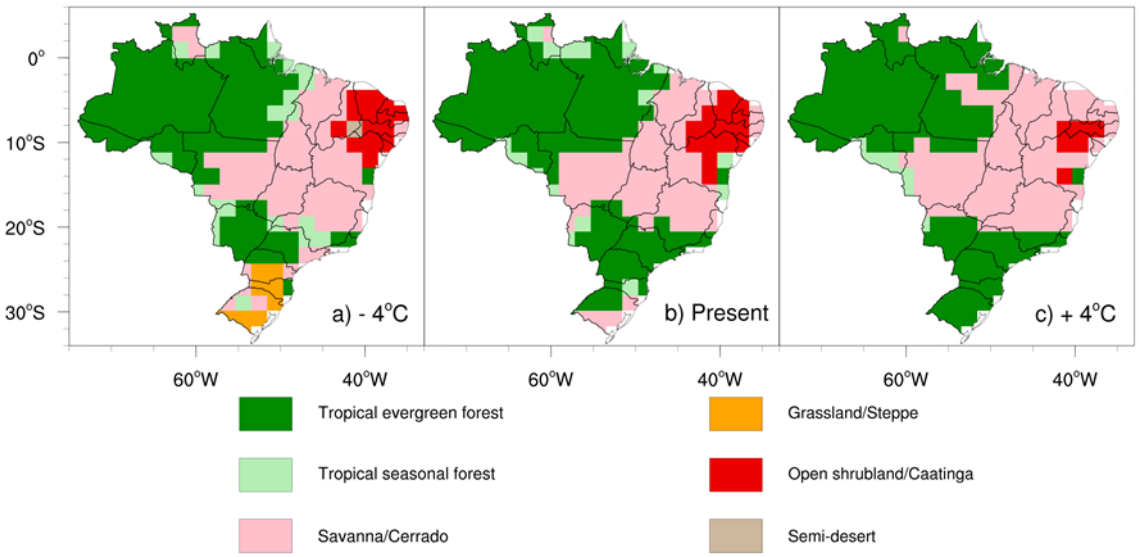

2.3.4 Validation of the biome simulations for the -4°C scenario using paleovegetation proxies

Most regions where the CPTEC-PVM2 model projected biome changes for the -4°C scenario are in high agreement with paleovegetation proxies (Figure 2.4). From 149 proxy data present in the compilation, where 77 deal with changes in vegetation, 49 vegetation proxies matching the changes suggested by the model. However, while paleorecords from southern and eastern Amazonia are in accordance with the model output, four paleorecords from the core of the Amazon forest contradict model projections (for full details see Proxy Compilation).

Figure 2.5 - Differences between biome projection for the -4°C (representing the Last Glacial Maximum) scenario and Present. Grey fields represent areas where the Center for Weather Forecasting and Climate Studies Potential Vegetation Model version 2 (CPTEC-PVM2) projection for the -4°C scenario and for the Present differ from each other. The approximate location of compiled vegetation proxy sites is presented by circles. Red(black) circles indicate vegetation change (no change), brown circles indicate unclear signals. The size of the circles are defined by the Chronological Reliability Index (CRI), indicating the reliability of the paleorecord (the higher the CRI value, the more reliable the paleorecord). For full details about proxies see https://doi.org/10.1594/PANGAEA.927527.

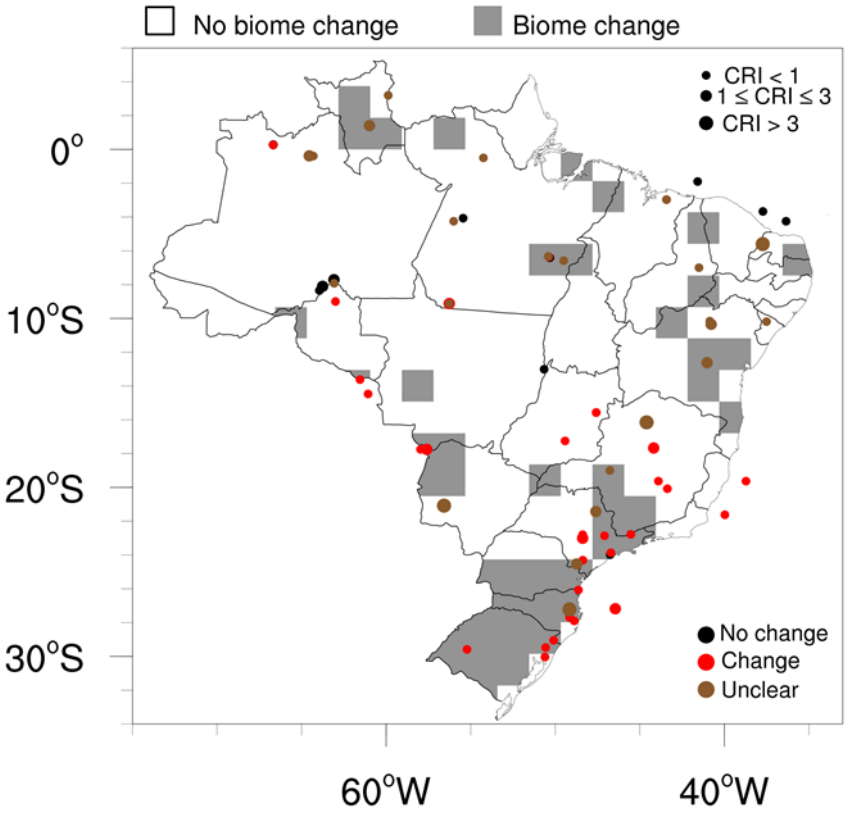

2.3.5 Sensitivity experiments

Sensitivity experiments were performed to evaluate the specific influence of precipitation, temperature and CO_2 over vegetation. Figure 2.6 shows that CO_2 and/or precipitation reduction of the -4°C scenario are able to induce ample changes in a large part of Amazonia and northeastern Brazil. The CO_2 reduction turns the Tropical evergreen forest into a less productive Tropical seasonal forest and enlarges the occurrence of Open shrubland/Caatinga

vegetation (Figure 2.6a). Changes in precipitation from the -4°C scenario drive Savanna/Cerrado expansion and produce great reduction of Tropical evergreen forest in the eastern and southern Amazonia (Figure 2.6b). Past temperature decrease in the -4°C scenario, in turn, mostly decreased the occurrence of Open shrubland/Caatinga, with a positive effect in the occurrence of Tropical evergreen forest (Figure 2.6c).

In the case of the future +4°C scenario, Tropical evergreen forests substantially expand its occurrence with elevated CO_2. Future precipitation anomalies induce Tropical evergreen forest reduction in Tropical evergreen forests to the north of the equator and the occurrence of semi-desert vegetation in northeastern Brazil. Future temperature increase of 4°C causes Tropical evergreen forest to be completely replaced by less productive biomes, while large extensions of Savanna/Cerrado turns into Open shrubland/Caatinga, and the occurrence of semi-desert vegetation over northeastern Brazil is increased.

Figure 2.6 - Sensitivity simulations for biome distribution projected by the Center for Weather Forecasting and Climate Studies Potential Vegetation Model version 2 (CPTEC-PVM2) for a) the -4°C scenario (representing the Last Glacial Maximum) and b) the +4°C scenario (representing RCP8.5 experiment period when the average global mean temperature reaches +4°C compared to the Historical run). Anomalies of the CO_2, precipitation and temperature were considered separately for the -4°C scenario (upper panels) and +4°C conditions (lower panels). The color scale displays different biomes. Details about sensitivity experiments are given in the Table 2.3.

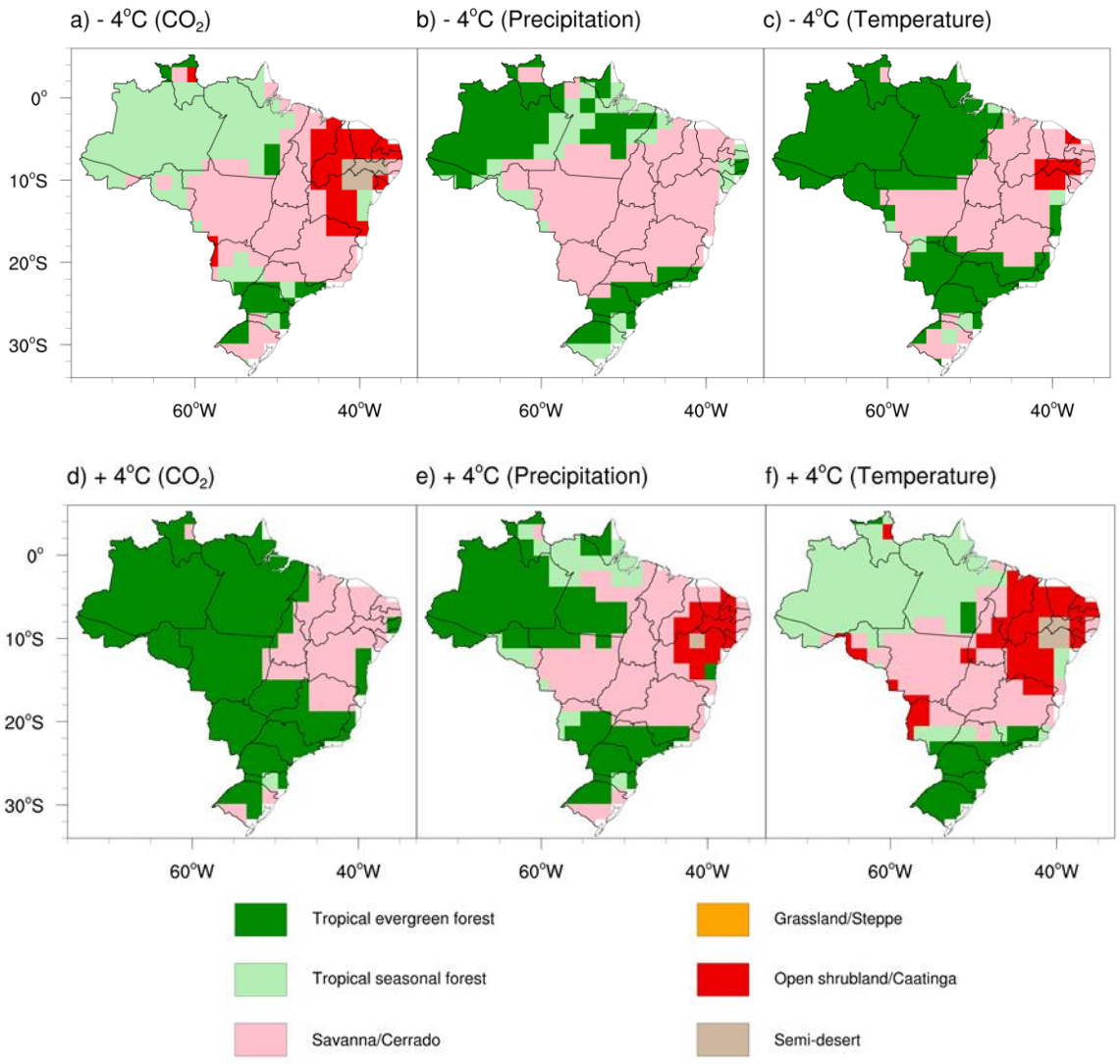

2.4 Discussion

2.4.1 Biome simulations: from the -4°C scenario to the Present

Prior to discussing the biome simulations, it is worth noting that although CMIP5/PMIP3 models improved the representation of physical processes and

resolution if compared to earlier intercomparison phases, some climatic processes are still simulated with high uncertainties (e.g., precipitation, clouds, aerosols, air–sea interactions), and some regional and seasonal climatology biases persist (KUMAR et al., 2014; WANG et al., 2014; ADAM et al., 2017). Models have clearly succeeded in reproducing the main features of past periods, but not all models resolve the topography and regional-scale features of the South American climate realistically. As simulated climatologies are used as the input for vegetation simulations, their validation for past conditions is of extreme importance.

Models in general agree about the sign and magnitude of temperature change for LGM, but due to the complexity in simulating precipitation and model differences, substantially different precipitation patterns are projected for LGM. Simulations of precipitation have shown even opposite signs, and great regional variations in some regions (Figure 2.1). One way to overcome this issue is the use of a multi-model ensemble mean instead of a single model output (TEBALDI; KNUTTI, 2007). The LGM inconsistencies possibly came from difference in the sensitivity of models to the extent, height, and topography of the ice sheets and dust dynamics (ALDER; HOSTETLER, 2019). Studies also show that better physical parameterizations and/or enhanced horizontal and vertical resolutions can eliminate precipitation bias (HARLASS et al., 2016; LEE et al., 2013; JUNQUAS et al., 2015). On the proxy side, the small number of well-dated, long and continuous records from South America (FLANTUA et al., 2015; DEININGER et al., 2019) are additionaly complicated by subjective vegetational and climatic interpretation (BUSH, 2002). The results from biological and geochemical proxies in some regions open the debate if tropical South America experienced wet or dry conditions during the LGM (i.e. -4^{o}C scenario) (PRENTICE et al. 2022).

Here the computed LGM temperature and precipitation anomalies are validated with compilation of paleorecords covering the LGM within South America. For the sake of making LGM a potential antianalog for future warming and symmetric comparison, the referent cooling of LGM at -4°C was set. The computed temperature reduction showed here (Figure 2.3) are consistent and

within the range of several estimates for the LGM over South America (STUTE et al, 1995; COLINVAUX et al., 2000; VAN DER HAMMEN; HOOGHIEMSTRA, 2000; WILLE et al., 2001; BUSH et al., 2004; URREGO et al., 2005; CHIESSI et al., 2015). The newest research on global temperature (TIERNEY et al., 2020) estimates LGM to pre-industrial warming to be 6.1°C.

The multi-model ensemble mean for the -4°C scenario shows a negative precipitation anomaly over the equatorial region, with the highest precipitation reduction projected for the northwestern part of the Amazon Basin. Validation with proxies shows that computed climate coincides with glacial conditions inferred from the paleorecords available in the region (Figure 2.1). High precipitation along the Andes is consistent with cave, lake, marine and ice core records (e.g., GROSJEAN, 1994; GOSSLING et al., 2008; NIEMANN; BEHLING 2008; URREGO et al. 2010; CHENG et al., 2013; GOVIN et al., 2014). Precipitation lower than present over tropical South America to the east of the Andes and north of the Equator are in agreement with paleorecords (e.g., ABSY et al., 1991; HÄGGI et al., 2017; CRUZ et al., 2009; ROSSETTI et al., 2012). The projected stronger SAMS is in agreement with high-resolution speleothem- and marine-based records (e.g., CRUZ et al., 2006; CRUZ et al., 2009; NOVELLO et al., 2018; HOU et al., 2020). However, precipitation reconstructions from biological proxies from the southern border of the Amazon and from southeastern Brazil appear to contradict the increased activity of the SAMS (e.g., DE OLIVEIRA, 1992; SALGADO-LABOURIAU et al., 1997; BEHLING, 2002; BURBRIDGE et al., 2004; MAYLE et al., 2000).

The reasons for discrepancies between the results of biological reconstructions on the one side and multi-model ensemble mean and geological reconstructions on the other side could lie in edaphic constraints (ROSSETTI et al., 2019). The improved spatial resolution of climate models or the use of regional models, in addition with better soil representation (QUESADA et al., 2010) would probably clarify these discrepancies. Scheff et al., (2017), calls for caution when paleo hydrologic conditions are inferred from plant-based proxies, as the low glacial CO_2 and temperatures, and not water scarcity, as generally assumed, can drive changes in vegetation. The low CO_2 acts on physiological effects of individual

plants to changes in ecosystem functioning. The direct effect of low CO_2 on plant physiological processes is favoring C4 plants, while C3 plants show an average reduction in photosynthesis and biomass production (GERHART; WARD, 2010; PRENTICE et al., 2011). There is also the possibility of a no-analog climate for large portions of South America during the LGM (i.e. extended dry season plus extreme runoff events) as well as no-analog plant communities (LEDRU, 2002; BUSH et al., 2004). Still, a comparison between climate proxies and multi-model ensemble mean precipitation shows high consistency over southern Brazil (Figure 3.1a). Thus, we conclude that the computed temperature and precipitation anomalies over Brazil are reliable as inputs for the potential vegetation model.

Once the reliability of inputs for the potential vegetation model is confirmed, I evaluate the relative biome distribution (Figure 2.5). Relative biome distribution (%) for the -4°C scenario shows that Tropical evergreen forest decreased 10% (Figure 2.7). This is the result of the transformation of Tropical seasonal forest on the eastern portion of the Amazon basin, which is consistent with vegetation reconstructions (ABSY et al., 1991; SIFEDDINE et al., 2001; BEHLING, 2002; ANHUF et al., 2006; HÄGGI et al., 2017) as well as transformation of Grassland and Tropical seasonal forest in southern Brazil (e.g., BEHLING et al., 2004; GU et al., 2018).

The performed sensitivity experiments suggest that with CO_2 reduction, from 350 ppm (Present scenario) to 180 ppm (LGM scenario), there is an almost complete disappearance of Tropical evergreen forest biome (Figure 3.6a). In the photosynthesis model used by CPTEC-PVM2 (FARQUHAR et al. 1980) the response for changes in CO_2 concentration is linear, due to the term applied in photosynthesis formulation which avoids an unrealistic steep decay of photosynthesis rates at low CO_2 concentrations (LAPOLA et al., 2009). Nevertheless, halving CO_2 in LGM induced a significant reduction of net primary production and shifted Tropical evergreen forest biome to less productive Tropical seasonal forest.

Lower LGM temperature counteracts the effect of lower CO_2 and prevents a more extensive forest replacement by savanna (Figure 2.6a, c). It is estimated that about 32% of Amazonian rainfall originates from evapotranspiration within the basin, two thirds of which originate as tree transpiration (STAAL et al., 2018). Thus, under decreased CO_2 and water vapor in the atmosphere, vegetation water use efficiency is lower (BEERLING; WOODWARD, 1993), implying a higher stomatal conductance and an increase in transpiration. That effect could be balanced with temperature decrease and improved soil moisture (reduced evaporation) (SCHEFF et al., 2017) and consequently reduced prevalence of fire, which is an important element for savanna establishment, promoting the presence of Tropical evergreen forest (STAVER et al., 2011). On the other hand, for savanna's C4 grasses, the Cerrado biome, which evolved under low CO_2 conditions and tolerates droughts and fire, LGM conditions created an opportunity for advancement into forested areas. Therefore, alteration in the eastern Amazon could be mainly the result of insufficient soil moisture due to LGM precipitation reduction. The model does not consider soil types and variations in soil fertility, which may play an important role in explaining species composition, and forest productivity across the Amazon Basin (QUESADA et al., 2012), besides climatic east-west gradient presented here.

Hence, the results suggest that the western and central Amazon forest was largely maintained during the LGM mainly due to negative temperature anomalies, while a decrease in past precipitation was responsible for biome changes in the eastern portion of the Amazon. The simulations reaffirm that changes in the monsoon intensity cannot be used as the main driver for vegetational changes/stability across the Amazon biome (GERHART; WARD, 2010; PRENTICE et al., 2011; SCHEFF et al., 2017) and that lower temperatures in combination with substantially lower CO_2 are most probably the main controlling factors over changes in plant communities here (MAYLE et al., 2000). Thus, according to the simulations, the synergistic effect of temperature, precipitation and CO_2 increase since LGM positively affected the Amazon forest. Synergy of rising temperature and CO_2 also induced advancement of

forests over grassland in southern Brazil, represented in the simulations with complete disappearance of the Grassland biome. This change has been seen in pollen records and isotopic soil profiles from the southern Brazilian highlands, which reveal an expansion of Araucaria forest at the expense of grassland vegetation in the Late Holocene (LEDRU et al.,1996; LEDRU et al., 2009; BEHLING et al., 2004; GU et al., 2017). It is important to highlight that the LGM Grassland biome seen in records is reproduced by the model only when all forcings are taken into account, as none of them separately is sufficient for producing adequate conditions necessary for it (Figure 2.3a; Figure 2.6a-c). The omission of these LGM vegetation changes in the experimental design for LGM climate simulations could induce underestimation of important climate-vegetation feedback.

Over northeastern Brazil, with warming, Open shrubland/Caatinga is rearranged and its central part modeled as semi-desert for the -4°C scenario is transformed into Open shrubland/Caatinga (Figure 2.3a). This is in agreement with marine sediment records that suggest vegetation changes during the LGM (BEHLING et al., 2000). Bouimetarhan et al. (2018), infer the presence of Open shrubland/Caatinga vegetation in periods of expansion of tropical rainforest and tree ferns during the Younger Dryas, indicating the coexistence of a variety of vegetation types in northeastern Brazil and challenging the idea that Caatinga is the result of long-term climatic stability (WERNECK et al., 2011). Previously, De Oliveira et al. (1999) found abundant cold and humid-adapted montane rainforest taxa during the Pleistocene/Holocene transition in northeastern Brazil. Montane rainforests expanded and reached lower levels during LGM, afterwards decreasing gradually until Caatinga was established at 4.2 ka BP. Today, with semi-arid climate, rainforest enclaves with different phylogeographic histories are isolated on scattered ancient peaks where the higher elevation increases humidity (SILVEIRA et al., 2019). The difficulty in finding permanent lakes, bogs or stable locations for soil profiles made vegetational and climate evolution history within the Caatinga domain very limited. It is important to remember that local climate, topography and soil conditions are likely to influence vegetation structure (e.g. changes in biomass

or canopy cover) and dynamics (e.g. mortality and productivity) within the biomes. It is also worth noting that here only the LGM time slice is evaluated, and that millennial fluctuations, before and after this period, could have a larger impact on biomes, as no two time slices had identical biome patterns (PINAYA et al., 2019; ALLEN et al., 2020).

To summarize, in the context of 4°C climate warming since the LGM to the present times, the relative distribution of Savanna/Cerrado and Tropical seasonal forest decreased, Tropical evergreen forest and Open shrubland/Caatinga increased, while grassland biome virtually disappeared. Presented results indicate that Amazon forest and Caatinga showed resilience to temperature increase of 4°C since LGM. Whether their resilience will continue with another step in forcing of the same magnitude or they will be significantly disturbed in the future requires further analysis.

2.4.2 Biome simulations: from the present to a future +4°C scenario

Future conditions show an expansion of Savanna/Cerrado, with projected coverage 10% higher than the present, and a decrease of both Tropical evergreen forest and Tropical seasonal forest (Figure 2.4c; Figure 2.7). The results suggest that an even greater savanna advancement into forests is prevented by the "CO_2-fertilization" effect (LENTON et al., 2000) (Figure 2.6d-f). This is in agreement with an observed increase in carbon sink in the tropics. From the observed greening trends in the Amazon Basin, 70% is attributed to the 46 ppm increase in CO_2 during the period between 1982 and 2009 (ZHU et al., 2016). The results show the full potential of the "CO_2-fertilization" effect. However, long-term permanence and uniformity of this effect can be modulated by age (KÖRNER et al., 2005), mycorrhizal association (TERRER et al., 2016) and nutrient limitations (TERRER et al., 2019), as well as stress responses above the optimal temperature.

Although Savanna/Cerrado expanded in future simulation (i.e., +4°C scenario), the sensitivity experiments show that with additional 4°C even Savanna/Cerrado is pushed to a critical threshold (Figure 2.6f) and future precipitation changes will be critical in determining the fate of this biome (Figure 2.6e). The ecotonal

regions of Amazonia projected to change in the future, had experienced shifts throughout LGM (Figure 2.4a, b), showing that forest–savanna transitions are dynamic and particularly sensitive to change.

Figure 2.7 - Relative biome distribution projected by the Center for Weather Forecasting and Climate Studies Potential Vegetation Model version 2 (CPTEC-PVM2) for -4°C, Present and +4°C scenarios.

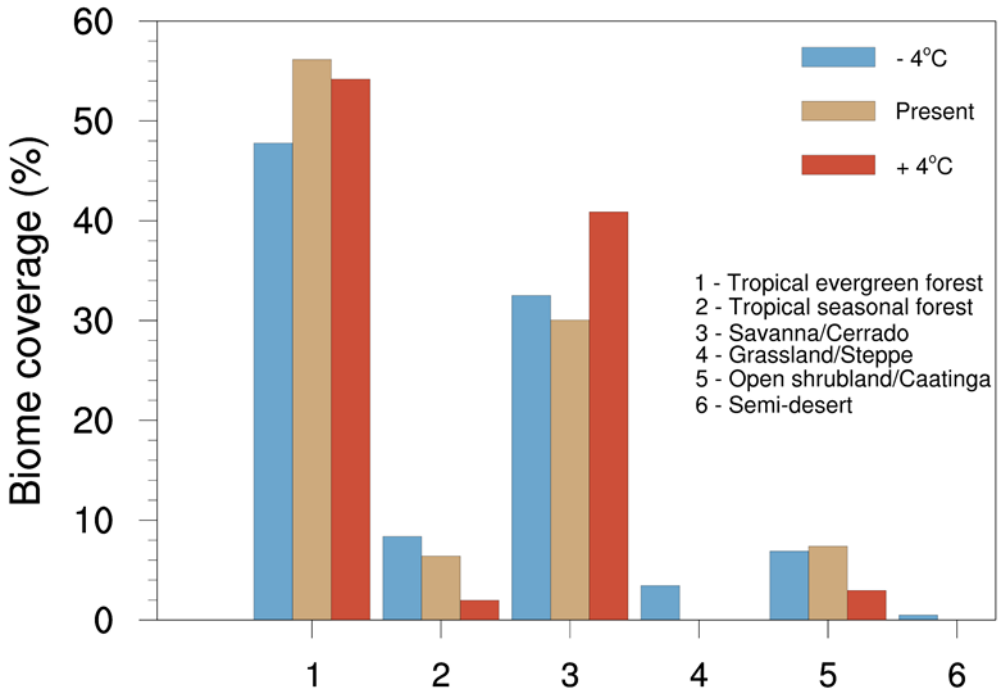

The model also suggests that the relative distribution of Caatinga will be ~50% lower. However, several issues have to be considered before interpreting this trend. First, with CO_2 = 900 ppm in the simulation, the modeled fertilization effect is strong enough to overweight temperature and precipitation impact and shift Open shrubland/Caatinga vegetation towards the more productive Savanna/Cerrado biome (Figure 2.6d-f). Previous experiments by Lapola et al. (2009) showed that halving the effect of CO_2 fertilization yields small changes in tropical forests, but considerable changes and higher permanence of shrubland in the Caatinga region. Moreover, Zhu et al. (2016) using three long-term satellite leaf area index records and ten global ecosystem models showed that for northeastern Brazil the key driver in vegetation change is climate and not

elevated CO_2. Second, high precipitation uncertainties for northeastern Brazil should also be taken into account (Figure 2.1). The sensitivity experiments indicate that with joined precipitation reduction and temperature increase, Caatinga vegetation, which is naturally highly adapted to water deficits (DOMBROSKI et al., 2011; LIMA; RODAL, 2010), could be replaced by semi-desert biome in its central domain (Figure 2.6e, f). Nevertheless, knowing that models do not agree about the sign of precipitation anomaly (MARENGO et al., 2020) (Figure 2.1, Figure 2.2), and with the possibility that the effect of CO_2 fertilization does not fully happen, the simulated Caatinga replacement by savanna in the future (+4^{o}C scenario) must be treated with caution (Figure 2.4b, c). In case of temperature increase and taking into account changes in frequency and intensity of droughts as well as aridization in northeastern Brazil (MARENGO et al., 2016), it is more likely that the Caatinga central domain will shift in the opposite direction and be replaced with semi-desert vegetation. In both cases (savannization or desertification), the Caatinga biome will experience an overall loss of biodiversity (SILVA et al., 2019).

Although the direct impact of warming on vegetation patterns is not easy to determine, as none of the evaluated driving factors (i.e. temperature, precipitation and CO_2) can be considered in isolation, the results indicate that two completely different biomes, when Tropical evergreen forests and Caatinga increased, both resilient to warming since the LGM, will be transformed in the future. In contrast to the warming of 4°C since the LGM, when Tropical evergreen forests and Caatinga increased, with additional warming those two biomes will be pushed to their thresholds. This is consistent with Ciemer et al, 2019, who claim higher resilience to climatic disturbances in regions exposed to a higher rainfall variability during their long-term past. Presented results suggest that only changes in the monsoon intensity cannot be used as the main driver for biomes changes in the past (Figure 2.4a, b; Figure 2.6a-c), but it is also found that with additional 4°C warming, changes and direction of biomes shifts in the eastern Amazon forest and Caatinga, will mostly depend on future precipitation changes. At the same time, the precipitation decrease will induce

decrease in biomass production and with that provoke additional local warming, preventing regeneration and adaptation (PERUGINI et al., 2017).

Precipitation changes in the last 30 years already increased the abundance of drought-tolerant genera and increased mortality of wet-affiliated trees in the areas where the drying trend was stronger across the Amazon forest (ESQUIVEL-MUELBERT et al., 2019), which indicates that this biome change is already underway. This relatively slow process of compositional change could continue in the future, and if it happens over larger spatial or temporal scales, there is potential for adaptation to changing conditions. However, under future global change, large changes in abiotic drivers in a short time-frame bring question whether ecosystems will have enough time to adapt to new warming conditions (ETTERSON; SHAW, 2001; HOFFMANN; SGRO, 2011; LAPOLA et al., 2023). On the other hand, even if compositional change happens that will lead to lower diversity, changes in evapotranspiration and forest resilience will likely decrease (AGUIRRE-GUTIÉRREZ et al., 2020). With interaction between droughts and fires, especially in the drier portions of the Amazon, forests could abruptly shift to new states (BRANDO et al., 2014).

Human land-use and land-use change will also alter the projected vegetation patterns over Brazil, through desertification and deforestation, and weaken the hydrological cycle even more (LEITE-FILHO et al., 2019; GATTI et al., 2021). Woody encroachment observed in recent years occurring within Cerrado and in transitional savanna zones, mostly caused by fire suppression, is a serious threat to Cerrado biodiversity (ROSAN et al., 2019).

Finally, the herein projected expansion of Tropical evergreen forest in southern Brazil (Figure 2.4b-c), that could possibly counteract forest loss due to Savanna/Cerrado expansion in the eastern Amazon, is already prevented by land use with high rates of areas converted into pastures and croplands in this region (LAPOLA et al., 2014, SONG et al., 2018). In this study land use changes were not modeled, but there is a need to consider this additional driver as regional human-driven pressures can lead to a cascade of tipping points in combination to the scrutinized driving factors (LAPOLA et al., 2023).

2.5 Conclusions

Because neither available paleorecords nor state-of-the-art models alone are conclusive, especially under extremely heterogeneous and complex environmental conditions, it is crucial to employ while both reconstructing and projecting past and future Brazilian biomes.

Before exploring the extent of Brazilian biome changes in the past (-4°C scenario, standing for the LGM) and in the future (+4°C scenario, standing for the end of the twenty-first century), I computed precipitation anomalies over Brazil and validated them with an updated compilation of 149 published reconstructions. Computed LGM anomalies showed decreased precipitation over equatorial (0°-10°S) Brazil. Over the SAMS region precipitation increased. In comparison with the compilation of published reconstructions, it was concluded that the computed climate anomalies over Brazil are reliable and valid as inputs for the potential vegetation model for the -4°C scenario.

These results are consistent with proxy reconstructions and suggest expansion of grassland in the southern Brazilian highlands and Amazon rainforest persistence through colder and drier conditions during the LGM. The results from the vegetation model reveal that the western and central Amazon forest were largely maintained during the LGM mainly due to negative temperature anomalies, while a decrease in past precipitation was responsible for Tropical evergreen forest to be substituted by Tropical seasonal forest and Savanna/Cerrado in its eastern portion. Results reaffirmed that changes in monsoon intensity cannot be used as the main driver for vegetational changes/stability across the Amazon biome, and that lower temperatures in combination with substantially lower CO_2 are important controlling factors during the LGM. In contrast, for the future +4°C scenario, biome shifts will mostly depend on future precipitation changes. Under future warming, the simulations show an expansion of Savanna/Cerrado, with projected coverage 10% higher than Present. Further, future warming will trigger a reduction of Amazon forest, Tropical seasonal forest and Caatinga (savannization or desertification). Results

suggest that the +4°C scenario will most probably impacts local biodiversity and regional climate.

3 INFLUENCE OF THE ATLANTIC MULTIDECADAL OSCILLATION ON SOUTH AMERICAN ATMOSPHERE DYNAMICS AND PRECIPITATION

3.1 Introduction

The Atlantic Multidecadal Oscillation (AMO) is a pattern of variability in the North Atlantic sea surface temperature (SST) with alternations between warm and cold conditions in most of the basin, that was first identified during the 1980s (FOLLAND et al, 1984). Majority of studies suggested the AMO to be induced by the Atlantic meridional overturning circulation (AMOC). Strong AMOC increased northward flowing of warm and salty surface water and leads to the warm AMO, which in turn changes the ocean surface density and surface winds, affecting the efficiency of deep-water formation and thus weakening meridional heat transport (BJERKNES, 1964; TANDON et al., 2015; DELWORTH et al., 2017; ZHANG et al., 2019). However, this role of the AMOC has been quite inconsistent among the models (YAN et al., 2019; KIM et al., 2021) and the AMO pattern is produced even in a model that does not include ocean circulation (CLEMENT et al.,2015).

Number of other studies challenge this conventional view of internally generated AMO, showing the link between AMO variability and combined solar activity and aerosols forcings (OTTERÅ et al., 2010; BOOTH et al., 2012; KNUDSEN et al., 2014; MURPHY et al., 2017). The most recent statistical analysis of instrumental records (WANG, X. et al, 2017; QIN et al., 2020) found the signatures of both internal and external forcings, thus, reconciling previous two hypotheses and suggesting that AMO index is not primarily driven by external forcings but simultaneously modulated by both internal and external forcings.

There are a variety of methods for constructing the AMO index (ENFIELD et al., 2001; TRENBERTH; SHEA, 2006; GUAN; NIGAM, 2009; KNIGHT, 2009; TING et al., 2009; YAN et al., 2019). Although these indices consider different aspects of the basin- or sub-basin scale variability they all capture large-scale multidecadal SST anomalies: (i) an anomalously warm North Atlantic characterizes the warm AMO phase; and (ii) an anomalously cold North Atlantic characterizes the cold AMO phase. The warm and cold phases swing with a

period of 60-90 years (SCHLESINGER; RAMANKUTTY, 1994; KNIGHT et al., 2006).

Regardless of the origins of the AMO, it is coherently linked to climate variations over many parts of the globe. It affects the Atlantic hurricane activity (ZHANG; DELWORTH, 2006), North American and European summer climate (SUTTON; HODSON, 2005), African Sahel rainfall (ZHANG; DELWORTH, 2006; WANG et al., 2012), Asian monsoon (LU et al., 2006; WANG et al., 2009; MIAO; JIANG, 2021), and summer rainfall over India (KRISHNAMURTHY; KRISHNAMURTHY, 2016). Over South America, important linkages with the AMO have been described for precipitation variability over northeastern Brazil (KNIGHT et al., 2006; KAYANO et al., 2016), surface air temperature of southern South America (KAYANO; SETZER, 2018) and, the dynamics of low-level jets (JONES; CARVALHO, 2018; CERÓN et al., 2020). More specifically, Jones and Carvalho (2018) analyzed the influence of the AMO on decadal-to-multidecadal variability of the South American low-level jet (SALLJ). They found a consistent pattern in which SALLJ days during cold AMO phases are associated with negative precipitation anomalies over northern Amazon and the Atlantic ITCZ. The results indicate a stronger influence of the cold AMO during austral winter (May-September) than during austral summer (December-February), while in the exit region of the SALLJ over southern Brazil, Uruguay and northern Argentina, precipitation increases.

Despite recent achievements, the mechanism by which the AMO influences regional precipitation over South America is not well understood. This is mostly due to the fact that observational data only contain two full cycles of the AMO. The prevailing view in the literature explains wet (dry) conditions in the SAMS domain by the southward (northward) shift of the Atlantic ITCZ and its influence on the SAMS and the South Atlantic Convergence Zone (SACZ) intensity. Both ITCZ and AMO are recognized to have strong imprints on the SAMS and the SACZ (GARREAUD et al., 2009; GARCIA; KAYANO, 2010). Instrumental records suggest that AMO phases are actually coupled with ITCZ north-south migrations (LEVINE et al., 2018).

An increasing number of records, summarized by Zhang et al. (2019), indicate that the AMO variability extends several millennia back in time. Recently, Lapointe et al. (2020) provided a reconstruction of the AMO for the past ~3 millennia, with unprecedented annual temporal resolution. By indirectly recording past precipitation changes, paleoclimate archives provide insights into the past behavior of the AMO. While there are records in which this multidecadal climate variability is not a persistent feature before 1750 AD (SAENGER et al., 2009), an increasing number of records, summarized by Zhang et al. (2019), indicate that the AMO variability extends several millennia back in time. Multiple paleoclimate records of the oxygen isotope composition ($\delta^{18}O$) within South America indicate periodicities in concordance with the AMO frequency of ~65 years and suggest the AMO signal to be imprinted in paleo precipitation proxy records. Multiple proxies within South America indicate that the AMO played a relevant role in modulating the South American Monsoon not only during LM (KNUDSEN et al., 2011; APAÉSTEGUI et al., 2014; BERNAL et al., 2016; NOVELLO et al., 2018) but also during the last deglaciation (CHIESSI et al., 2009).

Although several attempts have been made to extend instrumental data using terrestrial and marine proxies that indirectly record past behavior of the AMO (GRAY et al., 2004; MANN et al., 2009; WANG et al., 2017) much uncertainty still exists about the mechanism by which AMO influence both ITCZ and SAMS. Thus, the relationship of local and regional climate and to what extent they are directly influenced by AMO and how AMO phases impact precipitation isotopic ratios must rely on isotope-enabled models. Notwithstanding the continuous improvement of climate models over the past two decades (MEEHL et al., 2007; TAYLOR et al., 2012; EYRING et al., 2016), fully coupled models still show a large spread of the anomalies in regional precipitation associated to the AMO (KNIGHT et al., 2009; MURPHY et al., 2017; RUIZ-BARRADAS et al, 2013). They generaly lack in decadal to multidecadal variability (AULT et al., 2012), or underestimate their magnitude and fail to produce spatial patterns that match the observed signal (HAN et al., 2016).

The objective of this research is to determine the atmospheric response to the AMO and investigate the influence of the AMO on (sub)tropical South American regional precipitation and atmospheric circulation. The methodological approach taken in this study isolate the atmospheric response to the AMO using an Earth System model. By employing simplified approach which excludes the full range of feedbacks between different components of the climate system, as well as avoids the introduction of biases related to the way the atmosphere is coupled to land or ocean, that are present in fully coupled models (KOSTER et al., 2004; MUELLER; SENEVIRATNE, 2014; MYSTAKIDIS et al., 2017; HAWCROFT et al., 2017; HODSON et al, 2022).

3.2 Data and methods

3.2.1 Study area

This research is focused on South America, where the main driver of the difference in precipitation between winter dry and summer wet season is South America Monsoon System (SAMS) (VERA et al., 2006; GARREAUD et al., 2009). Two main precipitation features of SAMS are the ITCZ, an equatorial cloud band resulting from the low-level convergence of mass and moisture, and the SACZ, a northwest–southeast-oriented cloud band that connects the southern Amazon region with the western portion of the subtropical South Atlantic (HOREL et al., 1989; MARENGO et al., 2012).

3.2.2 iCESM model setup

Experiments for this study were carried with a water isotope-enabled version of the Community Earth System Model version 1.2 (iCESM1.2). The iCESM1.2 has active atmosphere, land, ocean, river transport, and sea ice component models linked through a coupler, and also simulates global variations in water isotopic ratios in the atmosphere, land, ocean, and sea ice. The ability of this model to simulate present and past δ18Op patterns has been documented previously (OTTO-BLIESNER et al. 2016; ZHU et al., 2017; HE et al., 2021). The atmospheric component of iCESM1.2, the isotope-enabled Community Atmosphere Model version 5 (iCAM5.3) (NUSBAUMER et al., 2017), is based

on the original, non-isotope enabled CAM5 (NEALE et al., 2010). It is coupled with the interactive Community Land Model version 4 (CLM4; OLESON et al., 2010) while sea surface temperature (SST) and sea ice concentrations (SICs) were prescribed. The model was configured to use a computational grid of 1.9° latitude × 2.5° longitude and 30 vertical levels from the surface to ~3.5 hPa.

3.2.3 Experiments

For this study, three experiments were conducted.

The list of experiments performed with iCESM1.2, as well as the initialization procedure and the datasets for sea-ice concentrations and SST, can be found in Table 3.1. All experiments were initialized from pre-industrial conditions, where the values for greenhouse gasses, aerosols, ozone, and solar irradiance were fixed at the year 1850.

Table 3.1 - Description of the experiments performed with the water isotope-enabled version of the Community Earth System Model version 1 (iCESM1.2).

Experiment	Initialization	Sea-surface temperatures (SST) and sea-ice concentrations (SIC)	Simulation
CONTROL	Pre-industrial conditions	HadISST dataset	One ensemble member / 30 yr
CAMO	Pre-industrial conditions	Cold SST anomaly superimposed on the HadISST dataset	Three ensemble members / 50 yr
WAMO	Pre-industrial conditions	Warm SST anomaly superimposed on the HadISST dataset	Three ensemble members / 50 yr

The control experiment (CONTROL) is with prescribed monthly-varying sea-surface temperatures and sea-ice concentrations (SST/SIC) from the Hadley Centre Global Sea Ice and Sea Surface Temperature (HadISST) dataset (RAYNER et al., 2003), while the values for greenhouse gases, aerosols, ozone, and solar irradiance were fixed at the year 1850 (pre-industrial level). The CONTROL simulation was integrated for 30 years and the first 10 years

were discarded as model spin-up. In further two experiments the annual cycle of the SST anomalies, representative of the cold (warm) SST anomaly, is superimposed on the prescribed climatology SST/SIC used in the control run.

The idealized cold and warm SST patterns were computed over time periods with opposite AMO index following Trenberth and Shea (2006) methodology. Both experiments are run as an ensemble of three 50-year long simulations generated with the same model but different initial conditions produced by slight variations in initial atmospheric conditions (Table 3.1). In order to be on the safe side of soil spin-up, for experiments spin-up period was extended on 20 years (YANG et al., 1995). The AMO index of Trenberth and Shea (2006) was adopted because it isolates the Atlantic variability from global warming and tropical influences.

The superimposed SST anomalies come from a composite analysis of the HadSST2 dataset (RAYNER et al., 2006), after linear detrending to remove the long-term influence. The cold AMO phase comprises the period between 1850 and 1928 and between 1964 and 1995, while the warm AMO phase includes the period between 1928 and 1964 and between 1995 and 2012. Thus, the two experiments, cold AMO (CAMO) and warm AMO (WAMO), only differ by the prescribed SST (Figure 3.1).

Figure 3.1 - Computed annual sea surface temperature (SST) difference between the warm Atlantic Multidecadal Oscillation (WAMO) and the cold Atlantic Multidecadal Oscillation (CAMO) phases (°C). Phases are defined based on AMO index (Trenberth and Shea, 2006) using the HadISST dataset for the period 1870–2015.

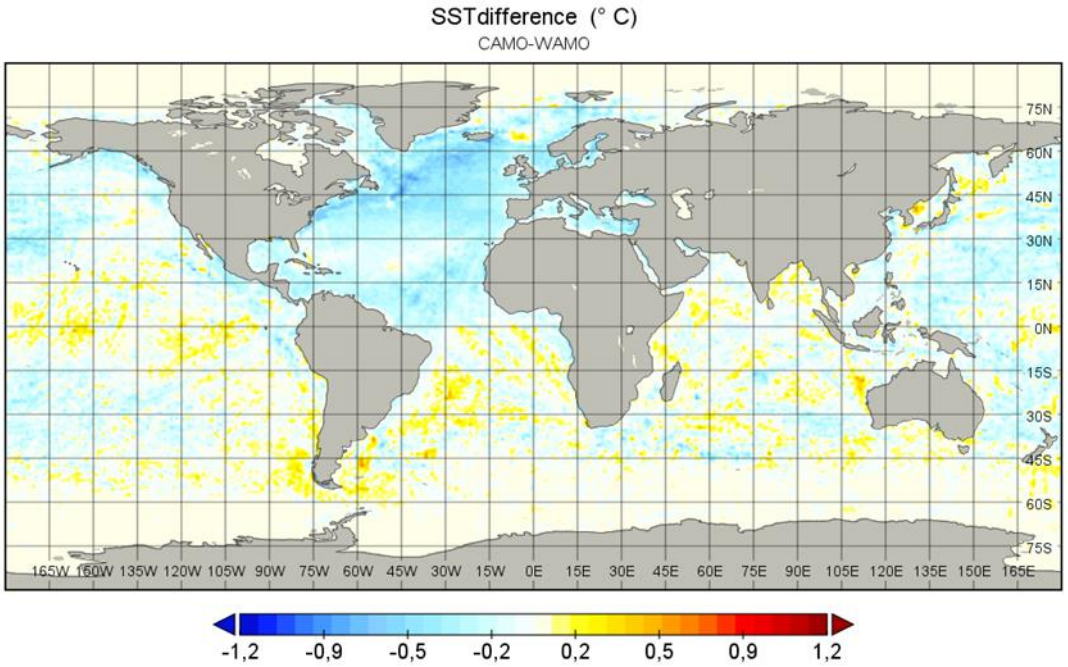

3.2.4 Climate variables and methods used in analyses

The climate variables used to identify the main differences in CAMO and WAMO simulations include: precipitation, meridional and zonal winds, and vertical velocity. Thus, the effects of AMO-related SST over South American climate were evaluated through the differences between CAMO and WAMO experiments for precipitation (seasonal and annual mean), atmospheric circulation at 850 hPa (seasonal mean) and 200 hPa (austral summer mean), 200 hPa divergence (annual), and zonal and meridional vertical velocity profiles.

Additionally, the upper-level divergence simulated by CAMO and WAMO experiments were compared with those obtained from composite analyses for both AMO phases using data derived from the National Oceanic and Atmospheric Administration / Cooperative Institute for Research in Environmental Sciences / U.S. Department of Energy (NOAA/CIRES/DOE) third version of the 20th Century Reanalysis data (20CRv3) (SLIVINSKI et al., 2019).

This comparison is important to detect aspects of the AMO-driven upper-level convective changes captured in presented simulations.

This study also aimed to analyze the influence of the SSTs in both AMO phases on the atmospheric circulation cells. In this study, the meridional mean of vertical pressure velocity between 0° and 15°S represents the Walker cell, while the zonal mean of vertical pressure velocity between 80°W and 30°W represents the Hadley cell. The Hadley cell intensity changes between CAMO and WAMO experiments were calculated as the mean maximum value of the zonal-mean meridional stream function between 900 and 200 hPa (NGUYEN et al., 2013). Finally changes in ITCZ position are analyzed through a zonal mean precipitation diagram.

3.3 Results

3.3.1 Changes in precipitation

The spatial distributions of changes in precipitation between CAMO and WAMO are shown in Figure 3.2. The annual mean shows increased precipitation during the cold AMO phase, mainly in the Amazon and northeastern Brazil (Figure 3.2e). In contrast, the model simulates precipitation reduction in most northern regions of South America. Figure 3.2 also shows that the atmospheric response to the prescribed SST anomalies is seasonally dependent. During austral summer (December to February-DJF), the precipitation over most of South America is increased in the CAMO experiment, with significant differences in the western Amazon (0°–10°S, 55°–75°W), northeastern Brazil (1°–18°S, 35°–47°W) and the Andes (Figure 3.2a). In austral autumn (March to May-MAM), wetter conditions remain over the northeastern Amazon basin and in the northernmost portion of northeastern Brazil, while over most of South America precipitation decreased (Figure 3.2b). On the other hand, during the winter season (June to August-JJA) the model suggests significantly wetter conditions over most of northern and central-southern South America in CAMO and drier conditions in a small eastern sector of northeastern Brazil (Figure 3.2c). Wetter conditions over northeastern Brazil and almost the entire Andes and Amazonia, and drier conditions over southeastern South America occur during austral

spring (September to November-SON) (Figure 3.2d). Significant differences in the amount of precipitation over the Atlantic Ocean can also be observed. There are significant differences in the amount of precipitation over the equatorial Atlantic Ocean for all seasons, with the largest increase occurring to the south of the equator close to northeastern Brazil, and the largest reduction to the north of the equator over the western and central Atlantic Ocean (Figure 3.2). These anomalies are likely associated with changes in the Atlantic ITCZ and further analyses on the ITCZ position and intensity are made and shown later in this section.

Figure 3.2 - Seasonal precipitation differences between the cold Atlantic Multidecadal Oscillation (CAMO) and the warm Atlantic Multidecadal Oscillation (WAMO) experiments (mm/day) in (a) December-February (DJF), (b) March-May (MAM), (c) June-August (JJA), and (d) September-November (SON) and (e) annual mean. Red (blue) shaded areas correspond to drier (wetter) conditions; grid points with statistically significant difference according to Student's t test with confidence level of 95% are marked with dots.

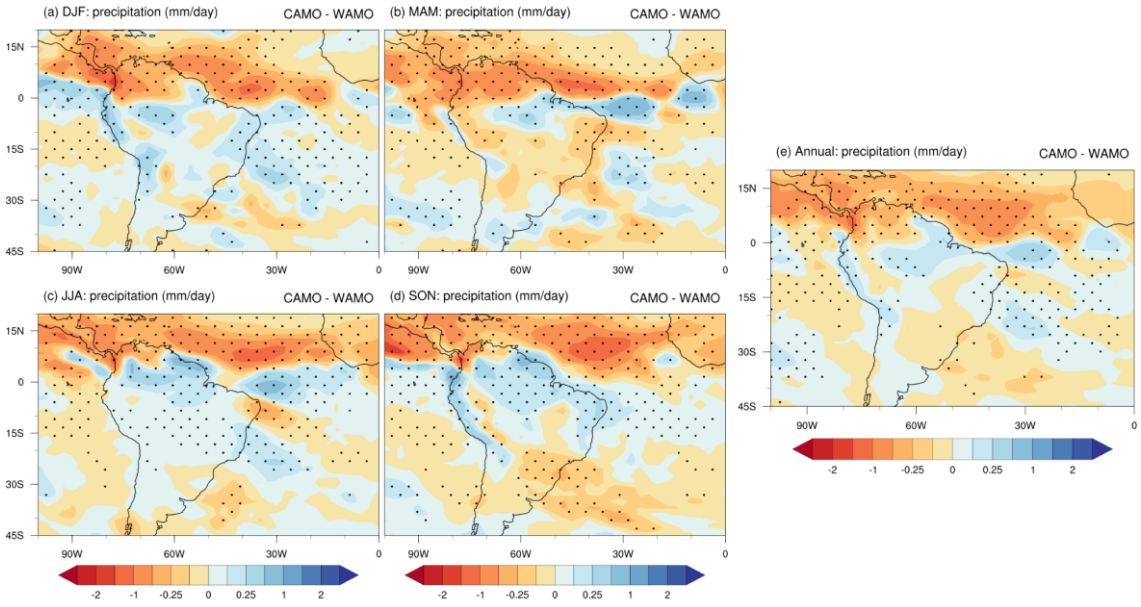

To understand the dynamical mechanisms that caused the changes in precipitation, the austral summer upper-level and lower-troposphere circulation (Figure 3.3 and Figure 3.4) was analyzed. The position of the upper-level anticyclonic circulation, known as the Bolivian High, is the same for both CAMO

and WAMO experiments, but the wind circulation is slightly intensified in WAMO (Figure 3.3b,c) in comparison with CAMO (Figure 3.3a,c) experiment, which enhanced the westerlies (200 hPa) over the North Atlantic Ocean, between the equator and 20N. Additionally, differences between CAMO and WAMO (Figure 3.3c) show that the subtropical jet stream is intensified in WAMO experiment, in relation to CAMO.

Figure 3.3 - Streamlines and wind intensity (m/s) at 200 hPa for December–February (DJF) for the cold Atlantic Multidecadal Oscillation (CAMO) (a) and the warm Atlantic Multidecadal Oscillation (WAMO) (b) experiments, as well as for the differences between CAMO and WAMO (c). In (c), only statistically significant differences calculated using Student's t test with a confidence level of 95% are shown.

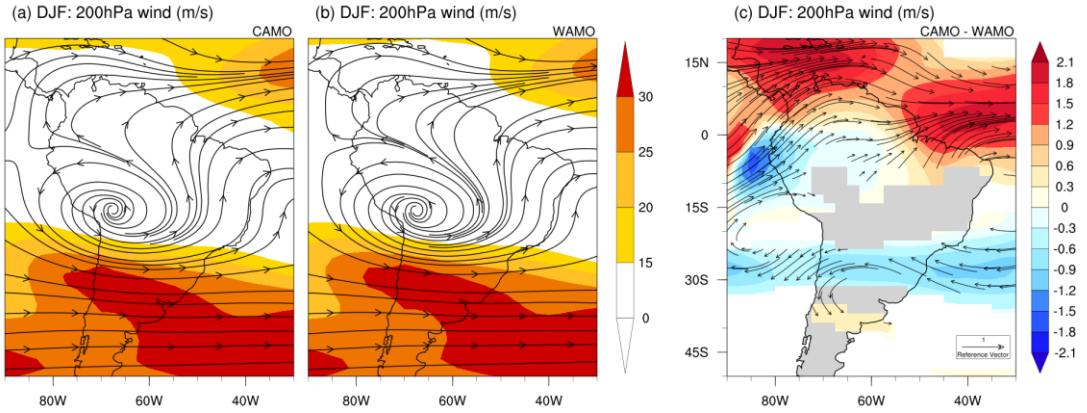

Comparing the 850 hPa wind field anomalies between both AMO phases (Figure 3.4), an increased easterly flow reaching 10° S is noted for CAMO. A stronger low-level easterly flow, over most of the Amazon, brings more moisture to the mainland and correlates with the increase in precipitation over the Amazon and coastal northeastern Brazil. These anomalies are present in all months, but are stronger in JJA and SON (Figure 3.4c,d). There are also slightly stronger northerly low-level winds in the Chaco low region in SON (Figure 3.4d). The differences in the SALLJ are only significant in JJA and SON, and show a weakening in CAMO, reducing the moisture flow from the Amazon to southeastern South America.

Figure 3.4 - Seasonal wind vectors and intensity at 850 hPa (m/s) for the differences between the cold Atlantic Multidecadal Oscillation (CAMO) and the warm Atlantic Multidecadal Oscillation (WAMO) phases in (a) December–February (DJF), (b) March–May (MAM), (c) June–August (JJA), and (d) September–November (SON). Only statistically significant differences calculated using Student's t test with confidence level of 95% are shown.

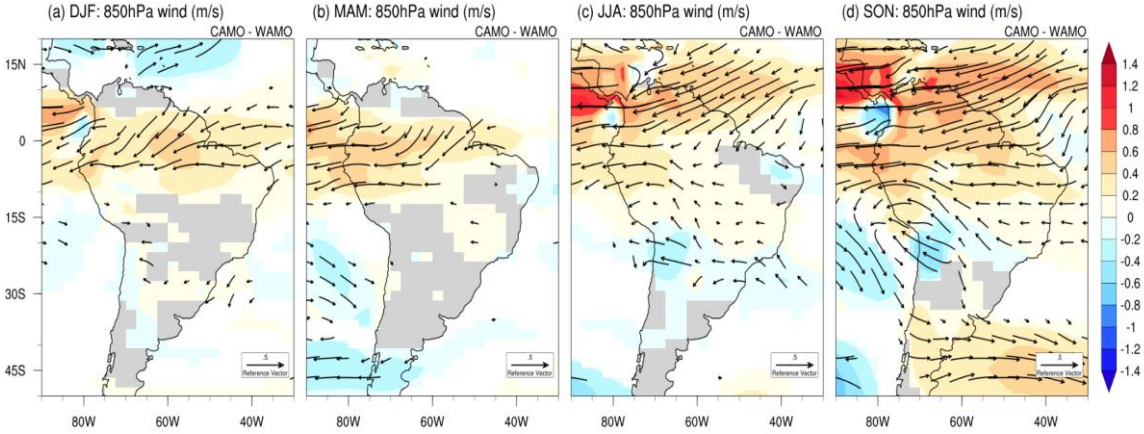

As ascending vertical motion at upper levels (200 hPa) is associated with important elements of the SAMS such as SACZ, the Bolivian High circulation and northeastern Brazil (LENTERS; COOK, 1997), the 200 hPa divergence fields for CAMO and WAMO are compared and their differences with the 20CRv3 reanalysis data (Figure 3.5) are analised. The cold AMO phase is characterized by lower divergence over the Amazon and the equatorial North Atlantic and higher divergence over northeastern Brazil, in relation to the warm AMO phase (Figure 3.5a–c). Although the model has some deficiencies in representing the intensity of the upper-level convergence change between AMO phases in the Amazon, the simulated annual mean is in good agreement with reanalysis profiles, and the model reproduces the main features of the divergent circulation over South America, associated with both the ITCZ and the SACZ convection. The differences between CAMO and WAMO show a dipole of lower/higher divergence over the tropical Atlantic, which is in agreement with the 20CRv3 data, and reflects the large SSTs anomalies over the region (Figure 3.2).

Figure 3.5 - Divergence at 200 hPa for the cold Atlantic Multidecadal Oscillation (CAMO) and the warm Atlantic Multidecadal Oscillation (WAMO) phases, as well as the differences between both phases from reanalysis (a-c) 20CRv3 and (d-f) iCESM model. Stippling areas represent statistically significant (Student's t test at 95%) composites (a, b) and differences (c, f).

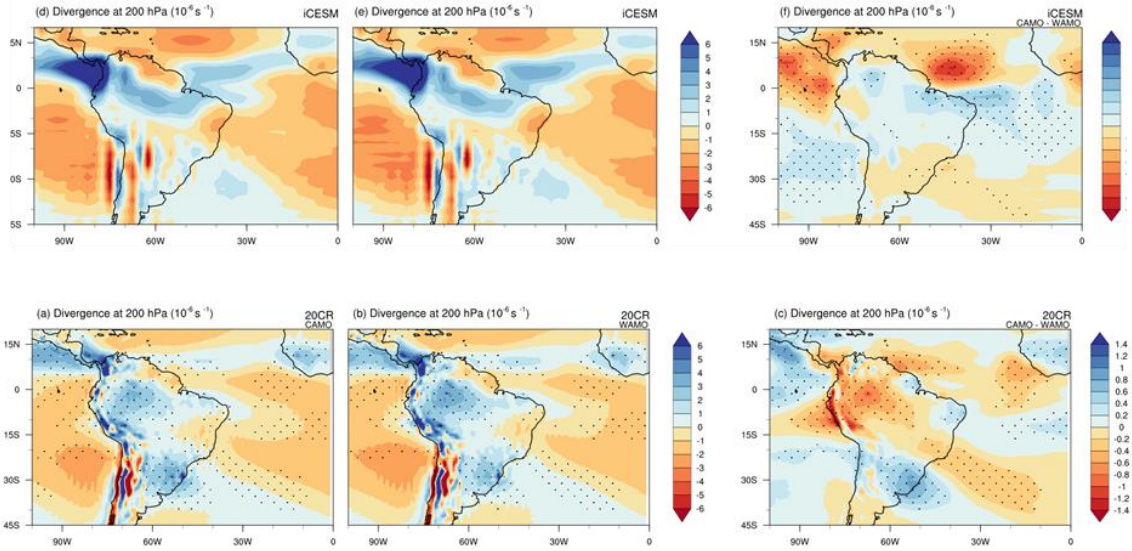

3.3.2 ITCZ and Atmospheric Circulation Cells

To identify changes in the Atlantic ITCZ, the annual cycle of precipitation over the Atlantic (15° N–15° S) averaged over 40° W–0° for CAMO and WAMO (Figure 3.6a, c) was analyzed, and the differences between these experiments averaged over the whole longitudinal band (Figure 3.6b) and over 30° W, where the anomaly was the highest (Figure 3.6d). Although clear shifts in the mean position of the precipitation band (Figure 3.6a, c) cannot be observed, distinct positive precipitation anomalies (CAMO-WAMO) are simulated from February to July between the equator and 10° S (highlighted by the blue rectangle on Figure 3.6b, d). It is worth noting the negative anomalies north and south of the positive anomaly field. It is also found that precipitation weakens (intensifies) in the ITCZ core region during the CAMO (WAMO) after July (highlighted by the pink ellipse in Figure 3.6a, c), and their difference (highlighted by the pink rectangle in Figure 3.6b, d).

Figure 3.6 - Annual cycle of precipitation for the cold Atlantic Multidecadal Oscillation (CAMO) (a) and the warm Atlantic Multidecadal Oscillation (WAMO) (c) experiments averaged over 40° W-0°, and their differences averaged over the whole longitudinal band (b) of the Atlantic Intertropical Convergence Zone (ITCZ) section (e) (15° N-15° S; 40° W-0°) and only at 30° W (d), where the precipitation anomaly was the highest.

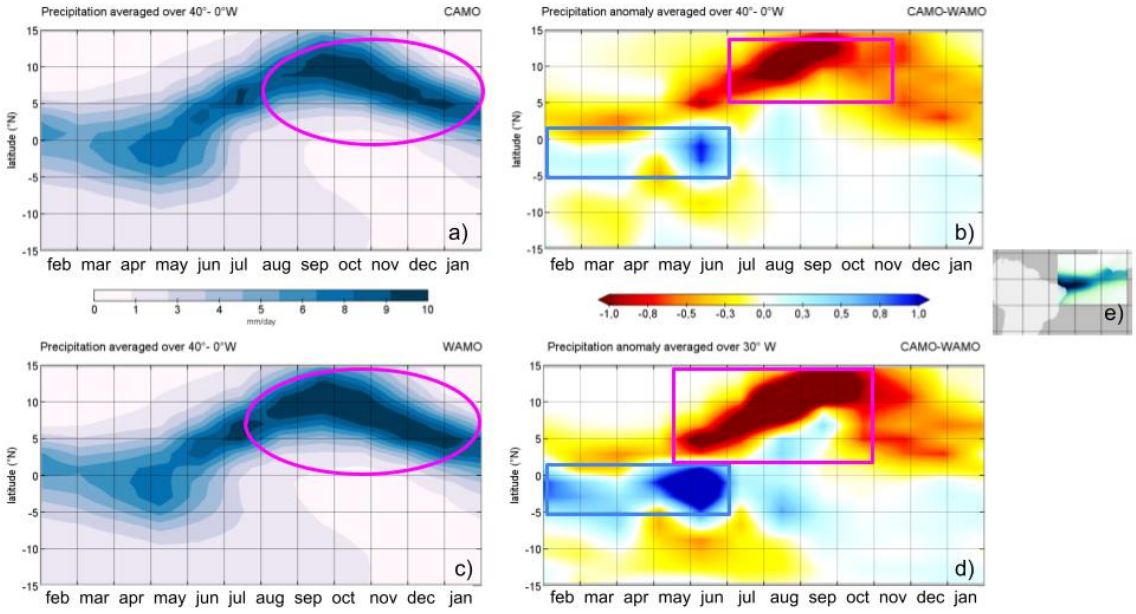

The zonal mean meridional streamfunction for both CAMO and WAMO experiments (Figure 3.7) show negative and positive cells north and south of the equator, respectively, which represents the Northern and Southern Hemisphere (NH and SH) Hadley cells. In the intersection of these cells lies the ITCZ (black line near the equator), which is located a few degrees north of the equator in both experiments. So, CAMO and WAMO experiments did not show substantial differences in the mean position of the Hadley cells and the ITCZ. However, the Hadley cell was stronger (weaker) in the NH (SH) for the CAMO experiment in relation to the WAMO experiment (Table 3.2).

Figure 3.7 - Climatological Hadley cell defined as the zonal mean stream function ψ (109 kg/s) for (a) CAMO, (b) WAMO and the differences between them (c). Red and blue contours (solid and dashed lines) denote clockwise and anti-clockwise mass stream functions. Black lines represent the zero-contour stream function. Stippled areas in (c) represent statistically significant (Student's t test at 95%) differences.

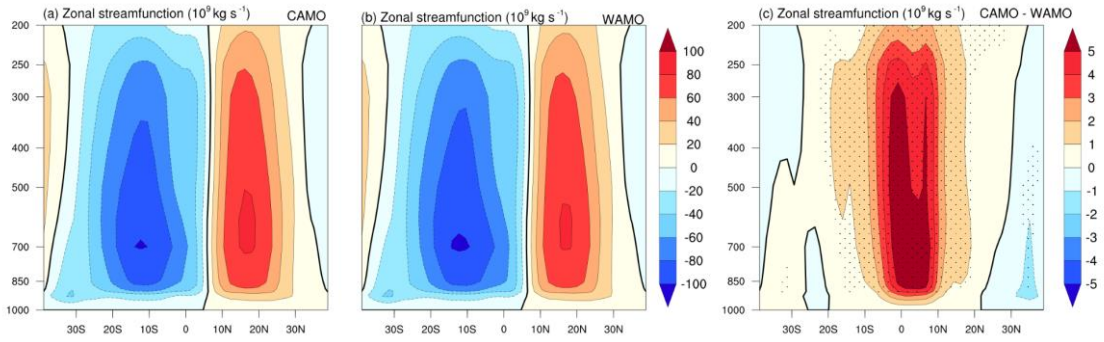

Table 3.2 - Mean intensity of the Northern Hemisphere (NH) and the Southern Hemisphere (HS) Hadley cells calculated in terms of vertical-mean (900–200 hPa) and zonal-mean meridional stream function ψ (109 kg/s) for CAMO and WAMO experiments, and the differences between them.

	CAMO (10^9 kg/s)	WAMO (10^9 kg/s)	CAMO - WAMO (10^9 kg/s)
NH	66.83	65.49	1.34
SH	-75.25	-78.23	2.98

For the vertical profile that represents the Hadley and Walker cells, it is noteworthy that both CAMO and WAMO experiments had the same spatial structure as that of the CONTROL run (Figure A.1 and Figure A.2).

The ascending branch of the section of the Atlantic Hadley cell, which is situated between the 5° N and 15° S and favors convective activity over this region (Figure 3.8) was analised. The difference (CAMO–WAMO) in vertical velocity at the pressure coordinates shows a dipole of negative/positive values south/north of the equator. This dipole is present in all seasons, with the highest positive anomalies being centered at 4° N in MAM, indicating a stronger inter-hemispheric atmospheric circulation. In Figure 3.8, positive anomalies can also be observed north of the equator, which are more pronounced in MAM.

Figure 3.8 - Difference between CAMO and WAMO of vertical pressure velocity (omega; hPa/s) representing the regional Hadley circulation: the latitude-height Section 15° N-15° S, zonally averaged over 80° W-30° W, for (a) December-February (DJF), (b) March-May (MAM), (c) June-August (JJA), and (d) September-November (SON). Stippled areas represent statistically significant (Student's t test at 95%) differences.

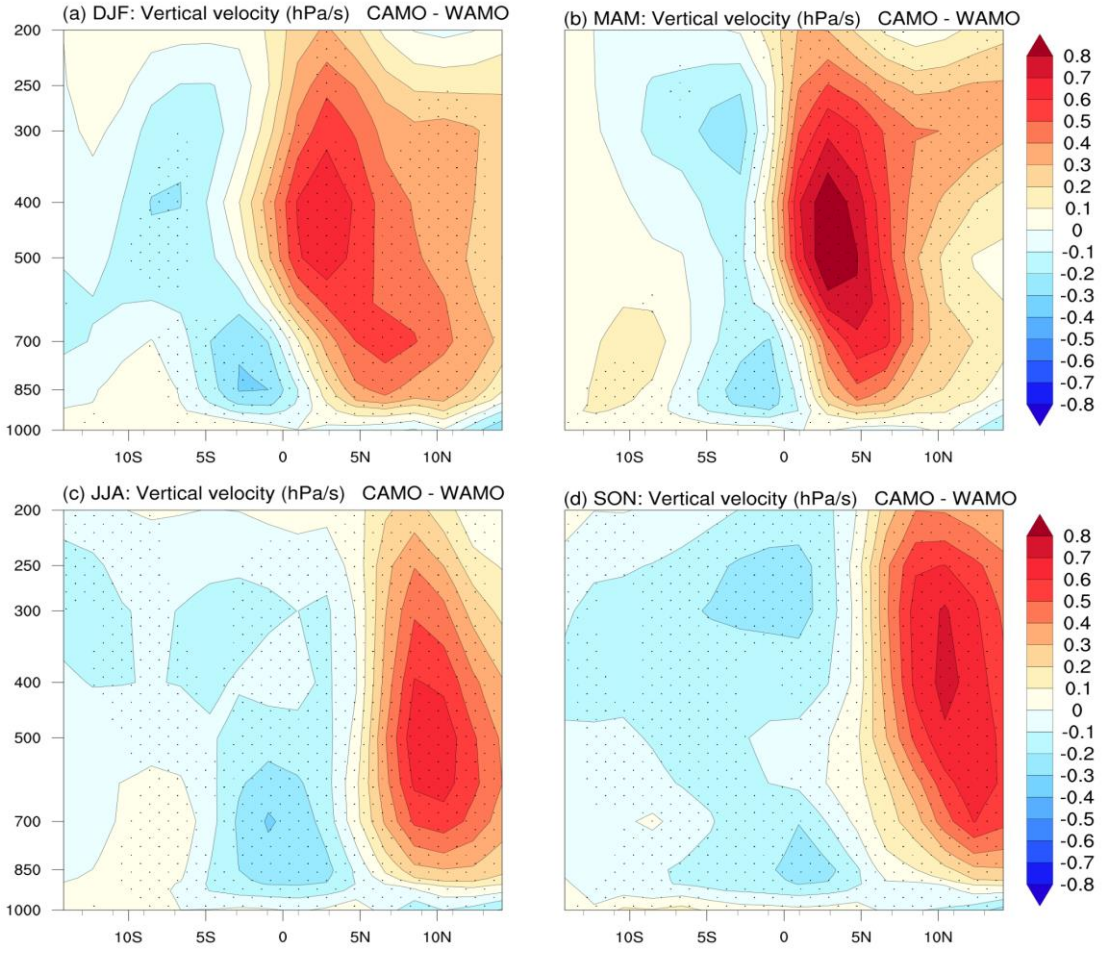

Simultaneously, changes in Walker circulation in which the ascending branch that is situated right over Amazonia, between the longitudes 80°W–40°W, and the descending motion occurs over longitudes 40°W–20°W, (Figure A.2) were found. During the cold AMO phase ascending motion is intensified (Figure 3.9a, b). In DJF and MAM seasons, this negative anomaly has distinct positive anomalies east and west of it, suggesting also change in the ascending branch position. In SON the opposite is observed (i.e., significant weakening of the ascending branch).

Figure 3.9 – Difference between CAMO and WAMO of vertical pressure velocity (omega; hPa/s) meridionally averaged over 0°-15°S, representing the regional Walker circulation for (a) December-February (DJF), (b) March-May (MAM), (c) June-August (JJA), and (d) September–November (SON). Stippled areas represent statistically significant (Student's t test at 95%) differences.

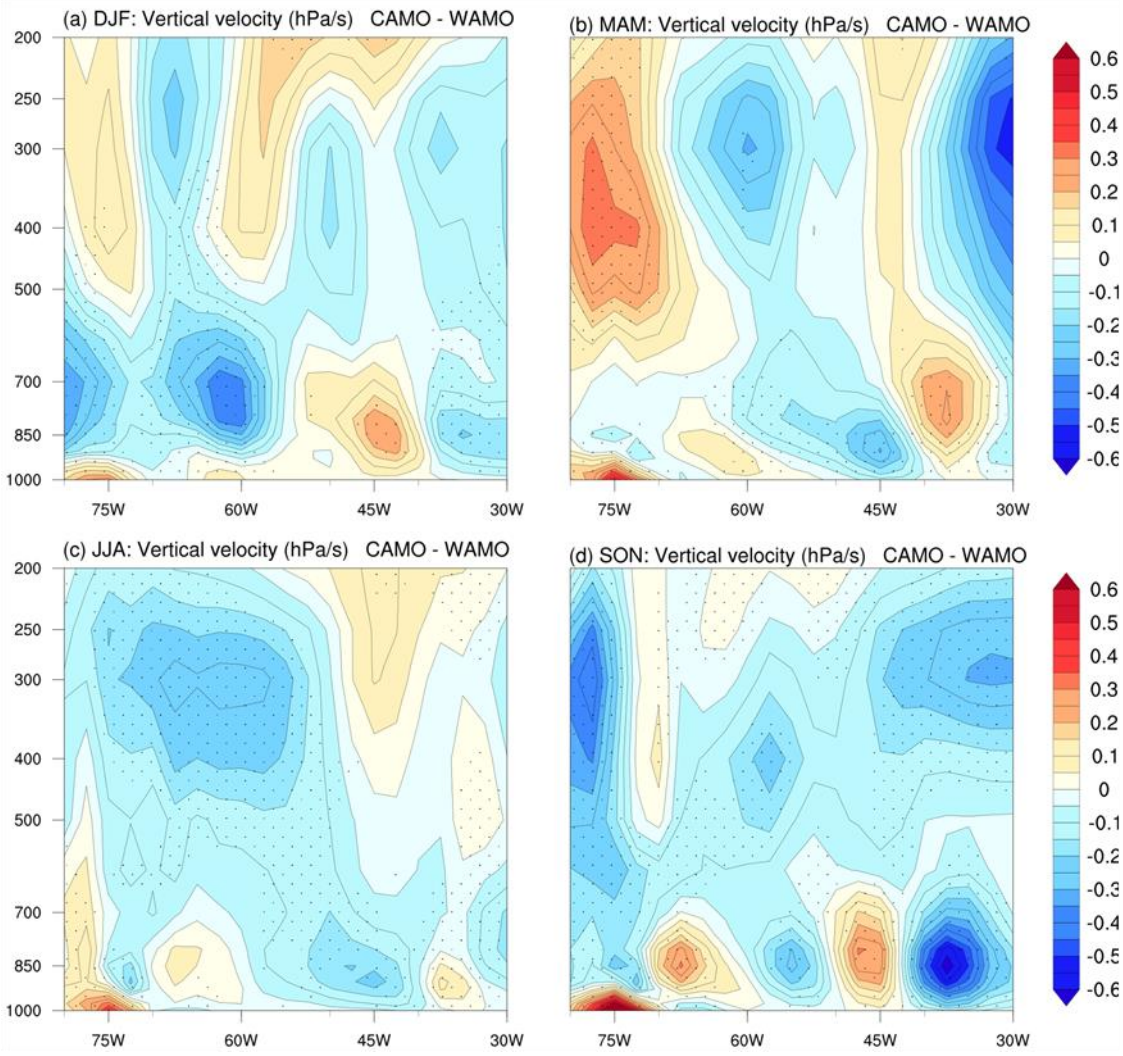

3.4 Discussion

This section explores the mechanisms by which the AMO influences regional precipitation patterns over South America. The idealized simulations show the AMO as an important driver of changes in precipitation over tropical South America. Mean annual precipitation anomalies indicate significant reduction over the northern equatorial Atlantic and in most regions of northern South America, as well as significant increase in the Amazon and northeastern Brazil

during the cold AMO phase (Figure 3.2). Although mean annual precipitation differences are generally consistent with the findings of previous studies which suggest that cold AMO force the ITCZ to shift meridionally (KNIGHT et al., 2006; YOON; ZENG, 2010; KAYANO et al., 2016), the spatial patterns of precipitation vary seasonally.

Amazonian precipitation changes in the simulations are in agreement with those shown by Yoon and Zeng (2010). The authors observed that warming (cooling) of the North Atlantic induced dry (wet) conditions over the Amazon basin. Presented results also corroborate their observation that the North Atlantic influence becomes significant over the southern edge of the Amazon basin during the dry season (JJA and SON). These precipitation changes are related to the weakening of SALLJ in JJA and SON, thus reducing the moisture flow from the Amazon to southeastern South America in the cold AMO phase. This differs from the findings presented in Jones and Carvalho (2018). More detailed analysis is necessary to determine the influence of AMO on SALLJ changes. On the other hand, results suggest the association between AMO and the Choco low-level jet (CJ) and Caribbean low-level jet (CLLJ) intensity. The results provide further support for the Cerón et al. (2020) hypothesis that in the cold (warm) AMO phase CJ is weakened (intensified) and CLLJ is intensified (weakened) (Figure 3.4d).

For northeastern Brazil, previous studies (KNIGHT et al., 2006; KAYANO et al., 2016) found an increased (decreased) precipitation induced by cold (warm) AMO in wet season (MAM) due to ITCZ shifting to a more southerly (northerly) position. In contrast, the model simulation showed an increase in precipitation over northernmost northeastern Brazil and over the adjacent tropical South Atlantic during the CAMO (WAMO) phase, but no clear wet (dry) signal over northeastern Brazil (Figure 3.2e).

Results indicate that precipitation anomalies over South America during AMO phases are mainly related to changes in the Hadley cell and subordinately to changes in the Walker cell (Figures 3.7-3.9). The global Hadley circulation was strengthened in the NH and weakened in the SH in a cold AMO phase (Table

3.2). This corroborates with previous studies that showed extratropical climate change as an important factor in modulation of Hadley and Walker circulation (FRIERSON et al., 2012; KANG et al., 2020). In addition, the findings are consistent with Liu et al. (2020) who identified the multidecadal variability in the hemispheric Hadley circulation strength, where the intensification in one hemisphere happens together with the weakening in the other, resulting in an interhemispheric seesaw in Hadley circulation strength as a response to AMO signal.

Here is also tested the hypothesis that the AMO phases force the ITCZ to shift meridionally, impacting precipitation over South America as suggested by previous studies (KNIGHT et al., 2006, TING et al., 2011). Recently, it was suggested that the ITCZ expansion/contraction may also drive tropical precipitation changes, potentially explaining diverging records (YAN et al., 2015; WODZICKI; RAPP, 2016; UTIDA et al., 2019; ASMERON et al., 2020; CHIESSI et al., 2021). To get further insight, focus is put on the Atlantic ITCZ position and strength. For the Atlantic ITCZ position, the results do not show a robust meridional shift of ITCZ. The zonal mean precipitation for both AMO phases did not present significant differences in the position of the maximum precipitation (Figure 3.6). On the other hand, the simulations show significant differences in the Atlantic ITCZ strength, which are evidenced by the positive (negative) precipitation anomalies (CAMO minus WAMO) to the south (north) of the equator. Moreover, the equator-symmetric changes present in precipitation fields have a remarkable agreement with the changes shown in Knight et al. (2006).

Atlantic ITCZ strength changes are associated with the Atlantic Hadley cell anomalies (Figure 3.8), with persistent negative vertical velocity anomalies in the low and middle tropospheric levels between 15°N and 5°S in all seasons during the cold AMO phases. Simultaneously, strengthening and eastward shifting of the Walker cell is observed, with the difference being the most pronounced in DJF and MAM.

The analyses also suggest that the ITCZ response to the AMO is regionally and seasonally dependent. Thus, these responses could be masked in analyses focusing on zonal and annual mean ITCZ shifts, as shown in Mamalakis et al. (2021). Precipitation anomalies (Figure 3.6b, d) suggest that the core region of ITCZ strengthens (weakens) from February to July, while from July to November the core region weakens (strengthens) during the cold (warm) AMO. This precipitation reduction over the ITCZ in the winter season during cold AMO accords with Jones and Carvalho, (2018). Likewise, Zhou et al. (2020) showed that decadal SST variability drives changes in Pacific ITCZ width, highlighting distinct ITCZ changes at seasonal and annual mean timescales.

It is interesting to note that the Atlantic ITCZ core region is seasonally dependent such that it is located in the NH most months of the year except during austral autumn when it is in the SH (CHIANG et al., 2002). Although the Atlantic ITCZ has a seasonal asymmetry, the AMO has a nearly symmetric effect in modulating the Atlantic ITCZ-related precipitation. This study has identified that during the cold AMO phase the ascending branch of the Walker circulation placed over western Amazonia is intensified and shifted eastward.

A recent reconstruction of surface seawater stable oxygen isotopes from the western tropical South Atlantic impacted by the ITCZ, a parameter that is related to changes in sea surface salinity, indicates a freshening trend from the 1940s to the 1970s (but mainly comprised between the 1960s and the 1970s). The freshening trend was attributed by the authors to a change in the ITCZ (PEREIRA et al., 2022). This change would be synchronous with the transition from the warm to the cold AMO, agreeing with the simulations (Figure 3.2e). However, instead of a southward migration of the ITCZ (PEREIRA et al., 2022), results presented here suggest that the observed decline in sea surface salinity in the western tropical South Atlantic was produced by a strengthening of the ITCZ during the cold AMO phase from February to July (Figure 3.6).

Presented results are also in line with Roldán-Gómez et al. (2022) who showed that ITCZ shifts in the Atlantic during the last millennium were only subordinately impacted by internal variability, but mainly driven by external

forcing. As the results of our study suggest, ITCZ expansion/contraction or changes in its strength are sufficient to produce observed AMO related signals even in the absence of marked changes in the ITCZ position. This implies that ITCZ shifts driven by external forcings (like the large number of strong volcanic eruptions during the Little Ice Age; TEJEDOR et al., 2021) and AMO induced ITCZ expansion/contraction contribute jointly to precipitation changes over South America during the last millennium (APAÉSTEGUI et al., 2014; NOVELLO et al., 2018).

3.5 Conclusions

This chapter shows analysis of the dynamical processes involved in South American precipitation changes in response to AMO phases. Unlike most earlier studies that suggest a displacement of the ITCZ, the results do not show robust changes in its zonal mean position between the different AMO phases. The results suggest that during the cold AMO phase, the NH Hadley circulation was stronger, while the SH Hadley circulation was weaker, in agreement with an interhemispheric seesaw in Hadley circulation strength. It is also found that the section of the Atlantic Hadley cell is marked by a stronger upward air component south of the equator during the cold AMO phase, which is consistent with distinct positive precipitation anomalies simulated from February to July south of the equator under the Atlantic ITCZ. Thus, the simulated precipitation anomalies can be interpreted as changes in the Atlantic ITCZ core strength, where in the cold (warm) AMO phase the core region of the ITCZ strengthens (weakens) from February to July, while from July to November the core region weakens (strengthens).

Presented results stress the importance of acknowledging the dynamics of season- and regional-dependent ITCZ responses as they are sufficient to produce observed AMO related signals even in the absence of marked changes in the ITCZ position. In addition, the results provide a better understanding of the physical basis of the AMO-related changes in South American precipitation. This understanding will serve as a base for the exploration of simulated water isotopes, with the aim to investigate the isotopic fingerprint of AMO and

precipitation variability found in paleoclimate reconstructions over South America.

4 ISOTOPIC FINGERPRINT OF THE ATLANTIC MULTIDECADAL OSCILLATION OVER SOUTH AMERICA AND ITS RELATION TO THE LITTLE ICE AGE

The previous section has shown the influence of the Atlantic Multidecadal Oscillation on South American atmosphere dynamics and precipitation. The following part describes in greater detail the effects of the AMO on simulated oxygen isotopic composition of precipitation over South America.

4.1 Introduction

The Atlantic Multidecadal Oscillation (AMO) is a mode of observed variability in North Atlantic sea surface temperatures (SST) that consists of an alternation between warm and cold SST anomalies (FOLLAND et al., 1984; KUSHNIR, 1994; SCHLESINGER; RAMANKUTTY, 1994). The AMO has a global-scale impact on climate that is well summarized in Zhang et al. (2019). Studies that analyzed the AMO impacts over South America found linkages with surface air temperature (KAYANO; SETZER, 2018), low-level jets (JONES; CARVALHO, 2018; CERÓN et al., 2020), precipitation over northeastern Brazil (KNIGHT et al., 2006; KAYANO et al., 2016) and southeastern South America (SEAGER et al., 2010). For northeastern Brazil, previous studies (KNIGHT et al., 2006; KAYANO et al., 2016) found increased (decreased) precipitation induced by cold (warm) AMO during the wet season, i.e., March-May (MAM). Instrumental records suggest that AMO phases are coupled with the Intertropical Convergence Zone (ITCZ) position (Levine et al., 2018).

Modeling studies also recognize changes in the ITCZ position as an important mechanism by which the AMO influences precipitation (KNIGHT et al., 2006, TING et al., 2011, LEVINE et al., 2018). Contrary to expectations, results from previous section (see also MAKSIC et al., 2022) show that AMO-related precipitation anomalies over northeastern South America are mainly related to changes in the Atlantic ITCZ core strength, instead of changes in its position. In the cold (warm) AMO phase, the core ITCZ region strengthens (weakens) from February to July, while from July to November the core region weakens (strengthens). Results also suggest an interhemispheric seesaw in the section

of the Atlantic Hadley cell, where a stronger upward atmospheric motion south of the equator marks the cold AMO phase. This is consistent with Liu et al. (2020) who suggested that the multidecadal variability in the hemispheric Hadley circulation strength is a response to the AMO, where the intensification in one hemisphere occurs synchronously with the weakening in the other. Nevertheless, uncertainties still exist about the mechanisms by which the AMO influences regional precipitation over South America, mostly because instrumental data contain, in the best case, two full cycles of the AMO (~130 years).

Several attempts have been made to extend instrumental data using terrestrial and marine proxies that indirectly record the past behavior of the AMO (GRAY et al., 2004; MANN et al., 2009; WANG, J. et al., 2017; LAPOINTE et al., 2020). An increasing number of records, summarized by Zhang et al. (2019), indicate that the AMO variability extends several millennia back in time. Recently, Lapointe et al. (2020) provided a reconstruction of the AMO with unprecedented annual resolution. According to this reconstruction, the Little Ice Age (LIA, ~1450-1850; Intergovernmental Panel on Climate Change (IPCC), 2013) is the longest period with a persistent cold anomaly in the North Atlantic over the past ~3 millennia. Recent evidence also suggests that the AMO played a keyrole in transition between the Medieval Climate Anomaly (MCA, ~950-1250; IPCC, 2013) and LIA. During the MCA, in the early 1400s, warm Atlantic water intrusion into the Nordic Seas provoked destabilisation of subpolar North Atlantic and weakening of the poleward oceanic heat transport followed by intensive cooling of North Atlantic (ARELLANO-NAVA et al., 2022; LAPOINTE; BRADLEY, 2021).

Multiple paleoclimate records of the stable oxygen isotope composition ($\delta^{18}O$) from South America (KNUDSEN et al., 2011; CHIESSI et al., 2009; APAÉSTEGUI et al., 2014; BERNAL et al., 2016; FLANTUA et al., 2015; NOVELLO et al., 2018) show typical AMO periodicities (~65 years) and suggest the AMO affected South American hydroclimate in the past. According to records from tropical Andes and and south central Brazil, the MCA is characterized as a warm period with weakened South American monsoon

system (NOVELLO et al., 2018; LÜNING et al., 2019). Isotopic records also suggest enhanced monsoon during the LIA (CAMPOS et al., 2019; ORRISON et al., 2022). On the other hand, speleothems (NOVELLO et al., 2012; NOVELLO et al., 2018) from northeastern Brazil indicate no changes in precipitation amounts during the MCA, but drier LIA period. Utida et al. (2019), however, suggest humid conditions along the coastal area of northeastern Brazil during LIA. At the same time, records from eastern Amazon region indicate variations in the overall aridity over past millenium, with pronounced humid phase in early and to drier conditions in late MCA and LIA (AZEVEDO et al., 2019). Although the number of available paleoprecipitation records from South America significantly increased during the last decade the relevance of the AMO in the precipitation anomalies over South America during LIA and MCA remains unclear. Therefore, the investigation of how the AMO affects precipitation and how that reflected on isotopic ratios requires the use of isotope-enabled climate models.

In this context, the main objective of this study was to simulate and evaluate the influence of the AMO on atmospheric dynamics, precipitation, and consequently $\delta^{18}O$ of precipitation over South America. For this purpose, the water isotope-enabled version of the Community Earth System Model version 1.2 (iCESM1.2) has been forced with cold and warm AMO-phase SST fields. In the following pages, it will also be discussed whether the AMO and related seasonally-dependent responses may potentially have been major drivers of LIA signal found in paleoclimate records (UTIDA et al., 2019; CAMPOS et al., 2019; ORRISON et al., 2022). In addition, $\delta^{18}O$ simulations were compared with a compilation of $\delta^{18}O_p$ published reconstructions within South America.

4.2 Material and methods

In the chapter that follows, for the purpose of clarity and completeness of the analysis methodology already employed in the previous chapter will be briefly presented, with additional explanation regarding stable oxygen isotope and paleoclimate records.

4.2.1 iCESM model setup

Experiments for this study were carried with a water isotope-enabled version of the Community Earth System Model version 1.2 (iCESM1.2). The iCESM1.2 has active atmosphere, land, ocean, river transport, and sea ice component models linked through a coupler, and also simulates global variations in water isotopic ratios in the atmosphere, land, ocean, and sea ice. The ability of this model to simulate present and past $\delta^{18}O_p$ patterns has been documented previously (OTTO-BLIESNER et al. 2016; ZHU et al., 2017; HE et al., 2021). The atmospheric component of iCESM1.2, the isotope-enabled Community Atmosphere Model version 5 (iCAM5.3) (NUSBAUMER et al., 2017), is based on the original, non-isotope enabled CAM5 (NEALE et al., 2010). The atmospheric component of iCESM1.2, the isotope-enabled Community Atmosphere Model version 5 (iCAM5) (NUSBAUMER et al., 2017), is coupled with the interactive Community Land Model version 4 (CLM4; OLESON et al., 2010) while sea surface temperature (SST) and sea ice concentrations (SICs) were prescribed. The model was configured to use a computational grid of 1.9° latitude × 2.5° longitude and 30 vertical levels from the surface to ~3.5 hPa.

This part of theses assesses the influence of the AMO on $\delta^{18}O$ of precipitation ($\delta^{18}O_p$) by analyzing simulations from isotope-enabled version of the Community Earth System Model version 1.2 (iCESM1.2) (BRADY et al., 2019). Isotope-enabled models integrate the mass-dependent kinetic fractionation with atmospheric circulation and oceanic evaporation, evaporation and transpiration from land, and the deposition of vapor onto ice. Isotope enabled models integrate the mass-dependent kinetic fractionation with atmospheric circulation and oceanic evaporation, evaporation and transpiration from land and the deposition of vapor onto ice. Model used in this study is designed so that isotope-specific processes respond directly to simulated physical processes, rather than tuning to match isotopic observations (BRADY et al, 2019). Description of the performed experiments can be found in Table 3.1. Illustration of the ability of the iCESM1.2 to accurately portray the modern seasonality of $\delta^{18}O_p$ can be found in Figure A.3.

4.2.2 Main variables and methods used in the analyses

The effects of AMO-related SST over South American climate were evaluated through the differences between CAMO and WAMO experiments, for both precipitation and $\delta^{18}O_p$. As in previos section, the analyses have been applied to the ensemble average. Here we investigated the austral summer (December, January and February, DJF) and autumn season (March, April and May, MAM). We also analyze summer and autumn seasons jointly (December, January, February, March, April, and May, DJFMAM) facilitating simultaneous observation of two major precipitation features, the ITCZ and the South Atlantic Convergence Zone (SACZ) that forms during the mature phase of South American Monsoon System (SAMS) (GARREAUD et al., 2009; SÖRENSSON; MENÉNDEZ, 2011).

To understand the dynamical mechanisms that caused the changes in precipitation and $\delta^{18}O_p$ we analyzed the upper- and lower-tropospheric circulation.

As the AMO has a strong impact on global atmospheric circulation, changes in Hadley and Walker circulation by comparing vertical velocity (omega; hPa/s) at different pressure levels in the troposphere (NGUYEN et al., 2013) were investigated. Hadley cells consists of the ascending branch (represented by upward motion, hence negative vertical velocity) situated in the tropics and associated with enhanced precipitation. At upper-tropospheric levels air is flowing poleward and finally descends in the subtropics (positive vertical velocity), suppressing precipitation. In this study, a latitude-height section 30°N-30°S of vertical velocity, averaged over 80°W-30°W, is analyzed to represent the regional Hadley circulation. The response of the regional Walker circulation over South America, where ascending branch is situated over the western Amazon region and descending motion occurs east of 40°W from December to March, was analyzed observing the longitude-height section 80°W-30°W, averaged over 0-15°S.

The simulated $\delta^{18}O_p$ responses in each AMO phase have been analysed in this section. The $\delta^{18}O_p$ denotes the ratio of H218O to H216O in precipitation

(DANSGAARD, 1964). The relative abundances of stable isotopologues of water (i.e., $^{16}O/^{18}O$) changes due to fractionation that accompany condensation and evaporation processes. Due to slight differences in chemical and physical properties heavier ^{18}O isotopes enter or remain in the liquid or solid phases, while lighter ^{16}O isotopes enter or remain in the vapor phase. The isotopic composition of precipitation is expressed as the per mil (‰) deviation of the heavy-to-light isotope ratio (R) from the Vienna Standard Mean Ocean Water standard (VSMOW) (KENDALL; CALDWELL, 1998). The $\delta^{18}O_p$ is calculated following equation:

$$\delta^{18}O_p = \left(\frac{\frac{O^{18}}{O^{16}\,sample}}{\frac{O^{18}}{O^{16}\,Standard}} - 1 \right) * 1000‰, \quad (4.1)$$

The statistical significance of these differences was assessed using Student's t-tests at a 95% confidence level to evaluate whether the means of two different groups were distinct, meaning that the change was significant, or not.

4.2.3 Compilation of proxy data from paleoclimate archives

According to Lapointe et al. (2020) the coldest AMO anomalies occurred during the LIA (Figure A.4). The LIA is also the longest period with a persistent cold anomaly in the North Atlantic over the past ~3 millennia. To test whether the AMO potentially may have been major driver of the LIA signal found in paleoclimate records, here are compared signals found in paleoclimate records with the simulated spatial footprint during the AMO cold and warm phase, respectively. We defined signals in the LIA and the MCA following the original interpretations of the authors in three categories: "drier" (meaning that the LIA was drier than the MCA), "wetter" (meaning that the LIA was wetter than the MCA) and "neutral" (meaning that the record shows no clear trend in humidity between the LIA and the MCA). We compiled 29 published records of hydroclimate and environmental reconstructions that cover both LIA and MCA (Table A.2).

4.3 Results

4.3.1 Changes in precipitation and $\delta^{18}O_p$

The precipitation has a strong seasonal variability over South America and in order to assess the impact of the AMO on two dominant precipitation features, the ITCZ and the SACZ, and consequently $\delta^{18}O_p$, we analyzed simulated austral summer (DJF), austral autumn (MAM), and both seasons together (DJFMAM) (Figure 4.1). The DJFMAM season shows continental-scale hydroclimate variability thus enables capturing the signal of the AMO during the peak of the monsoon season (DJF) as well as the period when ITCZ is reaching its southernmost position (MAM).

During austral summer (DJF), precipitation is significantly reduced over the Atlantic Ocean north of the equator, and in the northern portion of South America (10°N-0°, 75°W-60°W) in the CAMO experiment (Figure 4.1a). In contrast, precipitation over most of South America is increased in the CAMO experiment and the highest increase during DJF is simulated over the western Amazon (7°N-10°S, 70°-60°W), the northeastern Brazil (0°-25°S, 55°W-25°W) and the Andes.

During austral autumn (MAM), wetter conditions remain over the northeastern Amazon and in northern northeastern Brazil, while over most of South America precipitation decreased. The highest decreases are simulated over southeastern South America (25°S-40°S, 65°W-50°W), northeastern Brazil and the Andes.

Figure 4.1 - Precipitation and stable oxygen isotope composition ($\delta^{18}O_p$) (‰) differences between the cold Atlantic Multidecadal Oscillation (CAMO) and the warm Atlantic Multidecadal Oscillation (WAMO) experiments for austral summer (DJF), autumn (MAM) and for December, January, February, March, April, and May (DJFMAM). For precipitation red (blue) shaded areas correspond to drier (wetter) conditions. For in $\delta^{18}O_p$ (‰) red (blue) shaded areas correspond to an increase (decrease). Anomalies that are statistically significant at the 95% confidence level based on a Student's t test are marked with stippling. Panels a and b modified from Maksic et al. (2022).

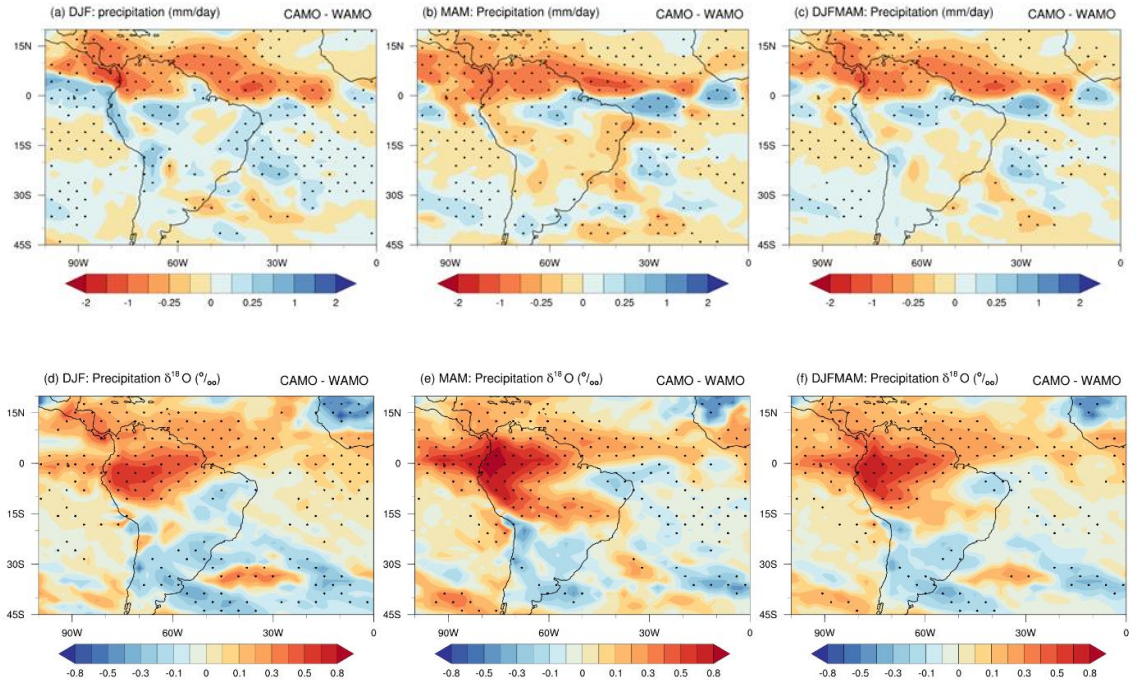

The DJFMAM mean shows increased precipitation during the cold AMO phase, mainly over the western Amazon region, northern northeastern Brazil and the Andes, while a significant precipitation reduction is present in the northernmost South America. There are also significant inter-hemispheric differences in the amount of precipitation over the Atlantic Ocean, with the largest increase occurring to the south of the equator close to northeastern Brazil and in the South Atlantic, while the largest reduction is observed to the north of the equator (Figure 4.1c).

The spatial distribution of $\delta^{18}O_p$ (‰) change between CAMO and WAMO is shown in Figure 4.1d-f. During the cold AMO phase $\delta^{18}O_p$ pattern shows an enriched (positive) signal over the Atlantic Ocean north of the equator and over

the entire Amazon region, reaching 15°S in DJF and 20°S in MAM. The highest enrichment in CAMO is simulated over the northwestern coast and the western Amazon (0°-10°S, 80°W-65°W) in MAM. The $\delta^{18}O_p$ values are significantly depleted (negative) in CAMO over the equatorial Atlantic Ocean to the south of the equator, northeastern Brazil and southern South America (20°S-30°S, 55°W-35°W) in MAM. The southeastern region (10°S-20°S, 60°W-35°W) is marked by shifting from negative to positive signal from DJF to MAM.

The DJFMAM mean (Figure 4.1c) shows that values remain significantly negative over northeastern Brazil and southern South America (2°S-30°S, 55°W-35°W) and positive over Amazon region and northernmost South America.

The spatial distribution of $\delta^{18}O_p$ (‰) change between CAMO and WAMO is shown in Figure 4.1d-f. During the cold AMO phase $\delta^{18}O_p$ pattern shows an enriched (positive) signal over the Atlantic Ocean north of the equator and over the entire Amazon region, reaching 15°S in DJF and 20°S in MAM. The highest enrichment in CAMO is simulated over the northwestern coast and the western Amazon (0°-10°S, 80°W-65°W) in MAM. The $\delta^{18}O_p$ values are significantly depleted (negative) in CAMO over the equatorial Atlantic Ocean to the south of the equator, northeastern Brazil and southern South America (20°S-30°S, 55°W-35°W) in MAM. The southeastern region (10°S-20°S, 60°W-35°W) is marked by shifting from negative to positive signal from DJF to MAM.

The DJFMAM mean (Figure 4.1c) shows that values remain significantly negative over northeastern Brazil and southern South America (2°S-30°S, 55°W-35°W) and positive over Amazon region and northernmost South America.

4.3.2 Changes in large-scale circulation

To understand the dynamical mechanisms that caused the changes in precipitation and $\delta^{18}O_p$, we analyzed the extended austral summer (DJFMAM) upper- and lower-tropospheric circulation (Figure 4.2 and Figure 4.3).

Figure 4.2 - The cold Atlantic Multidecadal Oscillation (CAMO) and the warm Atlantic Multidecadal Oscillation (WAMO) seasonal wind vectors and intensity at 200 hPa (m/s) (a,b) and their differences (c) during the extended summer season (December-May; DJFMAM). Only statistically significant differences calculated based on a Student's t test with confidence level of 95% are shown.

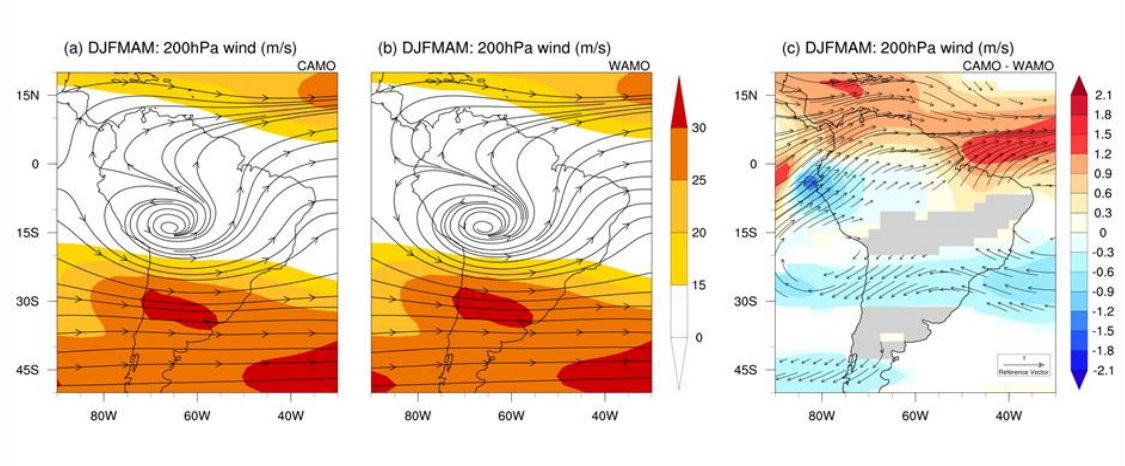

The position of the upper-level anticyclonic circulation, known as the Bolivian High, is the same for both CAMO and WAMO experiments, but the wind circulation is slightly intensified in WAMO (Figure 4.2a, b) in comparison with CAMO (Figure 4.2a, c). On the other hand, the westerlies (200 hPa) over the North Atlantic Ocean, between the equator and 20°N, are enhanced in CAMO. This inter-hemispheric contrast is reflected in the gradient of precipitation between northern South America and the Amazon region (Figure 4.1c). Differences between CAMO and WAMO (Figure 4.2c) show that the subtropical jet stream is intensified in the WAMO experiment, in relation to the CAMO experiment, which is related to the intensified Bolivian High. This subtropical jet stream intensification is the highest over the South Atlantic Ocean.

Comparing the 850 hPa wind field anomalies between both AMO phases (Figure 4.3), an increased easterly flow reaching 5°S is noted for CAMO. For DJFMAM the Caribbean low-level jet is weakened.

Figure 4.3 - Wind vectors and intensity at 850 hPa (m/s) for (a) the cold Multidecadal Oscillation (CAMO) and (b) the warm Atlantic Multidecadal Oscillation (WAMO), as well as for the differences between both phases (CAMO-WAMO) (c) for December-May (DJFMAM). Only statistically significant differences calculated by a Student's t test with confidence level of 95% are shown.

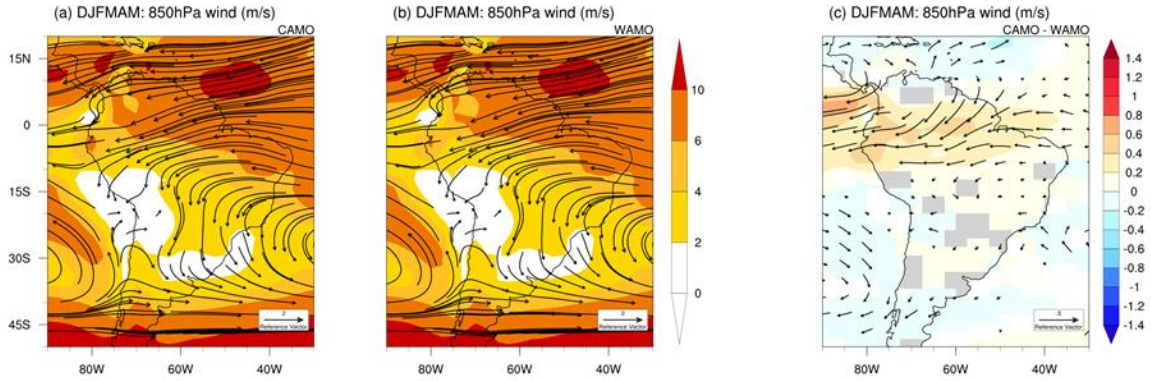

4.3.3 Changes in atmospheric circulation cells

Figure 4.4 reveals the difference (CAMO-WAMO) of the vertical profiles that represent the Hadley and Walker cells.

The Atlantic Hadley cell favors convective activity over the region situated between the 5°N and 15°S. The difference (CAMO-WAMO) of the vertical profile (Figure 4.4a) shows high positive anomalies centered between the equator and 15°N, indicating a stronger inter-hemispheric atmospheric circulation. The difference also shows a dipole of negative/positive values south/north of the equator in DJFMAM.

Figure 4.4b shows differences in the vertical profile of the Walker circulation. Anomalies show that during the cold AMO phase the ascent of warm and moist air is intensified, contributing to deep convective cloud formation. We also observe positive anomalies in the upper-troposphere east and west of intensification (negative anomaly) field, suggesting potential change in the ascending branch position.

Figure 4.4 - Difference between the cold Multidecadal Oscillation (CAMO) and the warm Atlantic Multidecadal Oscillation (WAMO) of vertical pressure velocity (omega; hPa/s) for December-May (DJFMAM). (a) Latitude-height section 30°N - 30°S, averaged over 80°W-30°W, representing the regional Hadley circulation. (b) Longitude-height section 80°W-30°W, averaged over 0-15°S, representing the regional Walker circulation. Anomalies statistically significant at the 95 % confidence level by Student's t test are marked with dots.

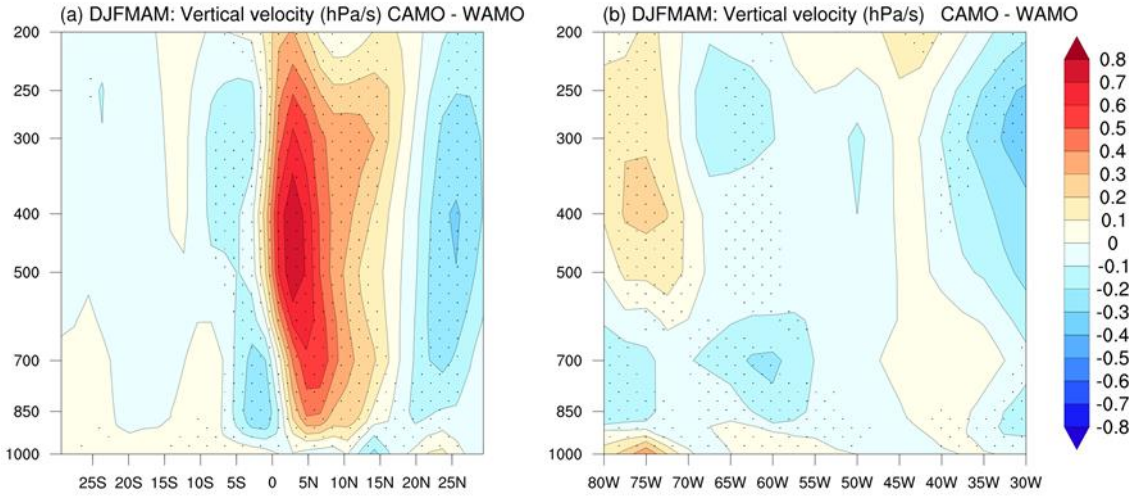

4.3.4 Paleoclimate reconstructions

Finally, we compare the LIA-MCA $\delta^{18}O$ anomalies from speleothems with simulated CAMO-WAMO $\delta^{18}O_p$ anomalies. We are comparing signals from LIA and MCA, based on the relative difference between LIA and MCA periods, following the original interpretations of the authors. Although we combine as many different paleo records in the compilation as possible (Table A.2), Figure 4.5 only shows the approximate location of speleothem records (presented by circles), that provide high-resolution and precisely dated $\delta^{18}O$ time series from the ITCZ and and monsoon regions in South America.

Figure 4.5 - Differences between the cold Multidecadal Oscillation (CAMO) and the warm Atlantic Multidecadal Oscillation (WAMO) experiments for $\delta^{18}O_p$. Red (blue) shaded areas correspond to simulated increase (decrease) in $\delta^{18}O_p$ (‰). Anomalies that are statistically significant at the 95 % confidence level based on a Student's t test are stippled. Paleoclimate record locations: circles, speleothems; triangle, ocean sediment. The anomalies between the Little Ice Age (LIA) and the Medieval Climate Anomaly (MCA), where red (blue) indicate an enriched(depleted) signal in $\delta^{18}O_p$, and grey circles indicate unclear signals (LIA-MCA) in paleoclimate record. For full details about proxies see Table A.2.

	Reference	Site name	Lat	Lon	Meters above sea level	Proxy
1	Asmerom et al., 2020	Yok Balum (YOKG), Belize	16.20° N	89.06° W	366	δ13C Speleothem
2	Haug et al., 2001	Cariaco, Venezuela	10.71° N	65.17 ° W		Ocean Sediment Titanium Conc.
3	Wang et al., 2017	Paraiso (PAR01,PAR03), Brazil	4.07 °S	55.45°W	60	δ18O / δ13C Speleothem
4	Apaéstegui et al., 2014	Palestina (PAL03,PAL04), Peru	5.92°S	77.35 °W	870	δ18O / δ13C Speleothem
5	Reuter et al., 2009	Cascayunga Cave, Peru	6.05° S	77.13° W	930	δ18O speleothem
6	Utida et al., 2019	RN caves (Trapia, Furna Nova)	5.14°S	37.62°W	70	δ18O speleothem composite
7	Bird et al., 2011	Pumacocha lake, Peru	10.70 °S	76.06 °W	4300	δ18Olw
8	Kanner et al., 2011	Huagapo cave, Peru	11.27°S	75.79°W	3550	δ18O speleothem
9	Della Libera et al., 2022	Cuíca cave (PIM4 and PIM5), Brazil	11.40°S	60.38°W	310	d18O and d13C speleothems
10	Azevedo et al., 2019	Mata Virgem Cave (MV3), Brazil	11.37°S	47.29°W	365	δ18O and δ13C Speleothem
11	Novello et al., 2012	Diva de Maura and Torinha cave, Brazil	12.22°S	41.34° W	480	Speleothem δ18O
12	Novello et al., 2018	São Bernardo and São Mateus caves, Brazil	13.81°S	46.35°W	631	Speleothem δ18O
13	Thompson et al., 1986	Quelccaya, Peru	13.93°S	70.83° W	5670	δ18Oic
14	Novello et al., 2016	Pau d'Alho (ALHO6), Brazil	15.12°S	56.48°W	600	δ18O stalagmite
15	Wortham et al., 2017	Tamboril Cave, Brazil	16.0°S	47.0°W	700	δ18O, δ13C, 87Sr/86Sr speleothem
16	Apaéstegui et al., 2018	Umajalanta, Bolivia	18.12°S	65.77°W	2650	δ18O Speleothem
17	Vuille et al., 2012	Cristal Cave (CR1), Brazil	24.58°S	48.58°W	130	δ18O Speleothem

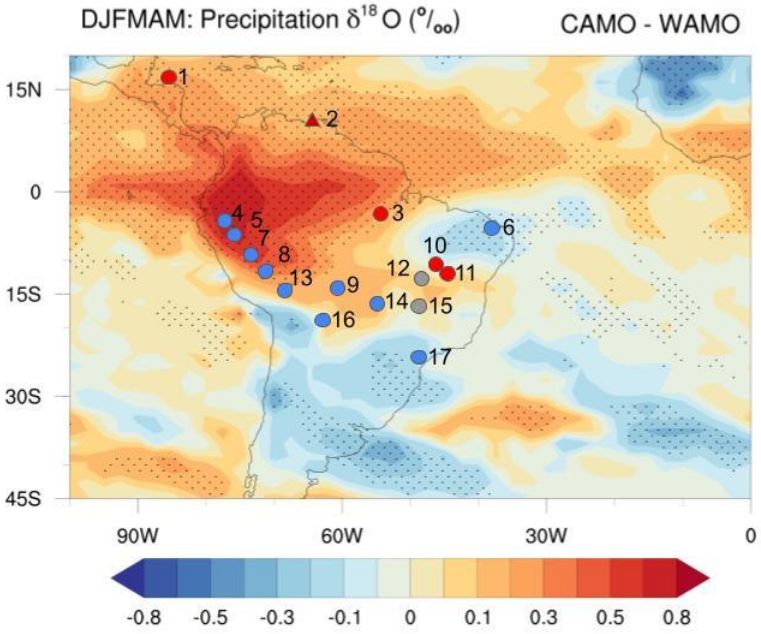

Simulated $\delta^{18}O_p$ anomalies over northeastern Brazil are in agreement with speleothem records from Rio Grande do Norte cave sites (UTIDA et al., 2022, in revision), as well as with lake sediments from Boqueirão Lake (UTIDA et al., 2019) located at about 5°S. Significant $\delta^{18}O_p$ enrichment is simulated for the cold AMO over northern South America, equatorial and western Amazon region

and the Andes. However, records from the southwestern Amazon region (DELLA LIBERA et al., 2022) suggest wetter conditions during the LIA and drier conditions during the MCA. This is in agreement with simulated precipitation (Figure 4.1) but not with simulated $\delta^{18}O_p$. Likewise, the simulated $\delta^{18}O_p$ signal differs from speleothem records from the Andes that suggest wetter conditions during the LIA (BIRD et al., 2011; KANNER et al., 2013; APAÉSTEGUI et al., 2014).

Simulated anomalies are not statistically significant in eastern Brazil, between 10 and 25°S, and this is also the region with a relative neutral signal between LIA and MCA (NOVELLO et al., 2012; NOVELLO et al., 2018; WORTHAM et al., 2017; AZEVEDO et al., 2019). On the other hand, statistically significant negative isotopic anomalies are observed in simulated oxygen isotope ratios over the southern part of tropical South America, which suggest an enhancement of the SASM during cold AMO. This result is in agreement with the signal recorded by speleothems from Cristal cave (VUILLE et al., 2012) and partly in agreement with Umajalanta–Chiflonkhakha cave system (APAÉSTEGUI et al., 2018) where records suggest change from wet to dry phase during MCA.

4.4 Discussion

Due to the complexity of the water cycle, $\delta^{18}O_p$ values in precipitation vary temporally and spatially, being influenced by several environmental factors (e.g., surface air temperature, amount of precipitation, orography, atmospheric humidity, distance from the ocean) (DANSGAARD, 1964). Over mid- and high latitude regions, fractionation processes and $\delta^{18}O_p$ variations are primarily governed by the temperature, while those at low latitudes are primarily governed by precipitation (DANSGAARD, 1964; ROZANSKI et al., 1992). In tropical regions, most precipitation arises from deep convection, with vertical motions dominating over horizontal transport, and, via Rayleigh distillation, the high condensation and precipitation results in water vapor with depleted (negative) $\delta^{18}O_p$ (BOWEN, 2008; VUILLE et al., 2003; VUILLE et al., 2012; CAMPOS et al., 2019; ORRISON et al., 2022). In areas with less strong

convergence, the $\delta^{18}O_p$ depends on a complex interplay between the amount effect, the continental effect (LACHNIET, 2009), moisture source and trajectory path (CRUZ et al., 2005; STURM et al., 2007), ocean-atmosphere interactions (BRADLEY et al., 2003; VUILLE; WERNER, 2005), and moisture recycling (AMPUERO et al., 2020). Given that $\delta^{18}O_p$ integrates information from all parts of the water cycle, proxy records of past hydroclimate preserve signal of large-scale climate dynamics related to changes in distant geographic area, such as North Atlantic SST (BACKER et al., 2009; WINTER et al., 2011; FENSTERERET al., 2012). Studies over the past two decades have provided important information on how AMO influences both ITCZ and SAMS, but very little was found in the literature on the isotopic fingerprint of AMO over South America. Statistical analyses show the dominant mode of variability characterized by frequencies of ~60-80 years in several speleothem records (APAÉSTEGUI et al., 2014), but the importance of AMO in the precipitation anomalies during LIA and MCA is still unknown. Recent work by Midhun et al. (2020) finds a globally-distributed, large spatial AMO footprint, but the signal is weak, possibly due to the difficulties of coupled models to appropriately simulate decadal to multidecadal variability (AULT et al., 2012; KRAVTSOV et al., 2018). Fully coupled models also underestimate the magnitude of decadal variability and fail to produce spatial patterns that match the observed signals (HAN et al., 2016).

The present study was designed to determine the effect of AMO on $\delta^{18}O_p$. The results show stronger low level easterly flow in CAMO (Figure 4.1c; Figure 4.3c) that brings more moisture to the mainland and correlates with the increase in precipitation over the western Amazon (7°N-10°S, 70°-60°W) and coastal northeastern Brazil (Figure 4.1c). While the increase in precipitation during CAMO corresponds with $\delta^{18}O_p$ simulated depletion over northeastern Brazil, significant increase in precipitation in western Amazon during CAMO, which is consistent with observations (YOON; ZENG, 2010), does not seem to correspond to simulated enriched (positive) $\delta^{18}O_p$ (Figure 4.1f). This finding was unexpected and suggests that even when the change in total precipitation amount is significant over the western Amazon this may not be reflected in

$\delta^{18}O_p$ depletion. Given that the total precipitation amount changed substantially, the simulation results indicate that different physical processes are compensating $\delta^{18}O_p$ depletion. This inconsistency may be due to changes in large-scale circulation (Figure 4.3c) where the $\delta^{18}O_p$ enrichment signal, related to precipitation reduction throughout the Atlantic Ocean north of the equator, propagates further inland reaching 20°S and diminishes the amount effect. This finding was also reported by Bowen (2008) who observed that isotope seasonality over relatively large regions may be strongly controlled by the strength of convergence over ITCZ. Another potential reason for enriched $\delta^{18}O_p$ values could be a reductions in overall evaporation in CAMO observed over the Amazon region and region under the SAMS influence (Figure A.5).

In comparison with reconstructions (Figure 4.5) we conclude that, contrary to expectations, the simulated $\delta^{18}O_p$ signal differ from speleothem records from the Andes that show wetter conditions during the LIA and $\delta^{18}O_p$ depletion (BIRD et al., 2011; KANNER et al., 2013; APAÉSTEGUI et al., 2014). More future analyses are needed to pinpoint the cause of this discrepancy and understand why significant total precipitation amount change over the western Amazon and Andes are not reflected in $\delta^{18}O_p$ depletion. It is important to bear in mind that the possible bias in these responses is in part due to the limited number of ensemble members to provide robust assessments of the forced response.

On the other hand, simulated $\delta^{18}O_p$ agree with speleothemes under the SAMS influence (Figure 4.1a, d), which show strengthening or southward displacement of the SACZ that occurred during the LIA (CAMPOS et al., 2019; ORRISON et al., 2022).

Depletion of $\delta^{18}O_p$ over northeastern Brazil is simulated in both DJF and MAM seasons, although simulated precipitation anomaly is positive in MAM only in its northernmost regions and over the adjacent tropical South Atlantic (Figure 4.1a,b). The precipitation increase over the equatorial Atlantic Ocean and northeastern Brazil can be dynamically understood as being associated with changes in the Atlantic ITCZ and the intensified easterly flow. The scientific literature has linked AMO phases and energetically driven meridional shift of

ITCZ with precipitation changes over South America (KNIGHT et al., 2006; TING et al., 2011; LEVINE et al., 2018). The same mechanism has been associated with drought conditions signal in the Cariaco Basin, located close to the northern limit of the ITCZ, and widespread aridity in the most northern regions of South America and during the LIA (HAUG et al., 2001; PETERSON; HAUG, 2006). Indeed, the LIA was the longest period with persistent cold anomalies in the North Atlantic (LAPOINTE et al., 2020). This could support the hypothesis of the ITCZ shifting southwards during the LIA (HAUG et al., 2001; BIRD et al., 2011; ZHANG et al., 2019). Displaced ITCZ could explain dry (wet) signals recorded in the Cariaco Basin and simultaneously wet (dry) signals over northeastern Brazil during LIA (UTIDA et al., 2019). However, paleoclimate records from Central America have recently challenged the hypothesis (POLISSAR et al., 2006; OBRIST-FARNER et al., 2023; MEDINA et al., 2023; ASMEROM et al., 2020), showing significant spatial variability in hydroclimate during the LIA (STEINMAN et al., 2022).

Surprisingly, the results of this study do not show substantial differences in the mean position of the Hadley cells and the ITCZ, but changes in intensity. The AMO in experiments presented here has a nearly symmetric effect in modulating the Atlantic ITCZ-related precipitation. Interesting finding is that the equator-symmetric changes present in the simulated precipitation fields are in remarkable agreement with the changes shown in Knight et al. (2006). It is important to bear in mind the importance of acknowledging the dynamics of season- and regional-dependent ITCZ responses as they are sufficient to produce observed AMO related signals even in the absence of marked changes in the ITCZ position. Therefore, we interpret the simulated changes in precipitation between different AMO phases as changes in the Atlantic ITCZ core strength. This is in agreement with Steinman et al. (2022) which shows multi century-long southerly shift in the ITCZ accompanied by a decrease in ITCZ strength.

Comparison of model-derived signal for region under the Atlantic ITCZ influence is also consistent with proxy reconstructions (AZEVEDO et al., 2019; DELLA LIBERA et al., 2022; UTIDA et al., 2022, submited) (Figure 4.5). Dipole pattern

of both precipitation and $\delta^{18}O_p$ simulated for coastal northeastern Brazil between northern portion and southern portion of northeastern Brazil resembles one found in records (NOVELO et al., 2012; NOVELO et al., 2018; AZEVEDO et al., 2021; UTIDA et al., 2022, submited). The results of this study are also in line with studies that suggested the ITCZ expansion/contraction as potential modulator of tropical precipitation changes (YAN et al., 2015; WODZICKI; RAPP, 2016; DENNISTON et al., 2016; CHIESSI et al., 2021). They also complement study that suggests external forcings as main drivers of the Atlantic ITCZ shifts during the last millennium (ROLDÁN-GÓMEZ et al., 2022). This implies that AMO-induced ITCZ seasonal strength changes and ITCZ shifts driven by strong volcanic eruptions during the LIA (STEVENSON et al., 2019; TEJEDOR et al., 2021) contribute jointly to changes in precipitation over South America during the last millennium.

Since the study was limited on one model it should be acknowledged that systematic biases could have influenced results. In addition, the AMO may not in fact be the only and primary control of precipitation $\delta^{18}O_p$ within South America over the last millennium, and that interactions among the three oceans can play an important role in initiating interactions and modulating climate over South America (WANG et al., 2019; HE et al., 2021). It is important to keep in mind that the proxy data reflect differences between LIA and MCA, while the experiments optimally represent only cold and warm phase from 1850-2012. Also, this study is limited to ocean–atmosphere interaction and the climate system is the result of many more complicated feedbacks and interactions. Thus, considerably more work will need to be done to determine which part of the signal found in proxies can be explained by the AMO.

Notwithstanding these limitations, this study support evidence from Utida et al. (2019) who found that regional precipitation along the coastal area of South America was not solely governed by north-south displacements of the ITCZ due to changes in NH climate, but also by the contraction and expansion of the tropical rainbelt. In addition, this mechanism potentialy explain zonal dipole between coastal area of northeastern Brazil and eastern Amazon region during the LIA (AZEVEDO et al., 2019; AZEVEDO et al., 2021). An implication of this

finding is the possibility that change in the ITCZ core strength, provoked by persistent cold AMO (LAPOINTE et al., 2020), contributed to dry conditions over northernmost South America and also increased precipitation along the coastal area of northeastern Brazil during LIA.

This study also explored the potential influence of the AMO on terrestrial ecosystem responses biome distribution. For this purpose the potential vegetation simulations with the CPTEC-PVM2, following methodology explained in the Section 2.2 (Table 2.2), were performed. To perform the potential vegetation simulations the CPTEC-PVM2 model was initialized with the observed monthly climatology plus the simulated monthly fields of CAMO and WAMO experiments. For both experiments, CO_2 was set on 280ppm. Contrary to expectations, this study did not find a significant difference between projected biome changes for the CAMO and WAMO experiments (Figure A.6). A possible explanation for this might be that responses to this large-scale change may be on structural complexity, community composition or phenological changes (NYE et al, 2014; VILELA et al., 2017) and not on biome level.

4.5 Conclusions

The findings of this study point out that Atlantic ITCZ strength is sensitive to the Atlantic Multidecadal Oscillation. Hence, teleconnection between the North Atlantic SST and ITCZ strength in simulations presented here drive seasonal variability of precipitation isotope ratios over tropics and subtropics. Model-derived AMO signal for region under the Atlantic ITCZ influence is consistent with proxy reconstructions and ITCZ strength change potentialy explain zonal dipole between northern portion and southern portion of northeastern Brazil, as well as northern portion of northeastern Brazil and eastern Amazon region during the LIA. An implication of this finding is the possibility that change in the ITCZ core strength, provoked by persistent cold AMO, contributed to dry conditions over northernmost South America and also increased precipitation along the coastal area of northeastern Brazil during LIA. These results also suggest that records reflecting annual means should be treated with caution as they potentialy record signal of seasonal variability and not ITCZ shift.

Hydroclimatic spatiotemporal patterns in other regions of South America, however, remain puzzling and cannot be explained by AMO, as model-derived AMO signal and signal in records are not consistent. The reasons for these discrepancies between the reconstructions on the one side and the model on the other side could lie in model systematic biases, limited interaction and feedback in experiments and additional uncontrolled factors. The AMO however may not be the only and primary control of precipitation within South America during LM, and that in different regions other factors were more dominant.

5 GENERAL CONCLUSIONS

This study tends to provide a past-present-future perspective of climate changes and terrestrial ecosystem responses in South America.

In the first part the vegetation response to a temperature increase since the Last Glacial Maximum to the pre-industrial period was analyzed using both simulations and records-based reconstructions. For the sake of making LGM a potential antianalog for future warming and symmetric comparison, the referent cooling of LGM at -4°C was set. Computed LGM anomalies showed decreased precipitation over equatorial (0°-10°S) Brazil and increased precipitation over regions under the SAMS influence. The compilation of published reconstructions shows that the computed multi-model ensemble mean precipitation and temperature fields are reliable over Brazil. The validation of past conditions is an important step that increased confidence in data that are used as the input for further vegetation simulations.

The investigation of LGM vegetation has shown that simulations are consistent with proxy reconstructions which suggests expansion of grassland in the southern Brazilian highlands (BEHLING et al., 2004; GU et al., 2018). One of the most significant findings to emerge from this study is that the model reproduces the LGM Grassland biome seen in records only considering all forcings, as none of them separately is sufficient for producing adequate conditions necessary for it. Model also suggests the Amazon rainforest persistence through colder and drier conditions during the LGM. This study has identified that the western and central Amazon forest were largely maintained during the LGM mainly due to negative temperature anomalies, while a decrease in past precipitation was responsible for Tropical evergreen forest to be substituted by Tropical seasonal forest and Savanna/Cerrado in its eastern portion. The results of this research support the idea that changes in monsoon intensity cannot be the main driver for vegetational changes/stability across the Amazon biome, as generally assumed. Thus, lower temperatures in combination with substantially lower CO_2 are also important controlling factors

during the LGM (GERHART; WARD, 2010; PRENTICE et al., 2011; SCHEFF et al., 2017).

A quantitative approach of classifying vegetation proxy data as reflecting “change”, “no change” and “unclear” could be the source of uncertainties that opens space for discussion and creates potentially fruitful area for further investigation. Although this approach has been used in other studies, this simplification can result in an agreement between the proxy record and the model scenario even in cases when they show opposite signals. A further study could assess the description of change and change evidence specified in the compilation created here and compare them with LGM climate produced by the regional climate models with more detailed topography and the consideration of paleo lake level fluctuations. More information by the regional climate models could bridge the gap between the coarse resolution of current global climate models and the regional-to-local scales, where the impacts of climate change are of primary interest. Also, climate affects land cover and land cover in turn affects climate, therefore further sensitivity tests with prescribed vegetation for LGM generated in this experiment could reveal the importance of more realistic vegetation boundary conditions for a more accurate representation of climate variability under LGM conditions.

Notwithstanding this limitation, this part of the thesis certainly contributes to our understanding of the main drivers behind LGM vegetation changes in the largest biomes of South America, and establishes the relationship between forcings (CO_2, precipitation and temperature) and reconstructed vegetation responses.

The results and insights from the LGM are then compared with projected vegetation response in conditions of potential future warming. The major finding is that, in contrast to LGM, biome shifts for the future +4°C scenario will mostly depend on future precipitation changes. Under future warming, simulations show an expansion of Savanna/Cerrado, with projected coverage 10% higher than Present. Further, future warming will trigger a reduction of Amazon forest, Tropical seasonal forest and Caatinga savannization or desertification. Results

reaffirmed that the +4°C scenario will most probably affect local biodiversity and regional climate. Knowing that the regional human-driven pressures are up to hundreds to thousands of times faster than they are for natural climatic and geological phenomena (ALBERT et al., 2023) and can lead to a cascade of tipping points in combination to the scrutinized driving factors there is, therefore, a definite need for consideration of land use changes in further research.

Recent observations show the Atlantic Ocean overturning circulation recently is weakening (AMOC) (CAESAR et al., 2018). Intensified (weakened) AMOC causes stronger (weaker) northward transport of oceanic heat and induces the warm (cold) anomalies in the North Atlantic (WANG; ZHANG, 2013). Observations also indicate emerging North Atlantic cooling in spite of warming in tropical Atlantic (FRAJKA-WILLIAMS et al., 2017). Simultaneously, evidence suggests that since 1979 the warming in the Arctic has been much faster than in the rest of the world (RANTANEN et al., 2022). The results of this study show that warming is nearly four times faster then the entire globe and that climate models highly underestimate it. With ongoing ice melting in the northern high latitudes, projected AMOC slowing under anthropogenic warming and surface temperature cooling in the Northern Hemisphere (DITLEVSEN; DITLEVSEN, 2023; LIU et al., 2020), it is likely that North Atlantic cooling will persist in future (FRAJKA-WILLIAMS et al., 2017). If these predictions were to occur in the future, the LIA as period with long cold AMO signal may potentially serve as an analogue for climatic conditions in the coming decades.

The experimental work presented in the second and third part of this thesis explores the AMO and hypothesis that the AMO is potentially a major driver of precipitation signals from the MCA and LIA seen in paleorecords. The influence of the AMO on $\delta^{18}O_p$ has been evaluated performing idealized experiments with the iCESM1.2 model.

Unlike earlier studies that suggest a displacement of the ITCZ, presented results do not show robust changes in its zonal mean position between the different AMO phases. The results suggest that the simulated precipitation anomalies can be interpreted as changes in the Atlantic ITCZ core strength,

where in the cold (warm) AMO phase the core region of the ITCZ strengthens (weakens) from February to July, while from July to November the core region weakens (strengthens). Notwithstanding that, interpretations here are based on experiments done with the use of only one model they indicate that season-dependent ITCZ responses are sufficient to produce observed AMO related signals even in the absence of marked changes in the ITCZ position. These results also suggest that records reflecting annual means should be treated with caution as they potentially record signals of seasonal variability and not ITCZ shift.

These simulations were primarily made with the aim to investigate the isotopic fingerprint of AMO and explain precipitation variability found in LM paleoclimate reconstructions over South America. This study is one of the first investigations about how the existence of a dipole mode in the SST over the North Atlantic reflects into $\delta^{18}O_p$ and tries to contribute to new insights into precipitation variability found in paleoclimate reconstructions. Model-derived AMO signal for regions under the Atlantic ITCZ influence is consistent with proxy reconstructions and ITCZ strength change potentially explain zonal dipole between coastal northern portion and southern portion of northeastern Brazil, as well as, northern portion of northeastern Brazil and eastern Amazon region during the LIA. eastern Amazon region during the LIA. An implication of this finding is the possibility that change in the ITCZ core strength, provoked by persistent cold AMO, contributed to dry conditions over northern South America and also increased precipitation along the coastal area of northeastern Brazil during LIA.

Hydroclimatic spatiotemporal patterns in other regions of South America, however, remain puzzling and cannot be explained only by AMO signal, as signals between the reconstructions on the one side and the model-derived signal on the other side are not consistent. The reasons for these discrepancies could lie in model systematic biases, limited interaction and feedback in experiments, as well as additional uncontrolled factors. It must also be acknowledged that the change of SST in other basins may also affect the South American precipitation from interannual to interdecadal time scales (KAYANO;

ANDREOLI, 2007; KAYANO et al., 2021). Recent studies show that the signals from the two different ocean basins can interact (KUCHARSKI et al., 2016) and that impact on local climate variability depends on the phase relationship of the Pacific decadal oscillation (PDO) and AMO (KAYANO et al., 2019; HONG et al., 2021; CERÓN et al., 2021). In addition, in years with cold AMO and cold PDO the South American precipitation anomaly patterns are strongly modulated by the El Niño-Southern Oscillation (KAYANO et al., 2022). Thus, the AMO may not be the only and primary control of precipitation within South America during LM and in different regions other factors could be more dominant, or result of combined effect of dominant patterns.

Given that the AMO is as a combination of both internal variability and response to external forcing, the AMO's interaction with the effects of anthropogenic climate change is certain. However, However, the extent of the AMO's impact in a warming world and its role in exacerbating or mitigating the effects of climate change on terrestrial ecosystem discussed in section two remains uncertain.

The present study makes several noteworthy contributions to our understanding of the main drivers behind LGM vegetation changes in the largest biomes of South America and establishes the relationship between forcings and reconstructed vegetation responses. A natural progression of this work is to analyze past climate and vegetation using regional models, providing more details, especially in regions with highly variable topography. It also indicates the potential for improving understanding millennial and decadal signals in records-based reconstructions, by discussing the mechanisms that take place at monthly timescales.

REFERENCES

ABE-OUCHI, A. et al. Ice-sheet configuration in the CMIP5/PMIP3 Last Glacial Maximum experiments. **Geoscientific Model Development**, v. 8, n. 11, p. 3621–3637, 2015.

ABSY, M.L. et al. Mise en évidence de quatre phases d'ouverture de la forêt dense dans le sud-est de l'Amazonie au cours des 60000 dernières années: première comparaison avec d'autres régions tropicales. **Comptes Rendus de L"Academie des Sciences, Serie II**, v. 312, p. 673–6788, 1991. Available from: https://repositorio.usp.br/item/000821773. Access on: 12 July 2023.

ADAM, O.; SCHNEIDER, T.; BRIENT, F. Regional and seasonal variations of the double-ITCZ bias in CMIP5 models. **Climate Dynamics**, v. 51, n. 1/2, p. 101–117, 2017.

AGUIAR, A. P. D. et al. Land use change emission scenarios: anticipating a forest transition process in the Brazilian Amazon. **Global Change Biology**, v. 22, n. 5, p. 1821–1840, 2016.

AGUIRRE-GUTIÉRREZ, J. et al. Long-term droughts may drive drier tropical forests towards increased functional, taxonomic and phylogenetic homogeneity. **Nature Communications**, v. 11, n. 1, 2020.

ALDER, J.R.; HOSTETLER, S. W. Applying the community ice sheet model to evaluate PMIP3 LGM climatologies over the North American ice sheets. **Climate Dynamics**, v. 53, n. 5/6, p. 2807–2824, 2019.

ALBERT, J. S. et al. Human impacts outpace natural processes in the Amazon. **Science**, v. 379, n. 6630, 2023.

ANNAN, J. D. ; HARGREAVES, J. C. A new global reconstruction of temperature changes at the Last Glacial Maximum. **Climate of the Past**, v. 9, n. 1, p. 367–376, 2013.

ALLEN, J. R. M. et al. Global vegetation patterns of the past 140,000 years. **Journal of Biogeography**, v. 47, n. 10, p. 2073–2090, 2020.

APAÉSTEGUI, J. et al. Hydroclimate variability of the northwestern Amazon Basin near the Andean foothills of Peru related to the South American Monsoon System during the last 1600 years. **Climate of the Past**, v. 10, n. 6, p. 1967–1981, 2014.

APAÉSTEGUI, J. et al. Precipitation changes over the eastern Bolivian Andes inferred from speleothem (δ18O) records for the last 1400 years. **Earth and Planetary Science Letters**, v. 494, p. 124–134, 2018.

ARBUSZEWSKI, J. A. et al. Meridional shifts of the Atlantic intertropical convergence zone since the Last Glacial Maximum. **Nature Geoscience**, v. 6, n. 11, p. 959–962, 2013.

ARELLANO-NAVA, B. et al. Destabilisation of the subpolar North Atlantic prior to the Little Ice Age. **Nature Communications**, v. 13, n. 1, 2022.

ARGOLLO, J.; MOURGUIART, P. Late quaternary climate history of the Bolivian Altiplano. **Quaternary International**, v. 72, n. 1, p. 37–51, 2000.

ARIAS, P. et al. **Climate change 2021: the physical science basis. contribution of working group14 i to the sixth assessment report of the Intergovernmental Panel on Climate Change: technical summary**. Available from: <https://elib.dlr.de/137584/>. Accesso on: 9 Dec. 2021.

ASMEROM, Y. et al. Intertropical convergence zone variability in the Neotropics during the common era. **Science Advances**, v. 6, n. 7, 2020.

AULT, T. R.; COLE, J. E.; ST. GEORGE, S. The amplitude of decadal to multidecadal variability in precipitation simulated by state-of-the-art climate models. **Geophysical Research Letters**, v. 39, n. 21, 2012.

AVILES, A. M. C. et al. Vegetation and climate changes in the forest of Campinas, São Paulo State, Brazil, during the last 25,000 cal yr BP. **Brazilian Journal of Geology**, v. 49, n. 3, 2019.

AZEVEDO, V. et al. Medieval climate variability in the eastern Amazon-Cerrado regions and its archeological implications. **Scientific Reports**, v. 9, n. 1, 2019.

AZEVEDO, V. et al. Paleovegetation seesaw in Brazil since the late pleistocene: a multiproxy study of two biomes. **Earth and Planetary Science Letters**, v. 563, p. 116880–116880, 2021.

BAKER, P. A. et al. Tropical climate changes at millennial and orbital timescales on the Bolivian Altiplano. **Nature**, v. 409, n. 6821, p. 698–701, 2001.

BAKER, P. A. et al. The history of South american tropical precipitation for the past 25,000 years. **Science**, v. 291, n. 5504, p. 640–643, 2001.

BAKER, A. et al. Global analysis reveals climatic controls on the oxygen isotope composition of cave drip water. **Nature Communications**, v. 10, n. 1, 2019.

BAKKER, J. **Tectonic and climatic controls on late quaternary sedimentary processes in a neotectonic intramontane basin, the Pitalito Basin, South Colombia**. 1990. Thesis (Master) - Wageningen University and Research, 1990.

BARBERI, M.; SALGADO-LABOURIAU, M. L.; SUGUIO, K. Paleovegetation and paleoclimate of “Vereda de Águas Emendadas”, central Brazil. **Journal of South American Earth Sciences**, v. 13, n. 3, p. 241–254, 2000.

BAUERMANN, S. G. **Análises palinológicas e evolução paleovegetacional e paleoambiental das turfeiras de Barrocadas e Águas Claras, Planície Costeira do Rio Grande do Sul, Brasil.** 2003. Tese (Doutorado) - Universidade Federal do Rio Grande do Sul, Porto Alegre, 2003.

BAUERMANN, S. G.; BEHLING, H.; BACKES, M. R. Biomas regionais e evolução da paisagem no Rio Grande do Sul com base em paleopalinologia. In: RIBEIRO, A. M. et al (Ed.). **Quaternário do Rio Grande do Sul integrando conhecimentos.** Porto Alegre: SBP, 2009. p. 81–93.

BEHLING, H. Investigations into the late pleistocene and holocene history of vegetation and climate in Santa Catarina (S Brazil). **Vegetation History and Archaeobotany**, v. 4, n. 3, 1995.

BEHLING, H. Late quaternary vegetation, climate and fire history from the tropical mountain region of Morro de Itapeva, SE Brazil. **Palaeogeography, Palaeoclimatology, Palaeoecology**, v. 129, n. 3/4, p. 407–422, 1997.

BEHLING, H. et al. Late quaternary vegetational and climate dynamics in northeastern Brazil, inferences from marine core GeoB 3104-1. **Quaternary Science Reviews**, v. 19, n. 10, p. 981–994, 2000.

BEHLING, H. et al. Late Quaternary vegetational and climate dynamics in southeastern Brazil, inferences from marine cores GeoB 3229-2 and GeoB 3202-1. **Palaeogeography, Palaeoclimatology, Palaeoecology**, v. 179, n. 3, p. 227–243, 2002.

BEHLING, H. et al. Late quaternary araucaria forest, grassland (Campos), fire and climate dynamics, studied by high-resolution pollen, charcoal and multivariate analysis of the Cambará do Sul core in southern Brazil. **Palaeogeography, Palaeoclimatology, Palaeoecology**, v. 203, n. 3/4, p. 277–297, 2004.

BEHLING, H.; HOOGHIEMSTRA, H. Environmental history of the Colombian savannas of the llanos orientales since the last glacial maximum from lake records El Pinal and Carimagua. **Journal of Paleolimnology**, v. 21, n. 4, p. 461–476, 1999.

BEHLING, H.; LICHTE, M. Evidence of dry and cold climatic conditions at glacial times in tropical southeastern Brazil. **Quaternary Research**, v. 48, n. 3, p. 348–358, 1997.

BEHLING, H.; LICHTE, M.; MIKLOS, A. W. Evidence of a forest free landscape under dry and cold climatic conditions during the last glacial maximum in the Botucatú region (São Paulo State), Southeastern Brazil. In: RABASSA, J.; SALEMME, M. (Ed.). **Quaternary of South America and Antarctica Peninsula**. Routledge: Taylor & Francis, 1998. p. 99–110.

BEHLING, H.; NEGRELLE, R. R. B. Tropical rain forest and climate dynamics of the atlantic lowland, southern Brazil, during the late quaternary. **Quaternary Research**, v. 56, n. 3, p. 383–389, 2001.

BEHLING, H. South and southeast Brazilian grasslands during late quaternary times: a synthesis. **Palaeogeography, Palaeoclimatology, Palaeoecology**, v. 177, n. 1/2, p. 19–27, 2002.

BEHLING, H.; PILLAR, V. D.; BAUERMANN, S. G. Late quaternary grassland (Campos), gallery forest, fire and climate dynamics, studied by pollen, charcoal and multivariate analysis of the São Francisco de Assis core in western Rio Grande do Sul (southern Brazil). **Review of Palaeobotany and Palynology**, v. 133, n. 3/4, p. 235–248, 2005.

BERGER, A.L. Long-term variations of daily insolation and quaternary climatic changes. **Journal of the Atmospheric Sciences**, v. 35, n. 12, p. 2362–2367, 1978.

BERNAL, B. P. et al. High-resolution holocene South American monsoon history recorded by a speleothem from Botuverá Cave, Brazil. **Earth and Planetary Science Letters**, v. 450, p. 186–196, 2016.

BIASUTTI, M.; VOIGT, A. Seasonal and CO2-Induced Shifts of the ITCZ: testing energetic controls in idealized simulations with comprehensive models. **Journal of Climate**, v. 33, n. 7, p. 2853–2870, 2020.

BISSA, W. M.; TOLEDO, M. B. Late quaternary vegetational changes in a marsh forest in southeastern Brazil with comments on prehistoric human occupation. **Radiocarbon**, v. 57, n. 5, p. 737–753, 2015.

BIRD, B. W. et al. A 2,300-year-long annually resolved record of the South American summer monsoon from the Peruvian Andes. **Proceedings of the National Academy of Sciences**, v. 108, n. 21, p. 8583–8588, 2011.

BJERKNES. J. Atlantic air-sea interaction. **Advances in Geophysics**, v. 10, n. 1964, p. 1–82, 1964.

BEERLING, D. J.; CHALONER, W. G. Evolutionary responses of stomatal density to global CO2 change. **Biological Journal of the Linnean Society**, v. 48, n. 4, p. 343–353, 1993.

BEHLING, H. et al. Late quaternary vegetational and climate dynamics in northeastern Brazil, inferences from marine core GeoB 3104-1. **Quaternary Science Reviews**, v. 19, n. 10, p. 981–994, 2000.

BEHLING, H. Late quaternary vegetation and climate dynamics in southeastern Amazonia inferred from Lagoa da Confusão in Tocantins State, northern Brazil. **Amazoniana: Limnologia et Oecologia Regionalis Systematis Fluminis Amazonas**, v. 17, n. 1/2, 2002.

BEHLING, H. et al. Late quaternary araucaria forest, grassland (Campos), fire and climate dynamics, studied by high-resolution pollen, charcoal and multivariate analysis of the Cambará do Sul core in southern Brazil. **Palaeogeography, Palaeoclimatology, Palaeoecology**, v. 203, n. 3/4, p. 277–297, 2004.

BEHLING, H.; PILLAR, V. D. Late quaternary vegetation, biodiversity and fire dynamics on the southern Brazilian highland and their implication for conservation and management of modern Araucaria forest and grassland ecosystems. **Philosophical Transactions of the Royal Society B: Biological Sciences**, v. 362, n. 1478, p. 243–251, 2006.

BEHLING, H.; BUSH, M. B.; HOOGHIEMSTRA, H. biotic development of quaternary Amazonia: a palynological perspective. In: HOORN, C.; WESSELINGH, F. P. (Ed.). **Amazonia: landscape and species evolution: a look into the past**. [S.l.]: Wiley, 2011. p. 335–345.

BOBST, A. L. et al. A 106ka paleoclimate record from drill core of the Salar de Atacama, northern Chile. **Palaeogeography, Palaeoclimatology, Palaeoecology**, v. 173, n. 1-2, p. 21–42, 2001.

BETANCOURT, J. L. et al. A 22,000-year record of monsoonal precipitation from northern Chile's Atacama desert. **Science**, v. 289, n. 5484, p. 1542–1546, 2000.

BLARD, P.-H. et al. Late local glacial maximum in the Central Altiplano triggered by cold and locally-wet conditions during the paleolake Tauca episode (17–15ka, Heinrich 1). **Quaternary Science Reviews**, v. 28, n. 27, p. 3414–3427, 2009.

BLARD, P.-H. et al. Lake highstands on the Altiplano (Tropical Andes) contemporaneous with Heinrich 1 and the Younger Dryas: new insights from 14C, U–Th dating and δ18O of carbonates. **Quaternary Science Reviews**, v. 30, n. 27/28, p. 3973–3989, 2011.

BOOTH, B. B. B. et al. Erratum: Aerosols implicated as a prime driver of twentieth-century North Atlantic climate variability. **Nature**, v. 485, n. 7399, p. 534–534, 2012.

BRACONNOT, P. et al. Evaluation of climate models using palaeoclimatic data. **Nature Climate Change**, v. 2, n. 6, p. 417–424, 2012.

BRADLEY, R. S.; JONEST, P. D. "Little Ice Age" summer temperature variations: their nature and relevance to recent global warming trends. **The Holocene**, v. 3, n. 4, p. 367–376, 1993.

BRADLEY, R. S et al. Low latitude ice cores record Pacific sea surface temperatures. **Geophysical Research Letters**, v. 30, n. 4, 2003.

BRADY, E. et al. The connected isotopic water cycle in the community earth system model version 1. **Journal of Advances in Modeling Earth Systems**, v. 11, n. 8, p. 2547–2566, 2019.

BRANDO, P. M. et al. Abrupt increases in Amazonian tree mortality due to drought–fire interactions. **Proceedings of the National Academy of Sciences**, v. 111, n. 17, p. 6347–6352, 2014.

BREHM, N. et al. Eleven-year solar cycles over the last millennium revealed by radiocarbon in tree rings. **Nature Geoscience**, v. 14, n. 1, p. 10–15, 2021.

BRÖNNIMANN, S. et al. Last phase of the Little Ice Age forced by volcanic eruptions. **Nature Geoscience**, v. 12, n. 8, p. 650–656, 2019.

BOUIMETARHAN, I. et al. Intermittent development of forest corridors in northeastern Brazil during the last deglaciation: Climatic and ecologic evidence. **Quaternary Science Reviews**, v. 192, p. 86–96, 2018.

BRUNSCHÖN, C.; BEHLING, H. Late quaternary vegetation, fire and climate history reconstructed from two cores at Cerro Toledo, Podocarpus National Park, southeastern Ecuadorian Andes. **Quaternary Research**, v. 72, n. 3, p. 388–399, 2009.

BUSH, M. B.; COLINVAUX, P. A. A pollen record of a complete glacial cycle from lowland Panama. **Journal of Vegetation Science**, v. 1, n. 1, p. 105–118, 1990.

BUSH, M. B. On the interpretation of fossil Poaceae pollen in the lowland humid neotropics. **Palaeogeography, Palaeoclimatology, Palaeoecology**, v. 177, n. 1-2, p. 5–17, 2002.

BUSH, M. B. 48,000 Years of climate and forest change in a biodiversity hot spot. **Science**, v. 303, n. 5659, p. 827–829, 2004.

BUSH, M. B.; SILMAN, M. R. Observations on late pleistocene cooling and precipitation in the lowland neotropics. **Journal of Quaternary Science**, v. 19, n. 7, p. 677–684, 2004.

BUSH, R. et al. Perspectives on data reproducibility and replicability in paleoclimate and climate science. **HDSR**, v. 2, n. 4, 2020.

BURBRIDGE, R. E.; MAYLE, F. E.; KILLEEN, T. J. Fifty-thousand-year vegetation and climate history of Noel Kempff Mercado National Park, Bolivian Amazon. **Quaternary Research**, v. 61, n. 2, p. 215–230, 2004.

BYRNE, M. P. et al. Response of the intertropical convergence zone to climate change: location, width, and strength. **Current Climate Change Reports**, v. 4, n.4, p.355-370, 2018.

CAESAR, L. et al. Observed fingerprint of a weakening Atlantic Ocean overturning circulation. **Nature**, v. 556, n. 7700, p. 191–196, 2018.

CASSINO, R. F. et al. Vegetation and fire variability in the central Cerrados (Brazil) during the Pleistocene-Holocene transition was influenced by oscillations in the SASM boundary belt. **Quaternary Science Reviews**, v. 232, p. 106209, 2020.

CAMPOS, J. L. P. S. et al. Coherent South American monsoon variability during the last millennium revealed through high-resolution proxy records. **Geophysical Research Letters**, v. 46, n. 14, p. 8261–8270, 2019.

CARNEIRO FILHO, A. et al. Amazonian paleodunes provide evidence for drier climate phases during the late pleistocene–holocene. **Quaternary Research**, v. 58, n. 2, p. 205–209, 2002.

CERÓN, W. L et al. The influence of the atlantic multidecadal oscillation on the Choco low-level jet and precipitation in Colombia. **Atmosphere**, v. 11, n. 2, p. 174, 2020.

CERÓN, W. L. et al. Pacific and Atlantic multidecadal variability relations with the Choco and Caribbean low-level jets during the 1900–2015 period. **Atmosphere**, v. 12, n. 9, p. 1120, 2021.

CHENG, H. et al. Climate change patterns in Amazonia and biodiversity. **Nature Communications**, v. 4, n. 1, 2013.

CHIESSI, C. M. et al. Possible impact of the Atlantic Multidecadal Oscillation on the South American summer monsoon. **Geophysical Research Letters**, v. 36, n. 21, 2009.

CHIESSI, C. M. et al. Thermal evolution of the western South Atlantic and the adjacent continent during Termination 1. **Climate of the Past**, v. 11, n. 6, p. 915–929, 2015.

CHIESSI, C. M. et al. Mid- to late holocene contraction of the intertropical convergence zone over northeastern South America. **Paleoceanography and Paleoclimatology**, v. 36, n. 4, 2021

CIEMER, C. et al. Higher resilience to climatic disturbances in tropical vegetation exposed to more variable rainfall. **Nature Geoscience**, v. 12, n. 3, p. 174–179, 2019.

CLARK, P. U. et al. The last glacial maximum. **Science**, v. 325, n. 5941, p. 710–714, 2009.

CLEMENT, A. et al. The Atlantic multidecadal oscillation without a role for ocean circulation. **Science**, v. 350, n. 6258, p. 320–324, 2015.

CLELAND, E. et al. Shifting plant phenology in response to global change. **Trends in Ecology & Evolution**, v. 22, n. 7, p. 357–365, 2007.

COMAS-BRU, L. et al. SISALv2: a comprehensive speleothem isotope database with multiple age–depth models. **Earth System Science Data**, v. 12, n. 4, p. 2579–2606, 2020.

COSTA, G. C. et al. Biome stability in South America over the last 30 kyr: inferences from long-term vegetation dynamics and habitat modelling. **Global Ecology and Biogeography**, v. 27, n. 3, p. 285–297, 2018.

COHEN, M. C. L. et al. Late pleistocene glacial forest of Humaitá: western Amazonia. **Palaeogeography, Palaeoclimatology, Palaeoecology**, v. 415, p. 37–47, 2014.

COLLINS, M. Long-term climate change: projections, commitments and irreversibility. In: STOCKER, T. F. et al. **Climate change 2013: the physical science basis. contribution of working group i to the fifth assessment report of the Intergovernmental Panel on Climate Change**. Cambridge: Cambridge University Press, 2013. p. 1029-1136.

COLINVAUX, P. A. et al. A long pollen record from lowland Amazonia: forest and cooling in glacial times. **Science**, v. 274, n. 5284, p. 85–88, 1996.

COLINVAUX, P. A.; OLIVEIRA, P. E.; BUSH, M. B. Amazonian and neotropical plant communities on glacial time-scales: the failure of the aridity and refuge hypotheses. **Quaternary Science Reviews**, v. 19, n. 1, p. 141–169, 2000.

COLINVAUX, P. A. et al. A paradigm to be discarded: geological and paleoecological data falsify the HAFFER & PRANCE refuge hypothesis of Amazonian speciation. In: CASPERS, H. (Ed.). **Amazoniana: limnologia et oecologia regionalis systematis fluminis Amazonas**. [S.l.]: Wiley, 2001.

CORDEIRO, R. C. et al. Biogeochemical indicators of environmental changes from 50Ka to 10Ka in a humid region of the Brazilian Amazon. **Palaeogeography, Palaeoclimatology, Palaeoecology**, v. 299, n. 3, p. 426–436, 2011.

ORDEIRO, R. C. et al. Palaeofires in Amazon: interplay between land use change and palaeoclimatic events. **Palaeogeography, Palaeoclimatology, Palaeoecology**, v. 415, p. 137–151, 2014.

COWLING, S. A.; SYKES, M. T. Physiological significance of low atmospheric CO_2 for plant–climate interactions. **Quaternary Research**, v. 52, n. 2, p. 237–242, 1999.

CRUZ, F. W. et al. Insolation-driven changes in atmospheric circulation over the past 116,000 years in subtropical Brazil. **Nature**, v. 434, n. 7029, p. 63–66, 2005.

CRUZ, F. W. et al. Reconstruction of regional atmospheric circulation features during the late Pleistocene in subtropical Brazil from oxygen isotope composition of speleothems. **Earth and Planetary Science Letters**, v. 248, n. 1, p. 495–507, 2006.

CRUZ, F. W. et al. Orbitally driven east–west antiphasing of South American precipitation. **Nature Geoscience**, v. 2, n. 3, p. 210–214, 2009.

D'APOLITO, C.; LATRUBESSE, E. M.; ABSY, M. L. Results confirm a relatively dry setting during the last glacial (MIS 3 and LGM) in Carajás, Amazonia: a comment on Guimarães et al. **The Holocene**, v. 28, n. 2, p. 330–331, 2017.

DANTAS, M. A. T. et al. Paleoecology and radiocarbon dating of the Pleistocene megafauna of the Brazilian Intertropical Region. **Quaternary Research**, v. 79, n. 1, p. 61–65, 2013.

DANSGAARD, W. Stable isotopes in precipitation. **Tellus**, v. 16, n. 4, p. 436–468, 1964.

DELLA LIBERA, M. E. et al. Paleoclimatic and paleoenvironmental changes in Amazonian lowlands over the last three millennia. **Quaternary Science Reviews**, v. 279, p. 107383, 2022.

DELWORTH, T.L. et al. The central role of ocean dynamics in connecting the North Atlantic Oscillation to the extratropical component of the Atlantic Multidecadal Oscillation. **Journal of Climate**, v.30, n.10, p.3789-3805, 2017.

DEININGER, M. W. et al. Late quaternary variations in the South American monsoon system as inferred by speleothems: new perspectives using the SISAL database. **Quaternary**, v. 2, n. 1, p. 6, 2019.

DE OLIVEIRA, P. E. **A palynological record of Late Quaternary vegetational and climatic change in southeastern Brazil - ProQuest**. 1992. Thesis (Phd) - The Ohio State University, 1992.

DE OLIVEIRA, P. E. et al. Climate change and biogeographic connectivity across the Brazilian cerrado. **Journal of Biogeography**, v. 47, n. 2, p. 396–407, 2019.

DITLEVSEN, P.; DITLEVSEN, S. Warning of a forthcoming collapse of the Atlantic meridional overturning circulation. **Nature Communications**, v. 14, n. 1, p. 4254, 2023.

DOMBROSKI, J. L. D. et al. Water relations of Caatinga trees in the dry season. **South African Journal of Botany**, v. 77, n. 2, p. 430–434, 2011.

DUFFY, P. B. et al. Projections of future meteorological drought and wet periods in the Amazon. **Proceedings of the National Academy of Sciences**, v. 112, n. 43, p. 13172–13177, 2015.

DUFRESNE, J.-L. et al. Climate change projections using the IPSL-CM5 Earth system model: from CMIP3 to CMIP5. **Climate Dynamics**, v. 40, n. 9/10, p. 2123–2165, 2013.

DUPONT, L. M. et al. Two-step vegetation response to enhanced precipitation in Northeast Brazil during Heinrich event 1. **Global Change Biology**, v. 16, n. 6, p. 1647–1660, 2009.

ENFIELD, D.B.; MESTAS-NUÑEZ, A.M.; TRIMBLE, P.J. The Atlantic multidecadal oscillation and its relation to rainfall and river flows in the continental US. **Geophysical Research Letters**, v28, n.10, p. 2077–2080, 2001.

ESQUIVEL-MUELBERT, A. et al. Compositional response of Amazon forests to climate change. **Global Change Biology**, v. 25, n. 1, p. 39–56, 2018.

ETTERSON, J. R.; SHAW, R. G. Constraint to adaptive evolution in response to global warming. **Science**, v. 294, n. 5540, p. 151–154, 2001.

EYRING, V. et al. Overview of the Coupled Model Intercomparison Project Phase 6 (CMIP6) experimental design and organization. **Geoscientific Model Development**, v. 9, n. 5, p. 1937–1958, 2016.

FLANTUA, S. G. A. et al. Updated site compilation of the Latin American pollen database. **Review of Palaeobotany and Palynology**, v. 223, p. 104–115, 2015.

FLATO, G. M. Earth system models: an overview. **Climate Change**, v. 2, n. 6, p. 783–800, 2011.

FONTES, D. et al. Paleoenvironmental dynamics in South Amazonia, Brazil, during the last 35,000 years inferred from pollen and geochemical records of Lago do Saci. **Quaternary Science Reviews**, v. 173, p. 161–180, 2017.

FOLLAND, C.K.; PARKER, D.E.; KATES, F.E. Worldwide marine temperature fluctuations 1856–1981. **Nature**, v.310, n.5979, p.670–673,1984.

FORNACE, K. L. et al. Late quaternary environmental change in the interior South American tropics: new insight from leaf wax stable isotopes. **Earth and Planetary Science Letters**, v. 438, p. 75–85, 2016.

FRAJKA-WILLIAMS, E.; BEAULIEU, C.; DUCHEZ, A. Emerging negative atlantic multidecadal oscillation index in spite of warm subtropics. **Scientific Reports**, v. 7, n. 1, 2017.

FREITAS, H. A. et al. Late quaternary vegetation dynamics in the southern Amazon basin inferred from carbon isotopes in soil organic matter. **Quaternary Research**, v. 55, n. 1, p. 39–46, 2001.

FRITZ, S. C. et al. Quaternary glaciation and hydrologic variation in the South American tropics as reconstructed from the Lake Titicaca drilling project. **Quaternary Research**, v. 68, n. 3, p. 410–420, 2007.

GARCIA, S. R.; KAYANO, M. T. Some evidence on the relationship between the South American monsoon and the Atlantic ITCZ. **Theoretical and Applied Climatology**, v. 99, n. 1-2, p. 29–38, 2009.

GARREAUD, R. D. et al. Present-day South American climate. **Palaeogeography, Palaeoclimatology, Palaeoecology**, v. 281, n. 3/4, p. 180–195, 2009.

GATTI, L. V. et al. Amazonia as a carbon source linked to deforestation and climate change. **Nature**, v. 595, n. 7867, p. 388–393, 2021.

GAYO, E. M. et al. Late quaternary hydrological and ecological changes in the hyperarid core of the northern Atacama Desert (~21°S). **Earth-Science Reviews**, v. 113, n. 3-4, p. 120–140, 2012.

GENT, P. R. et al. The community climate system model version 4. **Journal of Climate**, v. 24, n. 19, p. 4973–4991, 2011.

GERHART, L. M.; WARD, J. K. Plant responses to low [CO2] of the past. **New Phytologist**, v. 188, n. 3, p. 674–695, 2010.

GIORGETTA, M. A. et al. Climate and carbon cycle changes from 1850 to 2100 in MPI-ESM simulations for the Coupled Model Intercomparison Project phase 5. **Journal of Advances in Modeling Earth Systems**, v. 5, n. 3, p. 572–597, 2013.

GOMES, M. O. S.; MEYER, K. E. B.; PESSENDA, L. C. R. Reconstituição paleoambiental da Vereda Carrasco da Raposa, Parque Estadual da Serra do Cabral, MG, Brasil, por meio de estudos palinológico e isotópico. **Pesquisas em Geociências**, v. 44, n. 1, p. 41–62, 2017.

GONZÁLEZ-OROZCO, C. E. et al. Phylogenetic approaches reveal biodiversity threats under climate change. **Nature Climate Change**, v. 6, n. 12, p. 1110–1114, 2016.

GONZÁLEZ, C.; URREGO, L. E.; MARTÍNEZ, J. I. Late quaternary vegetation and climate change in the Panama Basin: palynological evidence from marine cores ODP 677B and TR 163-38. **Palaeogeography, Palaeoclimatology, Palaeoecology**, v. 234, n. 1, p. 62–80, 2006.

GOSLING, W. D. et al. Glacial-interglacial changes in moisture balance and the impact on vegetation in the southern hemisphere tropical Andes (Bolivia/Peru). **Palaeogeography, Palaeoclimatology, Palaeoecology**, v. 259, n. 1, p. 35–50, 2008.

GROOT, M. H. M. et al. Ultra-high resolution pollen record from the northern Andes reveals rapid shifts in montane climates within the last two glacial cycles. **Climate of the Past**, v. 7, n. 1, p. 299–316, 2011.

GROSJEAN, M. Paleohydrology of the Laguna Lejía (north Chilean Altiplano) and climatic implications for late-glacial times. **Palaeogeography, Palaeoclimatology, Palaeoecology**, v. 109, n. 1, p. 89–100, 1994.

GROSJEAN, M. A 22,000 14C year BP sediment and pollen record of climate change from Laguna Miscanti (23°S), northern Chile. **Global and Planetary Change**, v. 28, n. 1-4, p. 35–51, 2001.

GROVE, J.M. The Initiation of the “Little Ice Age” in Regions Round the North Atlantic. **Climatic Change**, v. 48, n. 1, p. 53–82, 2001.

GU, F. et al. Long-term vegetation, climate and ocean dynamics inferred from a 73,500 years old marine sediment core (GeoB2107-3) off southern Brazil. **Quaternary Science Reviews**, v. 172, p. 55–71, 2017.

GU, F. et al. Late quaternary environmental dynamics inferred from marine sediment core GeoB6211-2 off southern Brazil. **Palaeogeography, Palaeoclimatology, Palaeoecology**, v. 496, p. 48–61, 2018.

GUAN, B.; NIGAM, S. Analysis of Atlantic SST variability factoring interbasin links and the secular trend: clarified structure of the atlantic multidecadal oscillation. **Journal of Climate**, v. 22, n. 15, p. 4228–4240, 2009.

HABERLE, S. G.; MASLIN, M. A. Late quaternary vegetation and climate change in the Amazon basin based on a 50,000 year pollen record from the Amazon Fan, ODP Site 932. **Quaternary Research**, v. 51, n. 1, p. 27–38, 1999.

HAN, Z. et al. Simulation by CMIP5 models of the atlantic multidecadal oscillation and its climate impacts. **Advances in Atmospheric Sciences**, v.33, n.12, p.1329–1342, 2016.

HARRISON, S. P.; BARTLEIN, P. Records from the past, lessons for the future: what the palaeorecord implies about mechanisms of global change. In: HENDERSON, A.; MCGUFFIE, K. (Ed.). **Macquarie**. Amsterdam: Elsevier, 2012. p. 403–436.

HARLASS, J.; LATIF, M.; PARK, W. Improving climate model simulation of tropical Atlantic sea surface temperature: The importance of enhanced vertical atmosphere model resolution. **Geophysical Research Letters**, v. 42, n. 7, p. 2401–2408, 2015.

HARRISON, S. P. et al. Evaluation of CMIP5 palaeo-simulations to improve climate projections. **Nature Climate Change**, v. 5, n. 8, p. 735–743, 2015.

HAUG, G. H. Southward migration of the intertropical convergence zone through the holocene. **Science**, v. 293, n. 5533, p. 1304–1308, 2001.

HAWCROFT, M. et al. Southern Ocean albedo, inter-hemispheric energy transports and the double ITCZ: global impacts of biases in a coupled model. **Climate Dynamics**, v. 48, n. 7-8, p. 2279–2295, 2016.

HÄGGI, C. et al. Response of the Amazon rainforest to late Pleistocene climate variability. **Earth and Planetary Science Letters**, v. 479, p. 50–59, 2017.

HE, C. et al. Abrupt Heinrich Stadial 1 cooling missing in Greenland oxygen isotopes. **Science dvances**, v.7, n.25, eabh1007, 2021.

HEINE, K.; HEINE, J. T. Late-glacial climatic fluctuations in Ecuador: glacier retreat during younger dryas time. **Arctic and Alpine Research**, v. 28, n. 4, p. 496–501, 1996.

HEGERL, G. C. et al. Causes of climate change over the historical record. **Environmental Research Letters**, v. 14, n. 12, p. 123006, 2019.

HELMENS, K. F. et al. Warming at 18,000 yr B.P. in the Tropical Andes. **Quaternary Research**, v. 45, n. 3, p. 289–299, 1996.

HELMENS, K. F.; KUHRY, P. Middle and late quaternary vegetational and climatic history of the paramo de Agua Blanca (Eastern Cordillera, Colombia). **Palaeogeography, Palaeoclimatology, Palaeoecology**, v. 56, n. 3-4, p. 291–335, 1986.

HERMANOWSKI, B.; COSTA, M. L.; BEHLING, H. Environmental changes in southeastern Amazonia during the last 25,000 yr revealed from a paleoecological record. **Quaternary Research**, v. 77, n. 1, p. 138–148, 2012.

HERMANOWSKI, B.; COSTA, M. L.; BEHLING, H. Possible linkages of palaeofires in southeast Amazonia to a changing climate since the Last Glacial Maximum. **Vegetation History and Archaeobotany**, v. 24, n. 2, p. 279–292, 2015.

HEUSSER, L. E.; SHACKLETON, N. J. Tropical climatic variation on the pacific slopes of the ecuadorian andes based on a 25,000-year pollen record from deep-sea sediment core Tri 163-31B. **Quaternary Research**, v. 42, n. 2, p. 222–225, 1994.

HILLYER, R. et al. A 24,700-yr paleolimnological history from the Peruvian Andes. **Quaternary Research**, v. 71, n. 1, p. 71–82, 2009.

HODSON, D. et al. Coupled climate response to Atlantic multidecadal variability in a multi-model multi-resolution ensemble. **Climate Dynamics**, v. 59, n. 3/4, p. 805–836, 2022.

HOFFMANN, A. A.; SGRÒ, C. M. Climate change and evolutionary adaptation. **Nature**, v. 470, n. 7335, p. 479–485, 2011.

HOEGH-GULDBERG, O. et al. Impacts of 1.5°C global warming on natural and human systems. In: INTERGOVERNMENTAL PLANEL ON CLIMATE CHANGE (IPCC) (Ed.). **Global warming of 1.5° C**. [S.l.]: IPCC, 2018.

HONG, J.-S.; YEH, S.-W.; YANG, Y.-M. Inter-basin interactions between the Pacific and Atlantic Oceans depending on the phase of Pacific decadal Oscillation and Atlantic multi-decadal oscillation. **Journal of Climate**, p. 1–38, 2021.

HOURDIN, F. et al. The art and science of climate model tuning. **Bulletin of the American Meteorological Society**, v. 98, n. 3, p. 589–602, 2017.

HOU, A. et al. Insolation and greenhouse gas forcing of the South American monsoon system across three glacial-interglacial cycles. **Geophysical Research Letters**, v. 47, n. 14, 2020.

INTERGOVERNMENTAL PLANEL ON CLIMATE CHANGE (IPCC). **Climate change 2013:** the physical science basis. Cambridge: Cambridge University Press, 2013.

INTERGOVERNMENTAL PLANEL ON CLIMATE CHANGE (IPCC). **Sixth assessment report**. 2021. Available from: https://www.ipcc.ch/report/ar6/wg1/.

JACOB, J. et al. Paleohydrological changes during the last deglaciation in Northern Brazil. **Quaternary Science Reviews**, v. 26, n. 7, p. 1004–1015, 2007.

JACOB, J. et al. Major environmental changes recorded by lacustrine sedimentary organic matter since the last glacial maximum near the equator (Lagoa do Caçó, NE Brazil). **Palaeogeography, Palaeoclimatology, Palaeoecology**, v. 205, n. 3-4, p. 183–197, 2004.

JESKE-PIERUSCHKA, V.; BEHLING, H. Palaeoenvironmental history of the São Francisco de Paula region in southern Brazil during the late Quaternary inferred from the Rincão das Cabritas core. **The Holocene**, v. 22, n. 11, p. 1251–1262, 2012.

JESKE-PIERUSCHKA, V. et al. New insights into vegetation, climate and fire history of southern Brazil revealed by a 40,000 year environmental record from the State Park Serra do Tabuleiro. **Vegetation History and Archaeobotany**, v. 22, n. 4, p. 299–314, 2012.

JONES, C.; CARVALHO, L. M. V. Climate change in the South American monsoon system: present climate and CMIP5 projections. **Journal of Climate**, v. 26, n. 17, p. 6660–6678, 2013.

JONES, C.; CARVALHO, L. M. V. The influence of the Atlantic multidecadal oscillation on the eastern Andes low-level jet and precipitation in South America. **Climate and Atmospheric Science**, v. 1, n. 1, 2018.

JONES, P. D.; MANN, M.E. Climate over past millennia. **Reviews of Geophysics**, v. 42, n. 2, 2004.

JUNGCLAUS, J. H. et al. The PMIP4 contribution to CMIP6 – Part 3: the last millennium, scientific objective, and experimental design for the PMIP4 past1000 simulations. **Geoscientific Model Development**, v. 10, n. 11, p. 4005–4033, 2017. Available from: https://doi.org/10.5194/gmd-10-4005-2017.

JUNQUAS, C. et al. Influence of South America orography on summertime precipitation in Southeastern South America. **Climate Dynamics**, v. 46, n. 11/12, p. 3941–3963, 2015.

KANNER, L. C. et al. High-latitude forcing of the South American summer monsoon during the last glacial. **Science**, v. 335, n. 6068, p. 570–573, 2012.

KANNER, L. C. et al. High-resolution variability of the South American summer monsoon over the last seven millennia: insights from a speleothem record from the central Peruvian Andes. **Quaternary Science Reviews**, v. 75, p. 1–10, 2013.

KAGEYAMA, M. et al. The PMIP4 contribution to CMIP6 – Part 4: scientific objectives and experimental design of the PMIP4-CMIP6 Last Glacial Maximum experiments and PMIP4 sensitivity experiments. **Geoscientific Model Development**, v. 10, n. 11, p. 4035–4055, 2017.

KAGEYAMA, M. et al. The PMIP4 last glacial maximum experiments: preliminary results and comparison with the PMIP3 simulations. **Climate of the Past**, v. 17, n. 3, p. 1065–1089, 2021.

KAYANO, M. T.; ANDREOLI, R. V. Relations of South American summer rainfall interannual variations with the Pacific Decadal Oscillation. **Dynamics of Atmospheres and Oceans**, v. 27, n. 4, p. 531–540, 2007.

KAYANO, M. T. et al. A further analysis of the tropical Atlantic SST modes and their relations to north-eastern Brazil rainfall during different phases of Atlantic Multidecadal Oscillation. **International Journal of Climatology**, v. 36, n. 12, p. 4006–4018, 2016.

KAYANO, M. T.; SETZER, A. W. Nearly synchronous multidecadal oscillations of surface air temperature in Punta Arenas and the atlantic multidecadal oscillation index. **Journal of Climate**, v. 31, n. 18, p. 7237–7248, 2018.

KAYANO, M. T.; ANDREOLI, R. V.; SOUZA, R. A. F. Pacific and Atlantic multidecadal variability relations to the El Niño events and their effects on the South American rainfall. **International Journal of Climatology**, v. 40, n. 4, p. 2183–2200, 2019.

KAYANO, M. T. et al. Isolated effects of Indian Ocean basin-wide and El Niño–southern oscillation on austral winter rainfall over South America. **Atmosphere**, v. 12, n. 12, p. 1605, 2021.

KAYANO, M. T. et al. Does the El Niño-southern oscillation affect the combined impact of the atlantic multidecadal oscillation and pacific decadal oscillation on the precipitation and surface air temperature variability over South America? **Atmosphere**, v. 13, n. 2, p. 231, 2022.

KHAN, N. S. et al. Inception of a global atlas of sea levels since the Last Glacial Maximum. **Quaternary Science Reviews**, v. 220, p. 359–371, 2019.

KENDALL, C.; CALDWELL, E. A. Fundamentals of isotope geochemistry. In: KENDALL, C.; MCDONNELL, J. J. (Ed.). **Isoptope tracers in catchment hydrology**. Amsterdam: Elsevier, 1998. p. 51–86.

KIM, H.-J.; AN, S.-I.; KIM, D. Timescale-dependent AMOC–AMO relationship in an earth system model of intermediate complexity. **International Journal of Climatology**, v. 41, n. S1, 2020.

KNIGHT, J. R. The Atlantic Multidecadal Oscillation inferred from the forced climate response in coupled general circulation models. **Journal of Climate**, v. 22, n. 7, p. 1610–1625, 2009.

KNIGHT, J. R.; FOLLAND, C. K.; SCAIFE, A. A. Climate impacts of the Atlantic Multidecadal Oscillation. **Geophysical Research Letters**, v. 33, n. 17, 2006.

KNUTTI, R.; SEDLÁČEK, J. Robustness and uncertainties in the new CMIP5 climate model projections. **Nature Climate Change**, v. 3, n. 4, p. 369–373, 2012.

KNUDSEN, M. F. et al. Tracking the Atlantic Multidecadal Oscillation through the last 8,000 years. **Nature Communications**, v. 2, n. 1, p. 1–8, 2011.

KNUDSEN, M. F. et al. Evidence for external forcing of the Atlantic Multidecadal Oscillation since termination of the Little Ice Age. **Nature Communications**, v. 5, n. 1, 2014.

KONAPALA, G. et al. Climate change will affect global water availability through compounding changes in seasonal precipitation and evaporation. **Nature Communications**, v. 11, n. 1, p. 1–10, 2020.

KOSTER, R. D. Regions of strong coupling between soil moisture and precipitation. **Science**, v. 305, n. 5687, p. 1138–1140, 2004.

KRAVTSOV, S.; GRIMM, C.; GU, S. Global-scale multidecadal variability missing in state-of-the-art climate models. **Climate and Atmospheric Science**, v. 1, n. 1, p. 1–10, 2018.

KRISHNAMURTHY, L.; KRISHNAMURTHY, V. Teleconnections of Indian monsoon rainfall with AMO and Atlantic tripole. **Climate Dynamics**, v. 46, n. 7/8, p. 2269–2285, 2015.

KOCK, S. T. et al. Stable oxygen isotope records (δ18O) of a high-andean cushion peatland in NW Argentina (24° S) imply South American summer monsoon related moisture changes during the late holocene. **Frontiers in Earth Science**, v. 7, 2019a.

KOCK, S. T. et al. Late Holocene environmental changes reconstructed from stable isotope and geochemical records from a cushion-plant peatland in the Chilean Central Andes (27°S). **Journal of Quaternary Science**, v. 34, n. 2, p. 153–164, 2019b.

KÖRNER, C. et al. Carbon flux and growth in mature deciduous forest trees exposed to elevated CO2. **Science**, v. 309, n. 5739, p. 1360–1362, 2005.

KUCHARSKI, F. et al. Atlantic forcing of Pacific decadal variability. **Climate Dynamics**, v. 46, n. 7-8, p. 2337–2351, 2015.

KUMAR, D.; KODRA, E.; GANGULY, A. R. Regional and seasonal intercomparison of CMIP3 and CMIP5 climate model ensembles for temperature and precipitation. **Climate Dynamics**, v. 43, n. 9-10, p. 2491–2518, 2014.

KULL, C. et al. Evidence of an LGM cooling in NW-Argentina (22°S) derived from a glacier climate model. **Quaternary International**, v. 108, n. 1, p. 3–11, 2003.

KULL, C. et al. Late Pleistocene glaciation in the Central Andes: temperature versus humidity control: a case study from the eastern Bolivian Andes (17°S) and regional synthesis. **Global and Planetary Change**, v. 60, n. 1/2, p. 148–164, 2008.

KUTZBACH, J. E. et al. Climate and biome simulations for the past 21,000 years. **Quaternary Science Reviews**, v. 17, n. 6-7, p. 473–506, 1998.

LACHNIET, M.S. Climatic and environmental controls on speleothem oxygen-isotope values. **Quaternary Science Reviews**, v. 28, n. 5-6, p. 412–432, 2009.

LAPOLA, D. M.; OYAMA, M. D.; NOBRE, C. A. Exploring the range of climate biome projections for tropical South America: the role of CO2fertilization and seasonality. **Global Biogeochemical Cycles**, v. 23, n. 3, 2009.

LAPOLA, D. M. et al. Pervasive transition of the Brazilian land-use system. **Nature Climate Change**, v. 4, n. 1, p. 27–35, 2013.

LAPOLA, D. M. et al. The drivers and impacts of Amazon forest degradation. **Science**, v. 379, n. 6630, 2023.

LAPOINTE, F. et al. Annually resolved Atlantic sea surface temperature variability over the past 2,900 y. **Proceedings of the National Academy of Sciences**, v. 117, n. 44, p. 27171–27178, 2020.

LAPOINTE, F.; BRADLEY, R. S. Little ice age abruptly triggered by intrusion of Atlantic waters into the Nordic Seas. **Science Advances**, v. 7, n. 51, 2021.

LATORRE, C. et al. Vegetation invasions into absolute desert: A 45;th000 yr rodent midden record from the Calama–Salar de Atacama basins, northern Chile (lat 22°–24°S). **Geological Society of America Bulletin**, v. 114, n. 3, p. 349–366, 2002.

LATORRE, C.; BETANCOURT, J. L.; ARROYO, M. T. K. Late quaternary vegetation and climate history of a perennial river canyon in the Río Salado basin (22°S) of Northern Chile. **Quaternary Research**, v. 65, n. 3, p. 450–466, 2006.

LATRUBESSE, E. M.; FRANZINELLI, E. The late quaternary evolution of the Negro River, Amazon, Brazil: Implications for island and floodplain formation in large anabranching tropical systems. **Geomorphology**, v. 70, n. 3-4, p. 372–397, 2005.

LATRUBESSE, E. M. et al. Late quaternary megafans, fans and fluvio-aeolian interactions in the Bolivian Chaco, Tropical South America. **Palaeogeography, Palaeoclimatology, Palaeoecology**, v. 356-357, p. 75–88, 2012.

LEDRU, M.-P. et al. The last 50,000 years in the Neotropics (Southern Brazil): evolution of vegetation and climate. **Palaeogeography, Palaeoclimatology, Palaeoecology**, v. 123, n. 1/4, p. 239–257, 1996.

LEDRU, M.-P. **The Cerrados of Brazil: ecology and natural history of a Neotropical savanna**. [S.l.]: Columbia University Press, 2002.

LEDRU, M.-P. et al. Millenial-scale climatic and vegetation changes in a northern Cerrado (Northeast, Brazil) since the Last Glacial Maximum. **Quaternary Science Reviews**, v. 25, n. 9-10, p. 1110–1126, 2006.

LEDRU, M.-P.; MOURGUIART, P.; RICCOMINI, C. Related changes in biodiversity, insolation and climate in the Atlantic rainforest since the last interglacial. **Palaeogeography, Palaeoclimatology, Palaeoecology**, v. 271, n. 1/2, p. 140–152, 2009.

LEE, L. et al. The magnitude and causes of uncertainty in global model simulations of cloud condensation nuclei. **Atmospheric Chemistry and Physics**, v. 13, n. 17, p. 8879–8914, 2013.

LEITE-FILHO, A. T.; SOUSA PONTES, V. Y.; COSTA, M. H. Effects of deforestation on the onset of the rainy season and the duration of dry spells in southern Amazonia. **Journal of Geophysical Research: Atmospheres**, v. 124, n. 10, p. 5268–5281, 2019.

LEITE, Y. L. R. et al. Neotropical forest expansion during the last glacial period challenges refuge hypothesis. **Proceedings of the National Academy of Sciences**, v. 113, n. 4, p. 1008–1013, 2016.

LENTERS, J. D.; COOK, K. H. On the origin of the Bolivian high and related circulation features of the South American climate. **Journal of the Atmospheric Sciences**, v. 54, n. 5, p. 656–678, 1997.

LENTON, T. M. et al. Tipping elements in the Earth's climate system. **Proceedings of the National Academy of Sciences**, v. 105, n. 6, p. 1786–1793, 2008.

LENTON, T. M. Land and ocean carbon cycle feedback effects on global warming in a simple Earth system model. **Tellus B: Chemical and Physical Meteorology**, v. 52, n. 5, p. 1159–1188, 2000.

LEVINE, A. F. Z.; FRIERSON, D. M. W.; MCPHADEN, M. J. AMO Forcing of multidecadal Pacific ITCZ variability. **Journal of Climate**, v. 31, n. 14, p. 5749–5764, 2018.

LI, L. et al. The flexible global ocean-atmosphere-land system model, Grid-point Version 2: FGOALS-g2. **Advances in Atmospheric Sciences**, v. 30, n. 3, p. 543–560, 2013.

LIMA, A. L. A.; RODAL, M. J. N. Phenology and wood density of plants growing in the semi-arid region of northeastern Brazil. **Journal of Arid Environments**, v. 74, n. 11, p. 1363–1373, 2010.

LIU, W. et al. Climate impacts of a weakened Atlantic Meridional overturning circulation in a warming climate. **Science Advances**, v. 6, n. 26, eaaz4876, 2020.

LONDOÑO, A. I. et al. Episodic eolian deposition in the past ca. 50,000years in the Alto Ilo dune field, southern Peru. **Palaeogeography, Palaeoclimatology, Palaeoecology**, v. 346-347, p. 12–24, 2012.

LOVEJOY, T. E.; NOBRE, C. Amazon tipping point: Last chance for action. **Science Advances**, v. 5, n. 12, eaba2949, 2019.

LU, R.; DONG, B.; DING, H. Impact of the Atlantic multidecadal oscillation on the Asian summer monsoon. **Geophysical Research Letters**, v.33, n.24, 2006.

LÜNING, S. et al. The medieval climate anomaly in South America. **Quaternary International**, v. 508, p. 70–87, 2019.

MAKSIC, J. et al. Simulation of the Holocene climate over South America and impacts on the vegetation. **The Holocene**, v. 29, n. 2, p. 287–299, 2018.

MAKSIC, J.; VENANCIO, I. M.; SHIMIZU, M. H. **Compilation of proxy data from paleoclimate archives of South America.** 2021. Available from: https://doi.org/10.1594/PANGAEA.927527. Access on: 13 July 2023.

MAMALAKIS, A. et al. Zonally contrasting shifts of the tropical rain belt in response to climate change. **Nature Climate Change**, v. 11, n. 2, p. 143–151, 2021.

MANN, M. E.; JONES, P. D. Global surface temperatures over the past two millennia. **Geophysical Research Letters**, v. 30, n. 15, 2003.

MANN, M. E. et al. Global signatures and dynamical origins of the little ice age and medieval climate anomaly. **Science**, v. 326, n. 5957, p. 1256–1260, 2009.

MARENGO, J. A.; TORRES, R. R.; ALVES, L. M. Drought in Northeast Brazil: past, present, and future. **Theoretical and Applied Climatology**, v. 129, n. 3;4, p. 1189–1200, 2016.

MARENGO, J. A. et al. Extreme seasonal climate variations in the Amazon Basin: droughts and floods. In: NAGY, L.; FORSBERG, B.; ARTAXO, P. (Ed.). **Interactions between biosphere, atmosphere and human land use in the Amazon basin.** Heidelberg: Springer, 2016. p. 55–76.

MARENGO, J. A. et al. Assessing drought in the drylands of northeast Brazil under regional warming exceeding 4 °C. **Natural Hazards**, v. 103, n. 2, p. 2589–2611, 2020.

MAYLE, F. E. Millennial-scale dynamics of southern Amazonian rain forests. **Science**, v. 290, n. 5500, p. 2291–2294, 2000.

MCGEE, D. et al. Changes in ITCZ location and cross-equatorial heat transport at the Last Glacial Maximum, Heinrich Stadial 1, and the mid-Holocene. **Earth and Planetary Science Letters**, v. 390, p. 69–79, 2014.

MEDINA, M. M. et al. Atlantic ITCZ variability during the Holocene based on high-resolution speleothem isotope records from northern Venezuela. **Quaternary Science Reviews**, v. 307, p. 108056–108056, 2023.

MEEHL, G. A. et al. Overview of the coupled model intercomparison project. **Bulletin of the American Meteorological Society**, v. 86, n. 1, p. 89–93, 2005.

MEEHL, G. A. et al. THE WCRP CMIP3 multimodel dataset: a new era in climate change research. **Bulletin of the American Meteorological Society**, v. 88, n. 9, p. 1383–1394, 2007.

MIAO, J.; JIANG, D. Multidecadal variations in the east Asian winter monsoon and their relationship with the Atlantic multidecadal oscillation since 1850. **Journal of Climate**, v. 34, n. 18, p. 7525–7539, 2021.

MILLER, G. H. et al. Abrupt onset of the Little Ice Age triggered by volcanism and sustained by sea-ice/ocean feedbacks. **Geophysical Research Letters**, v. 39, n. 2, 2012.

MOURGUIART, P.; LEDRU, M.-P. Last glacial maximum in an Andean cloud forest environment (Eastern Cordillera, Bolivia): comment and reply. **Geology**, v. 31, n. 1, p. e27, 2003.

MUELLER, B.; SENEVIRATNE, S. I. Systematic land climate and evapotranspiration biases in CMIP5 simulations. **Geophysical Research Letters**, v. 41, n. 1, p. 128–134, 2014.

MULITZA, S. et al. Synchronous and proportional deglacial changes in Atlantic meridional overturning and northeast Brazilian precipitation. **Paleoceanography**, v. 32, n. 6, p. 622–633, 2017.

MURPHY, L. N. et al. The role of historical forcings in simulating the observed Atlantic multidecadal oscillation. **Geophysical Research Letters**, v. 44, n. 5, p. 2472–2480, 2017.

MYSTAKIDIS, S. et al. **Environmental Research Letters**, v. 12, n. 1, p. 014009, 2017.

NEALE, R. B. **Description of the NCAR community atmosphere model (CAM 5.0)**. [S.l].: NCAR, 2010.

NELSON, D.; SACHS, J. P. Galápagos hydroclimate of the Common Era from paired microalgal and mangrove biomarker ^{2}H/^{1}H values. **PNAS,** v. 113, n. 13, p. 3476–3481, 2016.

NEUKOM, R. et al. Multiproxy summer and winter surface air temperature field reconstructions for southern South America covering the past centuries. **Climate Dynamics**, v. 37, n. 1-2, p. 35–51, 2011.

NGUYEN, H. et al. The hadley circulation in reanalyses: climatology, variability, and change. **Journal of Climate**, v. 26, n. 10, p. 3357–3376, 2013.

NIEMANN, H.; BEHLING, H. Late quaternary vegetation, climate and fire dynamics inferred from the El Tiro record in the southeastern Ecuadorian Andes. **Journal of Quaternary Science**, v. 23, n. 3, p. 203–212, 2008.

NOBRE, C. A.; SELLERS, P. J.; SHUKLA, J. Amazonian deforestation and regional climate change. **Journal of Climate**, v. 4, n. 10, p. 957–988, 1991.

NOLAN, C. et al. Past and future global transformation of terrestrial ecosystems under climate change. **Science**, v. 361, n. 6405, p. 920–923, 2018.

NOVELLO, V. F. et al. Multidecadal climate variability in Brazil's Nordeste during the last 3000 years based on speleothem isotope records. **Geophysical Research Letters**, v. 39, n. 23, 2012.

NOVELLO, V. F. et al. A high-resolution history of the South American Monsoon from last glacial maximum to the holocene. **Scientific Reports**, v. 7, n. 1, p. 44267, 2017.

NOVELLO, V. F. et al. Two millennia of South Atlantic Convergence Zone variability reconstructed from isotopic proxies. **Geophysical Research Letters**, v. 45, n. 10, p. 5045–5051, 2018.

NOVELLO, V. F. et al. Vegetation and environmental changes in tropical South America from the last glacial to the Holocene documented by multiple cave sediment proxies. **Earth and Planetary Science Letters**, v. 524, p. 115717, 2019.

NUSBAUMER, J. et al. Evaluating hydrological processes in the Community Atmosphere Model Version 5 (CAM5) using stable isotope ratios of water. **Journal of Advances in Modeling Earth Systems**, v. 9, n. 2, p. 949–977, 2017.

OBRIST-FARNER, J. et al. Incoherency in Central American hydroclimate proxy records spanning the last millennium. **Paleoceanography and Paleoclimatology**, v. 38, n. 3, 2023.

OLSON, D. M. et al. Terrestrial ecoregions of the world: a new map of life on Earth. **BioScience**, v. 51, n. 11, p. 933, 2001.

OLESON, K. W. et al. **Technical description of version 4.0 of the Community Land Model (CLM) | TES-SFA**. Available from: https://tes-sfa.ornl.gov/bibcite/reference/131. Access on: 17 July 2023.

OTTO-BLIESNER, B. L. et al. Climate variability and change since 850 CE: an ensemble approach with the community earth system model. **Bulletin of the American Meteorological Society**, v. 97, n. 5, p. 735–754, 2016.

ORRISON, R. et al. South American Summer monsoon variability over the last millennium in paleoclimate records and isotope-enabled climate models. **Climate of the Past**, v. 18, n. 9, p. 2045–2062, 2022.

OTTERÅ, O. H. et al. External forcing as a metronome for Atlantic multidecadal variability. **Nature Geoscience**, v. 3, n. 10, p. 688–694, 2010.

OWENS, M. J. et al. The Maunder minimum and the Little Ice Age: an update from recent reconstructions and climate simulations. **Journal of Space Weather and Space Climate**, v. 7, n. A33, p. A33, 2017.

OYAMA, M. D.; NOBRE, C. A. A new climate-vegetation equilibrium state for Tropical South America. **Geophysical Research Letters**, v. 30, n. 23, 2003.

PADUANO, G. M. et al. A vegetation and fire history of Lake Titicaca since the Last Glacial Maximum. **Palaeogeography, Palaeoclimatology, Palaeoecology**, v. 194, n. 1/3, p. 259–279, 2003.

PAGES 2K CONSORTIUM. Continental-scale temperature variability during the past two millennia. **Nature Geoscience**, v. 6, n. 5, p. 339–346, 2013.

PASCALE, S. et al. Projected changes of rainfall seasonality and dry spells in a high greenhouse gas emissions scenario. **Climate Dynamics**, v. 46, n. 3/4, p. 1331–1350, 2015.

PESSENDA, L. C. R. et al. The evolution of a tropical rainforest/grassland mosaic in southeastern Brazil since 28,000 14C yr BP based on carbon isotopes and pollen records. **Quaternary Research**, v. 71, n. 3, p. 437–452, 2009.

PEREZ, L.; GARCÍA-RODRÍGUEZ, F.; HANEBUTH, T. J. J. Variability in terrigenous sediment supply offshore of the Río de la Plata (Uruguay) recording the continental climatic history over the past 1200 years. **Climate of the Past**, v. 12, n. 3, p. 623–634, 2016.

PERUGINI, L. et al. Biophysical effects on temperature and precipitation due to land cover change. **Environmental Research Letters**, v. 12, n. 5, p. 053002, 2017.

PETERSON, L. C.; HAUG, G. H. Variability in the mean latitude of the Atlantic Intertropical Convergence Zone as recorded by riverine input of sediments to the Cariaco Basin (Venezuela). **Palaeogeography, Palaeoclimatology, Palaeoecology**, v. 234, n. 1, p. 97–113, 2006.

PINAYA, J. L. D. et al. Brazilian montane rainforest expansion induced by Heinrich Stadial 1 event. **Scientific Reports**, v. 9, n. 1, p. 17912, 2019.

PIPERNO, D. R.; BUSH, M. B.; COLINVAUX, P. A. Paleoecological perspectives on human adaptation in central Panama. I. the pleistocene. **Geoarchaeology International Journal**, v. 6, n. 3, 1991.

PIPERNO, D. R. Phytoliths and microscopic charcoal from leg 155: a vegetational and fire history of the Amazon Basin during the last 75 Ky. In: FLOOD, R.D. et al. (Ed.). **Proceedings of the Ocean Drilling Program, Scientific Results**. [S.l.]: National Science Foundation, 1997. p. 411–420.

PLACZEK, C.; QUADE, J.; P. JONATHAN PATCHETT. Geochronology and stratigraphy of late Pleistocene lake cycles on the southern Bolivian Altiplano: implications for causes of tropical climate change. **Geological Society of America Bulletin**, v. 118, n. 5-6, p. 515–532, 2006.

POLISSAR, P. J. et al. Solar modulation of Little Ice Age climate in the tropical Andes. **Proceedings of the National Academy of Sciences of the United States of America**, v. 103, n. 24, p. 8937–8942, 2006.

PRADO, L. F. et al. A mid-Holocene climate reconstruction for eastern South America. **Climate of the Past**, v. 9, n. 5, p. 2117–2133, 2013.

PRENTICE, I. C.; HARRISON, S. P. Ecosystem effects of CO2 concentration: evidence from past climates. **Climate of the Past**, v. 5, n. 3, p. 297–307, 2009.

PRENTICE, I. C.; HARRISON, S. P.; BARTLEIN, P. J. Global vegetation and terrestrial carbon cycle changes after the last ice age. **New Phytologist**, v. 189, n. 4, p. 988–998, 2011.

PRENTICE, I. C.; VILLEGAS-DIAZ, R.; HARRISON, S. P. Accounting for atmospheric carbon dioxide variations in pollen-based reconstruction of past hydroclimates. **Global and Planetary Change**, v. 211, p. 103790, 2022.

QIN, M.; DAI, A.; HUA, W. Quantifying contributions of internal variability and external forcing to atlantic multidecadal variability since 1870. **Geophysical Research Letters**, v. 47, n. 22, 2020.

QIN, Y. et al. Carbon loss from forest degradation exceeds that from deforestation in the Brazilian Amazon. **Nature Climate Change**, v. 11, n. 5, p. 442–448, 2021.

QUESADA, C. A. et al. Variations in chemical and physical properties of Amazon forest soils in relation to their genesis. **Biogeosciences**, v. 7, n. 5, p. 1515–1541, 2010.

QUESADA, C. A. et al. Basin-wide variations in Amazon forest structure and function are mediated by both soils and climate. **Biogeosciences**, v. 9, n. 6, p. 2203–2246, 2012.

RANTANEN, M. et al. The Arctic has warmed nearly four times faster than the globe since 1979. **Communications Earth & Environment**, v. 3, n. 1, p. 1–10, 2022.

EIS, L. S. et al. Environmental and vegetation changes in southeastern Amazonia during the late Pleistocene and Holocene. **Quaternary International**, v. 449, p. 83–105, 2017.

REUTER, J. et al. A new perspective on the hydroclimate variability in northern South America during the Little Ice Age. **Geophysical Research Letters**, v. 36, n. 21, 2009.

RIAHI, K. et al. RCP 8.5: a scenario of comparatively high greenhouse gas emissions. **Climatic Change**, v. 109, n. 1-2, p. 33–57, 2011.

ROBERTS, W. H. G.; VALDES, P. J. Green mountains and white plains: the effect of northern hemisphere ice sheets on the global energy budget. **Journal of Climate**, v. 30, n. 10, p. 3887–3905, 2017.

ROJAS, M. et al. The South American monsoon variability over the last millennium in climate models. **Climate of the Past**, v. 12, n. 8, p. 1681–1691, 2016. Available from: https://doi.org/10.5194/cp-12-1681-2016.

ROOT, T. L. et al. Fingerprints of global warming on wild animals and plants. **Nature**, v. 421, n. 6918, p. 57–60, 2003.

ROSAN, T. M. et al. Extensive 21st-century woody encroachment in South America's Savanna. **Geophysical Research Letters**, v. 46, n. 12, p. 6594–6603, 2019.

ROSSETTI, D. F. et al. Reconstructing habitats in central Amazonia using megafauna, sedimentology, radiocarbon, and isotope analyses. **Quaternary Research**, v. 61, n. 3, p. 289–300, 2004.

ROSSETTI, D. F. et al. A Late pleistocene–holocene wetland megafan in the Brazilian Amazonia. **Sedimentary Geology**, v. 282, p. 276–293, 2012.

ROSSETTI, D. F.; COHEN, M. C. L.; PESSENDA, L. C. R. Vegetation change in southwestern Amazonia (Brazil) and relationship to the late pleistocene and holocene climate. **Radiocarbon**, v. 59, n. 1, p. 69–89, 2017.

ROSSETTI, D. F. et al. The role of late pleistocene-holocene tectono-sedimentary history on the origin of patches of savanna vegetation in the middle Madeira River, southwest of the Amazonian lowlands. **Palaeogeography, Palaeoclimatology, Palaeoecology**, v. 526, p. 136–156, 2019.

RUIZ-BARRADAS, A.; NIGAM, S.; KAVVADA, A. The Atlantic Multidecadal Oscillation in twentieth century climate simulations: uneven progress from CMIP3 to CMIP5. **Climate Dynamics**, v. 41, n. 11-12, p. 3301–3315, 2013.

RAYNER, N. A. Global analyses of sea surface temperature, sea ice, and night marine air temperature since the late nineteenth century. **Journal of Geophysical Research**, v. 108, n. D14, 2003.

RAYNER, N. A. et al. Improved analyses of changes and uncertainties in sea surface temperature measured in situ since the mid-nineteenth century: the HadSST2 dataset. **Journal of Climate**, v. 19, n. 3, p. 446–469, 2006.

SACHS, J. et al. Southward Shift of the Pacific ITCZ during the holocene. **Paleoceanography and Paleoclimatology**, v. 33, n. 12, p. 1383–1395, 2018.

SAENGER, C. et al. Surface-temperature trends and variability in the low-latitude North Atlantic since 1552. **Nature Geoscience**, v. 2, n. 7, p. 492–495, 2009.

SAMPAIO, G. et al. CO_2 fertilization effect can cause rainfall decrease as strong as large-scale deforestation in the Amazon. **Biogeosciences Discussions**, p. 1–21, 2020.

SAIA, S. E. M. G. et al. Last Glacial Maximum (LGM) vegetation changes in the Atlantic Forest, southeastern Brazil. **Quaternary International**, v. 184, n. 1, p. 195–201, 2008.

SALGADO-LABOURIAU, M. L. et al. Late quaternary vegetational and climatic changes in cerrado and palm swamp from Central Brazil. **Palaeogeography, Palaeoclimatology, Palaeoecology**, v. 128, n. 1-4, p. 215–226, 1997.

SALGADO-LABOURIAU, M. L. et al. A dry climatic event during the late Quaternary of tropical Brazil. **Review of Palaeobotany and Palynology**, v. 99, n. 2, p. 115–129, 1998.

SCHLEUSSNER, C. F.; FEULNER, G. A volcanically triggered regime shift in the subpolar North Atlantic Ocean as a possible origin of the Little Ice Age. **Climate of the Past**, v. 9, n. 3, p. 1321–1330, 2013.

SCHNEIDER VON DEIMLING, T. et al. How cold was the Last Glacial Maximum? **Geophysical Research Letters**, v. 33, n. 14, 2006.

SCHLESINGER, M. E.; RAMANKUTTY, N. An oscillation in the global climate system of period 65–70 years. **Nature**, v. 367, n. 6465, p. 723–726, 1994.

SCHMIDT, G. A. et al. Climate forcing reconstructions for use in PMIP simulations of the last millennium (v1.0). **Geoscientific Model Development**, v. 4, n. 1, p. 33–45, 2011.

SCHMIDT, G. A. et al. Configuration and assessment of the GISS ModelE2 contributions to the CMIP5 archive. **Journal of Advances in Modeling Earth Systems**, v. 6, n. 1, p. 141–184, 2014.

SCHEFF, J. et al. Are glacials dry? consequences for paleoclimatology and for greenhouse warming. **Journal of Climate**, v. 30, n. 17, p. 6593–6609, 2017.

SCHMITTNER, A: et al. Climate sensitivity estimated from temperature reconstructions of the last glacial maximum. **Science**, v. 334, n. 6061, p. 1385–1388, 2011.

SCHREVE-BRINKMAN, E. J. A palynological study of the upper quaternary sequence in the El Abra corridor and rock shelters (Colombia). **Palaeogeography, Palaeoclimatology, Palaeoecology**, v. 25, n. 1, p. 1–109, 1978.

SEDDON, A. W. R. et al. Sensitivity of global terrestrial ecosystems to climate variability. **Nature**, v. 531, n. 7593, p. 229–232, 2016.

SELTZER, G.; RODBELL, D.; BURNS, S. Isotopic evidence for late quaternary climatic change in tropical South America. **Geology**, v. 28, n. 1, p. 35, 2000.

SHANAHAN, T. M. et al. Atlantic forcing of persistent drought in west Africa. **Science**, v. 324, n. 5925, p. 377–380, 2009.

SHAKUN, J. D. et al. Global warming preceded by increasing carbon dioxide concentrations during the last deglaciation. **Nature**, v. 484, n. 7392, p. 49–54, 2012.

SHIMIZU, M. H. et al. Seasonal changes of the South American monsoon system during the Mid-Holocene in the CMIP5 simulations. **Climate Dynamics**, v. 54, n. 5/6, p. 2697–2712, 2020.

SIFEDDINE, A. et al. Variations of the Amazonian rainforest environment: a sedimentological record covering 30,000 years. **Palaeogeography, Palaeoclimatology, Palaeoecology**, v. 168, n. 3/4, p. 221–235, 2001.

SIFEDDINE, A. et al. A 21 000 cal years paleoclimatic record from Caçó Lake, northern Brazil: evidence from sedimentary and pollen analyses. **Palaeogeography, Palaeoclimatology, Palaeoecology**, v. 189, n. 1/2, p. 25–34, 2003.

SIEGENTHALER, U. stable carbon cycle-climate relationship during the late pleistocene. **Science**, v. 310, n. 5752, p. 1313–1317, 2005.

SILVA, J. L. S. E et al. Climate change will reduce suitable Caatinga dry forest habitat for endemic plants with disproportionate impacts on specialized reproductive strategies. **Plos One**, v. 14, n. 5, e0217028, 2019.

SILVEIRA, M. H. B. et al. Pleistocene climatic instability drove the historical distribution of forest islands in the northeastern Brazilian Atlantic Forest. **Palaeogeography, Palaeoclimatology, Palaeoecology**, v. 527, p. 67–76, 2019.

SLAWINSKA, J.; ROBOCK, A. Impact of volcanic eruptions on decadal to centennial fluctuations of arctic sea ice extent during the last millennium and on initiation of the little ice age. **Journal of Climate**, v. 31, n. 6, p. 2145–2167, 2018.

SLIVINSKI, L. C. et al. Towards a more reliable historical reanalysis: improvements for version 3 of the twentieth century reanalysis system. **Quarterly Journal of the Royal Meteorological Society**, v. 145, n. 724, p. 2876–2908, 2019.

SMIRNOV, D. A. et al. A regime shift in the sun-climate connection with the end of the medieval climate anomaly. **Scientific Reports**, v. 7, n. 1, p. 11131, 2017.

SONG, X.-P. et al. Global land change from 1982 to 2016. **Nature**, v. 560, n. 7720, p. 639–643, 2018.

STAVER, A. C.; ARCHIBALD, S.; LEVIN, S. A. The global extent and determinants of Savanna and forest as alternative biome states. **Science**, v. 334, n. 6053, p. 230–232, 2011.

STEFFEN, D.; SCHLUNEGGER, F.; PREUSSER, F. Drainage basin response to climate change in the Pisco valley, Peru. **Geology**, v. 37, n. 6, p. 491–494, 2009.

STEIGER, N. J. et al. ENSO-driven coupled megadroughts in North and South America over the last millennium. **Nature Geoscience**, v. 14, n. 10, p. 739–744, 2021.

STEINMAN, B. A. et al. Interhemispheric antiphasing of neotropical precipitation during the past millennium. **Proceedings of the National Academy of Sciences**, v. 119, n. 17, 2022.

STRÍKIS, N. M. et al. Timing and structure of Mega-SACZ events during Heinrich Stadial 1. **Geophysical Research Letters**, v. 42, n. 13, p. 5477–5477, 2015.

STRÍKIS, N. M. et al. South American monsoon response to iceberg discharge in the North Atlantic. **Proceedings of the National Academy of Sciences**, v. 115, n. 15, p. 3788–3793, 2018.

STUTE, M. et al. Cooling of tropical Brazil (5°C) during the last glacial maximum. **Science**, v. 269, n. 5222, p. 379–383, 1995.

SUTTON, R. T.; HODSON, D. L. Atlantic Ocean forcing of North American and European summer climate. **Science**, v. 309, n. 5731, p. 115–118, 2005.

SUN, W. et al. Pacific multidecadal (50–70 year) variability instigated by volcanic forcing during the Little Ice Age (1250–1850). **Science**, v. 59, n. 1/2, p. 231–244, 2022.

SYLVESTRE, F. et al. Lake-level chronology on the southern Bolivian Altiplano (18°–23°S) during late-glacial time and the early holocene. **Quaternary Research**, v. 51, n. 1, p. 54–66, 1999.

TAYLOR, K.; STOUFFER, R. J. S.; MEEHL, G. A. An overview of CMIP5 and the experiment design. **Bulletin of the American Meteorological Society**, v. 93, n. 4, 2012.

TANDON, N. F.; KUSHNER, P. J. Does external forcing interfere with the AMOC's influence on North Atlantic sea surface temperature? **Journal of Climate**, v. 28, n. 16, p. 6309–6323, 2015.

TAPIA, P. M. et al. A late quaternary diatom record of tropical climatic history from Lake Titicaca (Peru and Bolivia). **Palaeogeography, Palaeoclimatology, Palaeoecology**, v. 194, n. 1-3, p. 139–164, 2003.

TEBALDI, C.; KNUTTI, R. The use of the multi-model ensemble in probabilistic climate projections. **Philosophical Transactions of the Royal Society A: Mathematical, Physical and Engineering Sciences**, v. 365, n. 1857, p. 2053–2075, 2007.

TEEUW, R. M.; RHODES, E. J. Aeolian activity in northern Amazonia: optical dating of Late Pleistocene and Holocene palaeodunes. **Journal of Quaternary Science**, v. 19, n. 1, p. 49–54, 2004.

TERRER, C. et al. Mycorrhizal association as a primary control of the CO2 fertilization effect. **Science**, v. 353, n. 6294, p. 72–74, 2016.

TERRER, C. et al. Nitrogen and phosphorus constrain the CO2 fertilization of global plant biomass. **Nature Climate Change**, v. 9, n. 9, 2019.

THOMPSON, L. G. et al. The little ice age as recorded in the stratigraphy of the tropical quelccaya ice cap. **Science**, v. 234, n. 4774, p. 361–364, 1986.

THOMPSON, L. G. et al. Late glacial stage and holocene tropical ice core records from Huascarán, Peru. **Science**, v. 269, n. 5220, p. 46–50, 1995.

THOMPSON, L. G. et al. A 25,000-year tropical climate history from Bolivian ice cores. **Science**, v. 282, n. 5395, p. 1858–1864, 1998.

THOURET, J.-C. et al. Paleoenvironmental changes and glacial stades of the last 50,000 years in the Cordillera Central, Colombia. **Quaternary Research**, v. 46, n. 1, p. 1–18, 1996.

TIERNEY, J. E. et al. Glacial cooling and climate sensitivity revisited. **Nature**, v. 584, n. 7822, p. 569–573, 2020.

TING, M. et al. Forced and internal twentieth-century SST trends in the North Atlantic. **Journal of Climate**, v. 22, n. 6, p. 1469–1481, 2009.

TING, M. et al. Robust features of Atlantic multi-decadal variability and its climate impacts. **Geophysical Research Letters**, v. 38, n. 17, 2011.

TOOHEY, M.; SIGL, M. Volcanic stratospheric sulfur injections and aerosol optical depth from 500 BCE to 1900 CE. **Earth System Science Data**, v. 9, n. 2, p. 809–831, 2017.

TRENBERTH, K. E.; SHEA, D. J. Atlantic hurricanes and natural variability in 2005. **Geophysical Research Letters**, v. 33, n. 12, 2006.

TRISOS, C. H.; MEROW, C.; PIGOT, A. L. The projected timing of abrupt ecological disruption from climate change. **Nature**, v. 580, n. 7804, p. 496–501, 2020.

TURCQ, B.; PRESSINOTTI, M. M. N.; MARTIN, L. Paleohydrology and Paleoclimate of the Past 33,000 Years at the Tamanduá River, Central Brazil. **Quaternary Research**, v. 47, n. 3, p. 284–294, 1997.

URREGO, D. H.; SILMAN, M. R.; BUSH, M. B. The Last Glacial Maximum: stability and change in a western Amazonian cloud forest. **Journal of Quaternary Science**, v. 20, n. 7-8, p. 693–701, 2005.

URREGO, D. H.; BUSH, M. B.; SILMAN, M. R. A long history of cloud and forest migration from Lake Consuelo, Peru. **Quaternary Research**, v. 73, n. 2, p. 364–373, 2010.

UTIDA, G. et al. Tropical South Atlantic influence on Northeastern Brazil precipitation and ITCZ displacement during the past 2300 years. **Scientific Reports**, v. 9, n. 1, 2019.

VAN DER HAMMEN, T. et al. Glacial sequence and environmental history in the Sierra Nevada del cocuy (Colombia). **Palaeogeography, Palaeoclimatology, Palaeoecology**, v. 32, p. 247–340, 1980.

VAN DER HAMMEN, T.; ABSY, M. L. Amazonia during the last glacial. **Palaeogeography, Palaeoclimatology, Palaeoecology**, v. 109, n. 2/4, p. 247–261, 1994.

VAN DER HAMMEN, T.; HOOGHIEMSTRA, H. Neogene and quaternary history of vegetation, climate, and plant diversity in Amazonia. **Quaternary Science Reviews**, v. 19, n. 8, p. 725–742, 2000.

VAN DER HAMMEN, T.; HOOGHIEMSTRA, H. Interglacial–glacial Fuquene-3 pollen record from Colombia: an Eemian to Holocene climate record. **Global and Planetary Change**, v. 36, n. 3, p. 181–199, 2003.

VAN GEEL, B.; VAN DER HAMMEN, T. Upper quaternary vegetational and climatic sequence of the fuquene area (Eastern Cordillera, Colombia). **Palaeogeography, Palaeoclimatology, Palaeoecology**, v. 14, n. 1, p. 9–92, 1973.

VAUTARD, R. et al. The European climate under a 2° C global warming. **Environmental Research Letters**, v. 9, n. 3, p. 034006, 2014.

VELÁSQUEZ MONTOYA, R. E. **Paleoecología de alta resolución del final de la última glaciación y la transición al Holoceno en el páramo de Belmira (Antioquia)**. 2013. Thesis (PhD) - Universidad Nacional de Colombia, 2013.

VÉLEZ, M. I. et al. Pollen- and diatom based environmental history since the Last Glacial Maximum from the Andean core Fúquene-7, Colombia. **Journal of Quaternary Science**, v. 18, n. 1, p. 17–30, 2003.

VÉLEZ, M. I. et al. Late glacial and holocene environmental and climatic changes from a limnological transect through Colombia, northern South America. **Palaeogeography, Palaeoclimatology, Palaeoecology**, v. 234, n. 1, p. 81–96, 2006.

VERA, C. et al. Toward a unified view of the American Monsoon systems. **Journal of Climate**, v. 19, n. 20, p. 4977–5000, 2006.

VILELA, A. A. et al. Climate changes affecting biotic interactions, phenology, and reproductive success in a savanna community over a 10-year period. **Arthropod-Plant Interactions**, v. 12, n. 2, p. 215–227, 2017.

VILLOTA, A.; BEHLING, H. Late quaternary vegetation, climate, and fire dynamics: human impact and evidence of past Polylepis populations in the northern Andean depression inferred from the El Cristal record in southeastern Ecuador. **Ecotropica,** v.19, p.39-58, 2013.

VOLDOIRE, A. et al. The CNRM-CM5.1 global climate model: description and basic evaluation. **Climate Dynamics**, v. 40, n. 9/10, p. 2091–2121, 2012.

VUILLE, M. et al. A review of the South American monsoon history as recorded in stable isotopic proxies over the past two millennia. **Climate of the Past**, v. 8, n. 4, p. 1309–1321, 2012.

WANG, X. et al. Wet periods in northeastern Brazil over the past 210 kyr linked to distant climate anomalies. **Nature**, v. 432, n. 7018, p. 740–743, 2004.

WANG, Y.; LI, S.; LUO, D. Seasonal response of Asian monsoonal climate to the Atlantic Multidecadal Oscillation. **Journal of Geophysical Research**, v. 114, n. D2, 2009.

WANG, C.; ZHANG, L. Multidecadal ocean temperature and salinity variability in the Tropical North Atlantic: linking with the AMO, AMOC, and subtropical cell. **Journal of Climate**, v. 26, n. 16, p. 6137–6162, 2013.

WANG, C. et al. Multidecadal covariability of North Atlantic sea surface temperature, african dust, sahel rainfall, and atlantic hurricanes. **Journal of Climate**, v. 25, n. 15, p. 5404–5415, 2012.

WANG, C. et al. A global perspective on CMIP5 climate model biases. **Nature Climate Change**, v. 4, n. 3, p. 201–205, 2014.

WANG, X. et al. Hydroclimate changes across the Amazon lowlands over the past 45,000 years. **Nature**, v. 541, n. 7636, p. 204–207, 2017.

WANG, J. et al. Internal and external forcing of multidecadal Atlantic climate variability over the past 1,200 years. **Nature Geoscience**, v. 10, n. 7, p. 512–517, 2017.

WANG, T.; WANG, N.; JIANG, D. Last Glacial Maximum ITCZ changes from PMIP3/4 simulations. **Journal of Geophysical Research: Atmospheres**, v. 128, n. 10, 2023.

WANNER, H. et al. Structure and origin of Holocene cold events. **Quaternary Science Reviews**, v. 30, n. 21-22, p. 3109–3123, 2011.

WANNER, H.; PFISTER, C.; NEUKOM, R. The variable European little ice age. **Quaternary Science Reviews**, v. 287, p. 107531, 2022.

WATANABE, M. et al. Improved climate simulation by MIROC5: mean states, variability, and climate sensitivity. **Journal of Climate**, v. 23, n. 23, p. 6312–6335, 2010.

WATANABE, S. et al. MIROC-ESM 2010: model description and basic results of CMIP5-20c3m experiments. **Geoscientific Model Development**, v. 4, n. 4, p. 845–872, 2011.

WERNECK, F. P. et al. Revisiting the historical distribution of seasonally dry tropical forests: new insights based on palaeodistribution modelling and palynological evidencegeb. **Global Ecology and Biogeography**, v. 20, n. 2, p. 272–288, 2010.

WHITNEY, B. S. et al. A 45kyr palaeoclimate record from the lowland interior of tropical South America. **Palaeogeography, Palaeoclimatology, Palaeoecology**, v. 307, n. 1-4, p. 177–192, 2011.

WILLE, M.; NEGRET, J. A.; HOOGHIEMSTRA, H. Paleoenvironmental history of the Popayán area since 27 000 yr BP at Timbio, Southern Colombia. **Review of Palaeobotany and Palynology**, v. 109, n. 1, p. 45–63, 2000.

WILLE, M. et al. Environmental change in the Colombian subandean forest belt from 8 pollen records: the last 50 kyr. **Vegetation History and Archaeobotany,** v. 10, n. 2, p. 61–77, 2001.

WILLIAMS, J. J. et al. Vegetation, climate and fire in the eastern Andes (Bolivia) during the last 18,000years. **Palaeogeography, Palaeoclimatology, Palaeoecology**, v. 312, n. 1-2, p. 115–126, 2011.

WILLMOTT, C.J.; MATSUURA, K**. Terrestrial air temperature and recipitation: Monthly and annual time series (1950–1999) Version 1.02**. Newark: University of Delaware, 2001.

WORTHAM, B. E. et al. Assessing response of local moisture conditions in central Brazil to variability in regional monsoon intensity using speleothem 87Sr/86Sr values. **Earth and Planetary Science Letters**, v. 463, p. 310–322, 2017.

YAN, H. et al. Dynamics of the intertropical convergence zone over the western Pacific during the Little Ice Age. **Nature Geoscience**, v. 8, n. 4, p. 315–320, 2015.

YAN, X.; ZHANG, R.; KNUTSON, T. R. A multivariate AMV index and associated discrepancies between observed and CMIP5 externally forced AMV. **Geophysical Research Letters**, v. 46, n. 8, p. 4421–4431, 2019.

YANG, Z.-L. et al. Preliminary study of spin-up processes in land surface models with the first stage data of Project for Intercomparison of Land Surface Parameterization Schemes Phase 1(a). **Journal of Geophysical Research**, v. 100, n. D8, p. 16553, 1995.

YIN, L. et al. How well can CMIP5 simulate precipitation and its controlling processes over tropical South America? **Climate Dynamics**, v. 41, n. 11-12, p. 3127–3143, 2012.

YUKIMOTO, S. et al. A new global climate model of the meteorological research institute: MRI-CGCM3: model description and basic performance. **Journal of the Meteorological Society of Japan Serie II**, v. 90A, p. 23–64, 2012.

ZANI, H. et al. Influence of landscape evolution on the distribution of floristic patterns in northern Amazonia revealed by δ13 C data. **Journal of Quaternary Science**, v. 27, n. 8, p. 854–864, 2012.

ZHANG, R.; DELWORTH, T. L. Impact of Atlantic multidecadal oscillations on India/Sahel rainfall and Atlantic hurricanes. **Geophysical Research Letters**, v. 33, n. 17, 2006.

ZHANG, Y. et al. Equatorial Pacific forcing of western Amazonian precipitation during Heinrich Stadial 1. **Scientific Reports**, v. 6, n. 1, p. 35866, 2016.

ZHANG, R. et al. A review of the role of the atlantic meridional overturning circulation in atlantic multidecadal variability and associated climate impacts. **Reviews of Geophysics**, v. 57, n. 2, p. 316–375, 2019.

ZHU, Z. et al. Greening of the Earth and its drivers. **Nature Climate Change**, v. 6, n. 8, p. 791–795, 2016.

ZHU, J. et al. Reduced ENSO variability at the LGM revealed by an isotope-enabled Earth system model. **Geophysical Research Letters**, v. 44, n. 13, p. 6984–6992, 2017.

ZECH, R. et al. LGM and late glacial glacier advances in the Cordillera Real and Cochabamba (Bolivia) deduced from surface exposure dating. **Climate of the Past**, v. 3, n. 4, p. 623–635, 2007.

ZECH, M. et al. Late quaternary environmental changes in Misiones, subtropical NE Argentina, deduced from multi-proxy geochemical analyses in a palaeosol-sediment sequence. **Quaternary International**, v. 196, n. 1-2, p. 121–136, 2009.

ZECH, J. et al. Glacier and climate reconstruction at Tres Lagunas, NW Argentina, based on 10Be surface exposure dating and lake sediment analyses. **Palaeogeography, Palaeoclimatology, Palaeoecology**, v. 284, n. 3-4, p. 180–190, 2009.

APPENDIX A

Table A.1 - Compilation of proxy data from paleoclimate archives of South America. In the case of precipitation, anomalies are expressed aas the difference between LGM and present time, and the categories are "drier", "wetter" and "unclear (NA)". Also for vegetation anomalies are expressed as the difference between LGM and present time, and the categories are "change (y)", "no change (n)" and "unclear (NA)".

	Site	Latitude	Longitude	Reference	Proxy type	CRI	LGM-Today precipitation (study)	LGM biome change (study)	Ensemble mean LGM climate	Simulated LGM biome change
1	El Valle	08°36'55'' N	80°07'31'' W	Bush & Colinvaux 1990; Piperno et al., 1991	Palynology and diatom	0,03	Drier	n	Drier	n
2	Fúquene 2, valle de Ubaté	05°30' N	73°46'12'' W	Van Geel & Van der Hammen 1973	Pollen diagram	0,03	Drier	y	Drier	y
3	Fúquene 3	05°27' N	73°46' W	Van der Hammen & Hooghiemstra 2003	Pollen diagrams	0,70	Drier	y	Drier	y
4	Fúquene 7	05°27' N	73°46' W	Vélez et al., 2003; Vélez et al., 2006	Palynology and diatom (plus water chemistry, magnetic)	0,73	Drier	NA	Drier	y
5	La Laguna, Bogotá	04°55' N	74°20' W	Helmens et al., 1996	Pollen diagrams (plus morainic complexes)	0,73	NA	NA	Drier	y
6	Ruíz-Tolima massif, Cordillera Central	04°51' N	75°22' W	Thouret et al., 1996	Glacial geomorphology, tephra-soil stratigraphy in basins, the area has active volcanoes that produced wideand mineralogy, palynology	0,03	Drier	NA	Drier	y
7	Laguna el El Piñal	04°08' N	70°23' W	Behling and Hooghiemstra, 1999	Pollen diagram	0,83	Drier	NA	Drier	n
8	Rio Branco-Rupununi Savanna	03°12' N	59°53' W	Teeuw & Rhodes 2004	Particle size, paleodunes dose	0,37	NA	NA	Drier	n
9	Piagua, Popayán	02°30' N	76°30' W	Wille et al. 2001	Palynology, $\delta^{13}C$ in organic material	0,07	NA	NA	Drier	n
10	Timbio, Popayán	02°24' N	76°36' W	Wille et al., 2000	Pollen diagram	0,40	Drier	y	Drier	n
11	Viruá National Park	01°24'35'' N	60°59'16'' W	Rossetti et al., 2012; Zani et al., 2012	Paleomorphology, $\delta^{13}C$, C/N, TOC (organic)	1,03	Drier	NA	Drier	y
12	Hill of six lakes	0°17'10'' N	66°40'36'' W	Cordeiro et al., 2011	TOC, total organic nitrogen (TN), $\delta^{13}C$, $\delta^{15}N$, charcoal, Chlorophy ll, black carbon, elemental analyses	1,00	Drier	n	Drier	n

continue

Table A.1 - Continuation.

	Site	Latitude	Longitude	Reference	Proxy type	CRI	LGM-Today precipitation (study)	LGM biome change (study)	Ensemble mean LGM climate	Simulated LGM biome change
13	Hill of six lakes	00°16' N	66°41' W	Bush et al., 2004a	Pollen diagram, charcoal, chemical cation, loss-on-ignition (LOI)	1,40	NA	n	Drier	n
14	Hill of six lakes	00°16' N	66°41' W	Colinvaux et al., 1996	Lithology and pollen spectra	0,77	Drier	n	Drier	n
15	Hill of six lakes	00°16' N	66°41' W	Bush et al., 2004a	Pollen diagram, charcoal, LOI	0,70	Drier	n	Drier	n
16	Pichincha	00°10' S	78°35' W	Heine and Heine 1996	Glacier advance under humid condition	0,00	NA	NA	Wetter	y
17	Temedauí, Río Negro	00°23' S	64°33' W	Carneiro Filho et al., 2002	Paleodunes dose	1,03	Drier	NA	Dry	n
18	Tiquié, upper Negro River Basin	00°23'18'' S	64°18'25'' W	Latrubesse & Franzinelli 2005	Geomorphologic mapping, field surveys, ^{14}C dating of wood detritus and charcoal	0,00	NA	NA	Dry	n
19	Maicurú	00°30' S	54°15' W	Colinvaux et al., 2001	Pollen diagrams, lithology	0,03	NA	NA	Dry	y
20	Pantano de Monica	00°42' S	72°04' W	Van der Hammen and Hooghiemstra, 2000	Pollen diagram, lithology	0,03	Drier	y	Dry	n
21	Caquetá River	02°07'18'' S	70°42'33'' W	Van der Hemmen et al., 1992	River bank sections, radiocarbon dates and palynological analyses of organic layers	0,00	Drier	NA	Dry	n
22	Laguna Chorreras	02°45' S	79°10' W	Hansen et al., 2003	Pollen/spores, charcoal, magnetic susceptibility	0,40	NA	NA	Wet	y
23	Lagoa do Caçó	02°58' S	43°25' W	Ledru et a., 2006; Sifeddine et al., 2003	Palynology, mineralogy and geochemistry	0,50	Drier	y	Drier	n
24	Lagoa do Caçó	02°58' S	43°25' W	Jacob et al., 2004; Jacob et al., 2007	Lithology, organic petrography, C/N, $\delta^{13}C_{org}$ and $\delta^{15}N$, δD	0,83	Drier	NA	Drier	n
25	Santiago cave	03°01' S	78°08' W	Mosblech et al., 2012	$\delta^{18}O_{calcite}$ of stalagmite	3,00	NA	NA	Wetter	y
26	El Tiro Pass	03°50'26'' S	79°08'43'' W	Niemann & Behling 2008	Pollen, spores and charcoal analysis	0,83	Wetter	y	Wetter	y
27	Itaituba fossil quarry	04°15'02'' S	56°00'50'' W	Rossetti et al., 2004	Sedimentology of fossil bed, $\delta^{13}C$ in bone collagen, X-ray analysis of clay	0,33	Drier	NA	Drier	n
28	Cerro Toledo	04°22'29'' S	79°06'42'' W	Brunschön & Behling 2009	Pollen diagram, non-destructive magnetic susceptibility	0,83	Wetter	n	Wetter	y
29	Rio Grande do Norte [Rainha, Furna Nova and Abissal caves]	05°36' S	37°44' W	Cruz et al., 2009	$\delta^{18}O_{calcite}$ of stalagmite	4,33	Drier	NA	Drier	y

continue

Table A.1 - Continuation.

	Site	Latitude	Longitude	Reference	Proxy type	CRI	LGM-Today precipitation (study)	LGM biome change (study)	Ensemble mean LGM climate	Simulated LGM biome change
30	Cueva del Diamante Cave	05°44' S	77°30' W	Cheng et al., 2013	$\delta^{18}O_{calcite}$ of stalagmite	4,00	Wetter	NA	Wetter	n
31	El Condor Cave	05°56' S	77°18' W	Cheng et al., 2013	$\delta^{18}O_{calcite}$ of stalagmite	5,67	Wetter	NA	Wetter	n
32	Serra dos Carajás	06°20' S	50°25' W	Absy et al., 1991	Pollen diagram	0,03	Drier	NA	Drier	y
33	Pántano da Maurítia, Serra Sul dos Carajás	06°21'06'' S	50°23'37'' W	Hermanowski et al., 2012	Pollen, fern spore, micro-charcoal, sediment and mineral analyses	0,40	Drier	y	Drier	y
34	Serra dos Carajás	06°35' S	49°30' W	Sifeddine et al., 2001	Lithology, mineralogy, $\delta^{13}C$ of organic matter ($\delta^{13}C_{org}$)	0,70	Drier	NA	Drier	n
35	Laguna La Compuerta, Peru	07°30' S	78°36' W	Weng et al., 2006	Pollen diagram, charcoal, magnetic susceptibility, and bulk density	0,37	NA	NA	Wet	n
36	Humaitá	07°55'26'' S	63°04'59'' W	Cohen et al., 2014	Pollen diagrams, sedimentary facies, $\delta^{13}C_{org}$ and C/N_{molar}	0,40	Drier	NA	Drier	n
37	Porto Velho to Humaitá (BR319), 8 locations in details in the ref.	08°21' S	63°57' W	Freitas et al., 2001	TOC, $\delta^{13}C$ of soil organic matter	0,37	NA	n	Drier	n
38	Katira Creek, Rondonia	09° S	63° W	Van der Hammen and Absy, 1994;	Palynology, sedimentology, $\delta^{13}C$	0,33	Drier	y	Drier	n
39	Huascarán, Peru	09°06'41'' S	77°36'53'' W	Thompson et al., 1995	$\delta^{18}O_{ice}$ and water chemistry	0,43	NA	NA	Neutral	y
40	Lago Saci	09°07' S	56°16'10'' W	Cordeiro et al., 2014	Sedimentology, charcoal, $\delta^{13}C_{org}$	0,83	Drier	NA	Neutral	n
41	Toca da Boa Vista	10°09'45'' S	40°51'35'' W	Wang et al., 2004	U-Th dating of speleothem/travertine formation	0,33	NA	NA	Wetter	y
42	Canhoba/Cel. João Sá	10°05'06'' S-10°17'27'' S	37°01'14'' W-37°59'20'' W	Dantas et al., 2013	$\delta^{13}C$ of Notiomastodon platensis (enamel)	0,67	NA	NA	Wetter	n
43	Cordillera Huayhuash	10°18' S	76°54' W	Hall et al., 2009	ASTER imagery, aerial photographs, ^{14}C and ^{10}Be dating of quaternary glacial landscape	0,67	NA	NA	Wetter	y
44	Salgadinho, Salitre valley	10°21' S	40°46'40'' W	Wang et al., 2004	U-Th dating of travertine formation	1,67	NA	NA	Wetter	y
45	Junin	11° S	76°10' W	Seltzer G., 2000	$\delta^{18}O_{calcite}$, $\delta^{13}C_{calcite}$, magnetic susceptibility	0,70	Drier	NA	Wetter	y

continue

Table A.1 - Continuation.

	Site	Latitude	Longitude	Reference	Proxy type	CRI	LGM-Today precipitation (study)	LGM biome change (study)	Ensemble mean LGM climate	Simulated LGM biome change
46	Laguna Junín, Peru	11°03'45'' S	76°06'35'' W	Hansen et al., 1984	Pollen diagram	0,70	NA	y	Wetter	y
47	Pacupahuain	11°14'24'' S	75°49'12'' W	Kanner et al., 2012	$\delta^{13}C$, $\delta^{18}O_{calcite}$	23,33	Wetter	NA	Wetter	y
48	Bananal Basin	13°0'20.61'' S	50°39'33'' W	Valente & Latrubesse. 2012.	Geomorphologic mapping, sedimentary and dating [i.e. TL,OSL,^{14}C] of fluvial sediments and organic debris	1,00	Drier	n	Wetter	n
49	Pacucha	13°36'26'' S	73°29'42'' W	Hillyer et al., 2009	Pollen & fossil diatoms, LOI, benthic/salt-tolerant diatoms and $CaCO_3$	0,70	NA	NA	Wetter	n
50	Laguna Bella Vista	13°37' S	61°33' W	Mayle et al., 2000; Burbridge et al., 2004	Pollen spectra and charcoal, LOI	0,40	Drier	y	Neutral	n
51	Pisco valley	13°42' S	75°42' W	Steffen et al., 2009	Optically stimulated luminescence (OSL) dating of quaternary deposit	1,00	Wetter	NA	Wetter	y
52	Lago Consuelo	13°57' S	68°59' W	Bush et al., 2004b	Pollen diagram	1,03	NA	n	Wetter	y
53	Laguna Chaplin	14°28' S	61°04' W	Mayle et al., 2000; Burbridge et al., 2004	Pollen spectra and charcoal, LOI	0,73	Drier	y	Dry	y
54	Vereda de Aguas Emendadas	15°34' S	47°35' W	Salgado-Labouriau et al., 1998	Pollen diagram	0,03	Drier	y	Wetter	n
55	Titicaca	16°03'27'' S	69°05'14'' W	Fritz et al., 2007	Magnetic susceptibility, lithology, TOC, %$CaCO_3$ $\delta^{13}C_{TOC}$, diatom	0,73	Wetter	NA	Neutral	y
56	Lago Grande, Titicaca	16°08'0.24'' S	69°09'12'' W	Baker et al., 2001a; Paduano et al., 2003; Tapia et al., 2003	Pollen diagram and charcoal, magnetic susceptibility, $CaCO_3$, $\delta^{13}C_{TOC}$	1,10	Wetter	y	Neutral	y
57	Huinãmimarca	16°20' S	68°57'45'' W	Argollo & Mourguiart. 2000	Geomorphological and pollen diagram	0,70	Drier	NA	Neutral	y
58	Huara Loma Valley, Cordillera de Cochabamba	17°12' S	66°17' W	May et al., 2011	Morphostratigraphic mapping, Mineralogy and geochemistry, and ^{14}C/OSL dating of glacial landforms	2,33	NA	NA	Drier	n
59	Wara Wara, Valle Huara Loma	17°17' S-17°13' S	66°07' W-66°16' W	Zech et al., 2007; Kull et al., 2008	^{10}Be dating of morine deposits & mass balance and climate modeling	1,00	NA	NA	Drier	n
60	Vereda, Cromínia	17°15' S	49°25' W	Salgado-Labouriau et al., 1997	Pollen diagram, spore and geochemical analyses	0,07	Wetter	y	Wetter	n

continue

Table A.1 - Continuation.

	Site	Latitude	Longitude	Reference	Proxy type	CRI	LGM-Today precipitation (study)	LGM biome change (study)	Ensemble mean LGM climate	Simulated LGM biome change
61	Laguna Khomer Kocha Upper	17°16'31'' S	65°43'57'' W	Williams et al., 2011	Physical and chemical analysis, pollen and spore analysis	0,40	NA	NA	Wetter	n
62	Alto Ilo, Pampa Inalambrica	17°41'31″ S-17°42'13″ S	71°15'55'' W-71°15'34″ W	Londoño et al., 2012	Stratigraphic assessment, sedimentologic, pedologic observations, optical OSL dating	1,00	NA	NA	Wetter	y
63	Laguna La Gaiba	17°45' S	57°35' W	Whitney et al., 2011	Pollen diagram, $\delta^{13}C$ of soil organic matter, LOI, magnetic susceptibility	1,07	Drier	y	Wetter	y
64	Siberia	17°50' S	64°43'08'' W	Mourguiart and Ledru, 2003	Pollen diagram, TOC, Quartz	0,70	Drier	y	Drier	y
65	Sajama	18°06' S	68°53' W	Thompson et al., 1998	$\delta^{18}O$, water chemistry	0,47	Wetter	NA	Wetter	y
66	Salar de Uyuni	18°00'28'' S-18°18'55'' S	67°02'31'' W-67°34'05'' W	Placzek et al., 2006	^{14}C dating of buried and surficial soil stratigraphic units that formed between deep-lake cycles, ake hydrologic budget models	0,33	NA	NA	Wetter	y
67	Rio Seco, Gran Chaco	18°41'47'' S	63°12'56'' W	Latrubesse et al., 2012	Geomorphologic mapping, field surveys, OSL dating	0,67	NA	NA	Drier	y
68	Cabezas-Río Grande,Bolivian Chaco	18°48'05'' S	63°18'02'' W	May et al., 2008	Stratigraphical, grain size and geochemical analyses [Pedogenic iron], ^{14}C dating of Terrestrial shell	0,70	Drier	y	Drier	y
69	Lagoa Campestre, Salitre de Minas	19° S	46°46' W	Ledru et al., 1996	Pollen diagram and spores	0,50	NA	NA	Wetter	n
70	Outuquis megafan, Gran Chaco	19°00'16'' S	58°31'09'' W	Latrubesse et al., 2012	Geomorphologic mapping, field surveys, OSL dating	0,67	Drier	NA	Wetter	y
71	Pocoyu (Poopó-Coipasa-Uyuni basin)	19°18' S-19°19'12'' S	68°00' W-67°31' W	Sylvestre et al., 1999; Argollo & Mourguiart 2000	^{14}C dating of Mollusc shells, Characea, Aragonite, Calcareous crust	0,33	NA	NA	Wetter	y
72	Quebrada Negrojahuila, Salar de Uyuni	19°34'12'' S	67°32'31'' W	Blard et al., 2011	Ages of Columnar microbialite, laminated stromatolithes, $\delta^{18}O$ of carbonates	0,33	Wetter	NA	Wetter	y
73	Minas Gerais	19°37'37'' S	43°53'24'' W	Auler et al., 2006	^{14}C on bone of fossil remains	1,33	Wetter	NA	Wetter	n
74	Pocoyu (Poopó-Coipasa-Uyuni basin)	19°43'12'' S	67°31' W	Sylvestre et al., 1999; Argollo & Mourguiart 2000	^{14}C dating of Mollusc shells, Characea	0,33	NA	NA	Wetter	y

continue

Table A.1 - Continuation.

	Site	Latitude	Longitude	Reference	Proxy type	CRI	LGM-Today precipitation (study)	LGM biome change (study)	Ensemble mean LGM climate	Simulated LGM biome change
75	Cerro Azanaques	19°45' S	67°39' W	Clayton & Clapperton 1997;	^{14}C dating of glacial landforms on an andesitic volcano, modeling of the ELA depression	0,00	NA	NA	Wetter	y
76	Chalchala valley, Cerro Tunupa	19°51'36'' S	67°36'36'' W	Blard et al., 2009	Cosmogenic $^{3}H_e$ dating of glacial landforms on an andesitic volcano, modeling of the ELA depression	0,33	NA	NA	Wetter	y
77	Salar de Uyuni	19°40'50'' S-20°09'03'' S	67°09'04'' W-67°48'34'' W	Placzek et al., 2006	^{14}C or U-Th dating of buried and surficial soil stratigraphic units that formed between deep-lake cycles, Lake hydrologic budget models	1,00	Wetter	NA	Wetter	y
78	Salar de Uyuni	19°38'57'' S-20°05'42'' S	68°05'47'' W-68°13'27'' W	Placzek et al., 2006	^{14}C or U-Th dating of buried and surficial soil stratigraphic units that formed between deep-lake cycles, Lake hydrologic budget models	0,33	Wetter	NA	Wetter	y
79	Salar de Uyuni	20°14'58'' S	67°30'02'' W	Baker et al., 2001b	γ-ray diffraction, diatom, $\delta^{18}O$ of lacustrine carbonates	0,70	Wetter	NA	Wetter	y
80	Salar de Uyuni	20°50'43'' S-21°02'21'' S	68°00'30'' W-68°15'09'' W	Placzek et al., 2006	^{14}C dating of buried and surficial soil stratigraphic units that formed between deep-lake cycles, lake hydrologic budget models	0,33	Wetter	NA	Wetter	y
81	Pampa del Tamarugal	21°25'48'' S	69°11'24'' W	Gayo et al., 2012	$\delta^{13}C_{org}$, fossil assemblage	0,33	NA	NA	Wetter	y
82	Pampa del Tamarugal	21°25'48'' S	69°15' W	Gayo et al., 2012	$\delta^{13}C_{org}$, fossil assemblage	0,33	NA	NA	Wetter	y
83	Rio Tamanduá valley	21°26' S	47°36' W	Turcq et al.,1997	Lithology	1,33	NA	NA	Wetter	y
84	Tres Lagunas, Laguna Grande Valley; Sierra de Santa Victoria	22°12' S-22°15' S	65°07' W-65°08' W	Zech et al., 2009a; Kull et al, 2003	Chronology of moraine deposits, grain-size, TOC of sediment core nearby Laguna III and mass-balance model	0,67	Wetter	NA	Wetter	y
85	Río Salado Basin	22°20' S	68°34' W	Latorre et al., 2006	$\delta^{13}C$ of plant Macrofossils, displacement of Andean steppe/Puna shrubs species	0,67	NA	NA	Wetter	n
86	Laguna Miscanti	22°45' S	67°45' W	Grosjean et al., 2001	Pollen diagram, spores, algae, geochemical composition	0,70	Drier	NA	Wetter	n
87	Morro de Itapeva	22°47' S	45°32' W	Behling 1997	Pollen diagram and charcoal	0,43	Drier	y	Wetter	y

continue

Table A.1 - Continuation.

	Site	Latitude	Longitude	Reference	Proxy type	CRI	LGM-Today precipitation (study)	LGM biome change (study)	Ensemble mean LGM climate	Simulated LGM biome change
88	Salar de Atacama	23°30' S	68°30' W	Bobst et al., 2001	$\delta^{18}O$ & δD (LWML) from modern water and aquifers under desiccated lake beds, salt core SQM#2005	0,33	Wetter	NA	Wetter	n
89	Laguna Lejía	23°30' S	67°42' W	Grosjean 1994	Water chemistry, the climate/water budget model, $\delta^{13}C$, $\delta^{18}O$, diatom assemblages	0,33	Wetter	NA	Wetter	y
90	Salar de Atacama	23°30' S	68°30' W	Betancourt et al., 2000	Plant macrofossils, lithology	0,67	Drier	y	Wetter	n
91	Vegas de Tilocalar, Salar de Atacama basins	23°47' S	68°09' W	Latorre et al., 2002	Fecal-pellet $\delta^{13}C$, plant-cuticle contents of 14C dated plant macrofossils	0,67	Drier	y	Wetter	n
92	Colônia, Brazil	23°52' S	46°42'20'' W	Ledru et al., 2009	Pollen diagram, Shannon-Wiener Indexes	0,50	Drier	y	Wetter	n
93	Curucutu, Itanhaém	23°59' S	46°44'45'' W	Pessenda et al., 2009	Pollen diagram, $\delta^{13}C$	0,83	Drier	n	Wetter	n
94	Bairro Lajeado	24°18'18'' S	48°21'54'' W	Saia et al., 2008	$\delta^{13}C$ of soil organic matter, TOC, charcoal fragments	0,37	Drier	y	Wetter	y
95	Santana Cave	24°31'51'' S	48°43'36'' W	Cruz et al., 2006	$\delta^{18}O$	1,67	Drier	NA	Wetter	y
96	Quebrada del Chaco	25°24'44'' S	69°13' W	Maldonado et al., 2005	Pollen assemblages from 17 fossil rodent middens	0,67	Wetter	NA	Wetter	n
97	Quebrada del Chaco	25°26'11'' S	69°27'04'' W	Maldonado et al., 2005	Pollen assemblages from 14 fossil rodent middens	1,00	Wetter	NA	Wetter	n
98	Volta Velha	26°04' S	48°38' W	Behling and Negelle, 2001	Pollen diagram	0,03	Drier	y	Wetter	y
99	Botuverá cave	27°13'24'' S	49°09'20'' W	Cruz et al., 2005	$\delta^{18}O$, $\delta^{13}C$ and growth rate	3,67	Wetter	NA	Wetter	y
100	Oberá, Misiones	27°23'35'' S	55°31'52'' W	Zech et al., 2009b	Elements, C_{org}, N,HI,OI, $\delta^{13}C_{org}$, n-alkanes andcompound-specific $\delta^{13}C$ analysesof biomarkers	0,73	Drier	n	Drier	y
101	Serra da Boa Vista	27°42' S	49°09' W	Behling et al., 1995	Pollen diagram	0,10	NA	y	Wetter	y
102	Cambará do Sul	29°03'09'' S	50°06'04'' W	Behling et al., 2004	Pollen diagram and charcoal	0,63	Drier	y	Drier	y
103	Rincão das Cabritas	29°28'35'' S	50°34'22'' W	Jeske-Pieruschka et al., 2012	Pollen diagram and charcoal	0,43	Drier	y	Drier	y

continued

Table A.1 - Continuation.

	Site	Latitude	Longitude	Reference	Proxy type	CRI	LGM-Today precipitation (study)	LGM biome change (study)	Ensemble mean LGM climate	Simulated LGM biome change
104	Lagoa da Cachoeira	6°21'18'' S	50°23'35'' W	Hermanowski et al., 2015	Pollen diagram and charcoal	0,67	Drier	y	Drier	y
105	Serra do Tabuleiro	27°53'48.46'' S	48°52'5.33'' W	Jeske-Pieruschka et al., 2013	Pollen diagram and charcoal	0,83	Drier	y	Wetter	y
106	Botucatú	22°48' S	48°23'' W	Behling et al., 1998; Behling, 2002	Pollen diagram and charcoal	0,00	Drier	y	Wetter	y
107	Lago dos Olhos	19°38' S	43°54'' W	De Oliveira, 1992; Behling, 2002	Pollen diagram	0,40	Wetter	y	Wetter	n
108	Catas Altas	20°05' S	43°22' W	Behling and Lichte, 1997	Pollen diagram	0,37	Drier	y	Wetter	n
109	Southeastern Brazil margin	19°38'5'' S	38°43'0'' W	Behling et al. 2002	Pollen diagram	0,03	Drier	y	Wetter	y
110	Southeastern Brazil margin	21°37'0'' S	39°58'7'' W	Behling et al. 2002	Pollen diagram	0,70	Drier	y	Wetter	y
111	Norheastern Brazil margin	3°40' S	37°43' W	Behling et al. 2000	Pollen diagram	0,70	Drier	n	Drier	n
112	Amazon fan	5°12.7' N	47°1.8' W	Haberle & Maslin, 1999	Pollen, stable isotopes forams	0,03	Drier	y	Drier	n
113	Lago do Saci	9°7'0'' S	56°16'0'' W	Fontes et al., 2017	Pollen, grain size, TOC, δ13C, δ15N, black carbon	1,47	Drier	y	Drier	n
114	area of the Amazon plume	6°39.38' N	52°04.99'W	Häggi et al., 2017	isotopic composition (δD and δ13C) of plant-waxes	1,10	Drier	n	Drier	n
115	Paraiso Cave	4°4′ S	55°27′ W	Wang et al., 2017	δ18O, δ13C	5,40	Drier	n	Drier	n
116	off southern Brazil	27.18°S	46.45°W	Gu et al., 2017	Pollen and dinocysts	1,03	Drier	y	Neutral	y
117	off southern Brazil	32.50°S	50.24°W	Gu et al., 2018	Pollen and dinocysts	0,70	Drier	y	Neutral	y
118	Paixao Cave NE Brazil	12°37′S	41°01′W	Strikis et al., 2018	δ18O	3,00	Drier	NA	Wetter	y
119	Lapa sem Fim Cave CE Brazil	16°09′S	44°36′W	Strikis et al., 2018	δ18O	4,00	Drier	NA	Wetter	n
120	Jaragua Cave, Bonito, Mato Grosso do Sul	21°05′S	56°35′W	Novello et al., 2017	δ18O	9,17	Wetter	NA	Wetter	y
121	Hill of six lakes	00°16' N	66°41' W	D'Apolito et al., 2013	Pollen analysis	0,40	Drier	y	Drier	n

continue

Table A.1 - Continuation.

	Site	Latitude	Longitude	Reference	Proxy type	CRI	LGM-Today precipitation (study)	LGM biome change (study)	Ensemble mean LGM climate	Simulated LGM biome change
122	off northeastern Brazil	1°54.50' S	41°35.50' W	Mulitza et al., 2017	δD and δ13C of plant-waxes, Pa/Th	0,93	Drier	y	Drier	y
123	Maranhao Basin (Piaui)	7°S	41.5°W	Stute et al., 1995	Noble gas record	0,03	NA	NA	Drier	y
124	Lago Consuelo	13°57.1′S	68°59.45' W	Urrego et al., 2010	Pollen, LOI	1,07	Wetter	n	Drier	y
125	Southwestern Amazonia	7°42′43″S	63°05′32″W	Rossetti et al., 2017	δ13C, C/N, 14C, sedimentology	1,03	Wetter	n	Drier	n
126	Southwestern Amazonia	8°06′02″S	63°45′31″W	Rossetti et al., 2017	δ13C, C/N, 14C, sedimentology	1,37	Wetter	n	Drier	n
127	Serra Sul, Southeastern Amazonia	6°24′35″S	50°19′05″W	Reis et al., 2017	Pollen, δ13C, δ15N	1,07	Drier	n	Drier	y
128	Lake Titicaca (Huiñaimarca)	17.5° S	70° W	Gosling et al., 2008	Pollen	0,70	Wetter	y	Wetter	y
129	Lake Fúquene	5°28' N	73°45' W	Groot et al., 2011	Pollen	0,97	NA	y	Drier	y
130	Pitalito Basin	1°87' N	76°03' W	Bakker, 1990	Pollen	0,37	Drier	y	Drier	y
131	El Abra, Sabana de Bogota	5°02' N	73°95' W	Schreve-Brinkman, E.J., 1978	Pollen	0,40	NA	y	Drier	y
132	Agua Blanca	5°00' N	74°10' W	Helmens & Kuhry, 1986	Pollen	0,03	NA	y	Drier	y
133	Panama Basin	1°12.1440' N	83°44.2200' W	González et al., 2006	Pollen	0,40	NA	NA	Wetter	y
134	Panama Basin	3°37' S	83°58' W	Martínez et al., 2003; Heusser & Shackleton, 1994	Pollen	1,07	NA	y	Wetter	y
135	Ciénaga El Morro, Belmira (Antioquia) Colombia	6°42'07,88'' N	75°40'50,74'' W	Velásquez Montoya, 2013	Pollen	0,47	NA	NA	Wetter	y
136	Laguna Ciega (I; III)	6.5°N	72.3°W	Van der Hammen et al., 1980	Pollen diagrams, ice/snow	0,37	Drier	n	Wetter	y
137	El Cristal	3°51'38.5" S	79°03'40.1"W	Villota & Behling, 2013	Pollen	0,43	NA	n	Wetter	y
138	off northeastern Brazil	4°15' S	36°21' W	Dupont et al., 2010	Pollen and geochemical analyses	0,83	Drier	n	Drier	y
139	Amazon fan	5°12.7' N	47°1.8' W	Piperno, 1997	Phytoliths and microscopic charcoal	0,37	Drier	y	Wetter	y

continue

Table A.1 - Conclusion.

	Site	Latitude	Longitude	Reference	Proxy type	CRI	LGM-Today precipitation (study)	LGM biome change (study)	Ensemble mean LGM climate	Simulated LGM biome change
140	Barrocadas	30°02'41.5"S	50°36'51.9"W	Bauermann, 2003; Bauermann et al., 2009	Pollen	0,03	Drier	y	Wetter	y
141	São Francisco de Assis	29°35'12"S	55°13'02"W	Behling et al., 2005	Pollen and charcoal	0,73	Drier	y	Wetter	y
142	Vereda Carrasco da Raposa	44°11'W	17°40'S	Gomes et al, 2017	Pollen and stable isotopes (C and N)	1,10	Drier	y	Wetter	n
143	Lagoa Feia	15.34° S	47.18° W	Cassino et al, 2020	Pollen and charcoal	1,03	NA	y	Wetter	n
144	Serra de Botucatu	23°00′43″S	48°22′40″W	Bissa et al, 2015	Pollen	1,03	Wetter	y	Wetter	n
145	Jaraguá cave	21°05′S	56°35′W	Novello et al., 2019	Total Organic Carbon, δ13C, XRF analysis, 87Sr/86Sr	1,03	NA	y	Wetter	y
146	Águas Emendadas, Brasilia	15°34′S	47°35′W	Barberi et al, 2000	Pollen	0,70	Drier	y	Wetter	n
147	Laguna La Gaiba	17°45' S	57°58' W	Fornace et al, 2016	Stable isotope analysis of leaf waxes	0,73	Drier	y	Wetter	y
148	Santa Elisa Farm	22°51'22.08"S	47°05'35.50"W	Aviles et al, 2019	Pollen and stable isotope analyses (δ 13C and δ 15N)	0,70	Drier	y	Wetter	y
149	Lagoa do Chapadão Lake of Serra Negra	18 °S	46 °W	De Oliveira et al, 2020	Pollen	0,40	Drier	NA	Wetter	n

Figure A.1 - Vertical pressure velocity (omega; units: hPa/s) representing regional Hadley circulation: the latitude-height section 15N-15°S, zonally averaged over 80°W–30°W, for (a) December–February (DJF), (b) March–May (MAM), (c) June–August (JJA), and (d) September–November (SON).

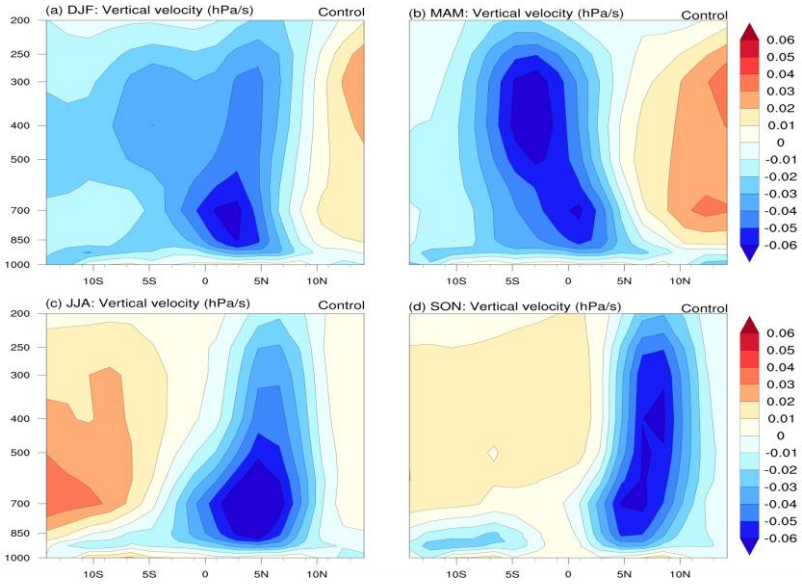

Figure A.2 - Vertical pressure velocity (omega; units: hPa/s) representing regional Walker circulation: the longitude-height section 80°W–30°W, meridionally averaged over 0°-15°S, for (a) December–February (DJF), (b) March–May (MAM), (c) June–August (JJA), and (d) September–November (SON).

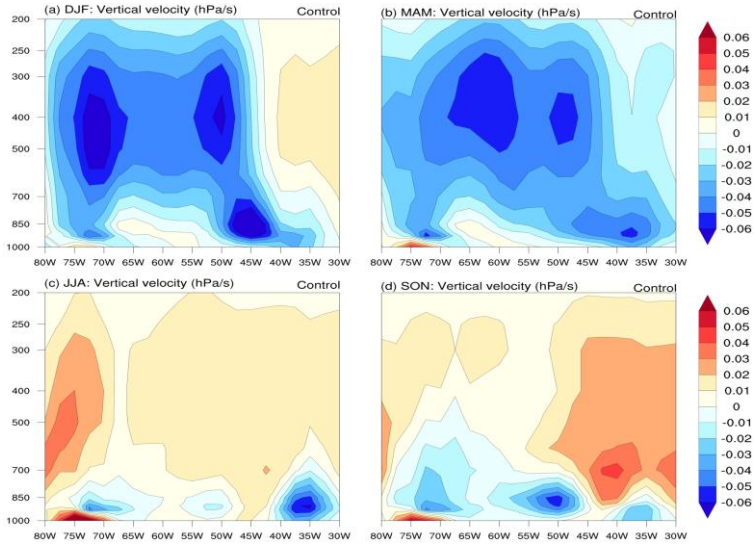

Figure A.3 - DJF-JJA $\delta^{18}O$ of precipitation illustrates the ability of the isotope-enabled version of the Community Earth System Model version 1 (iCESM1.2) to accurately portray the modern seasonality of precipitation.

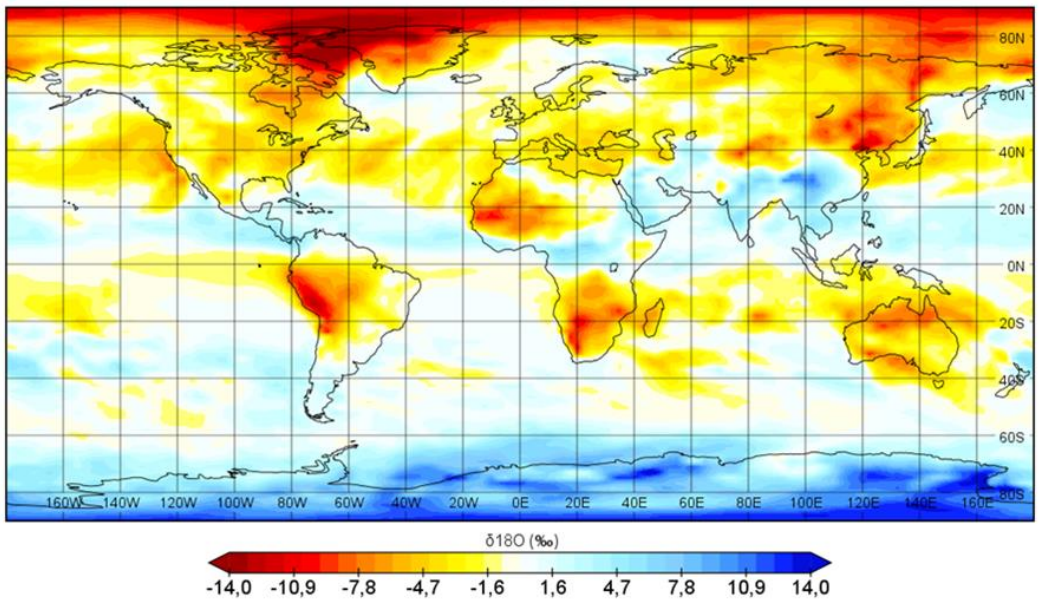

Figure A.4 - Annual AMV changes over the past 2,900 y with a 30-y loess first-order low-pass filter (red). The gray horizontal line is the estimated average SST over the past 2,900 y (22.19°C). CWP denotes Current Warm Period.

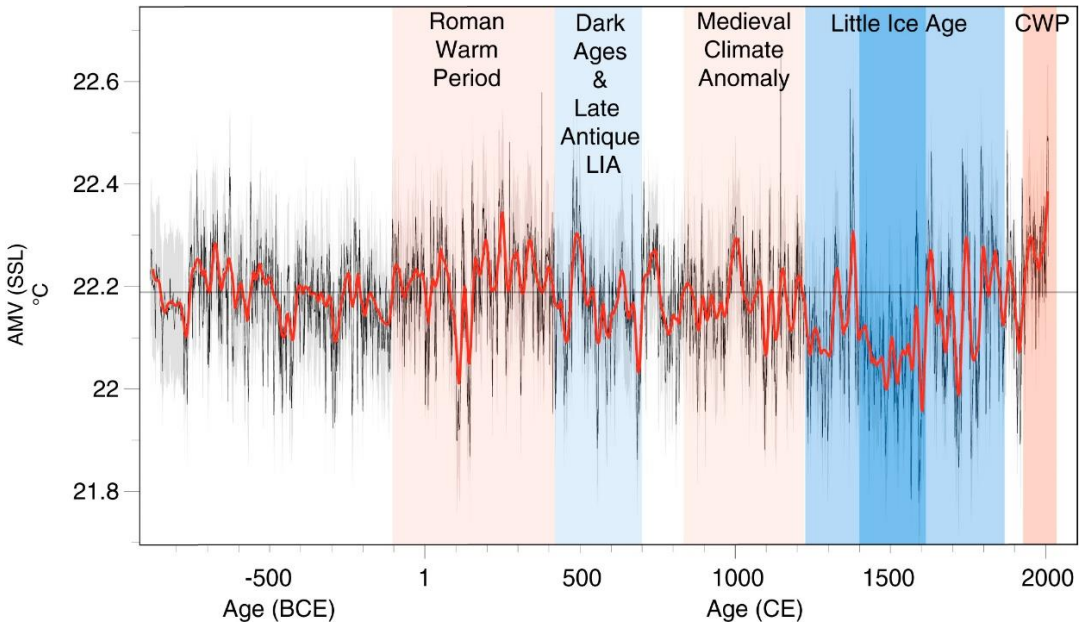

Source: Lapointe et al. (2020).

Figure A.5 - Simulated evaporation differences between the cold Atlantic Multidecadal Oscillation (CAMO) and the warm Atlantic Multidecadal Oscillation (WAMO) experiments (mm/day) for December, January, February, March, April, and May (DJFMAM).

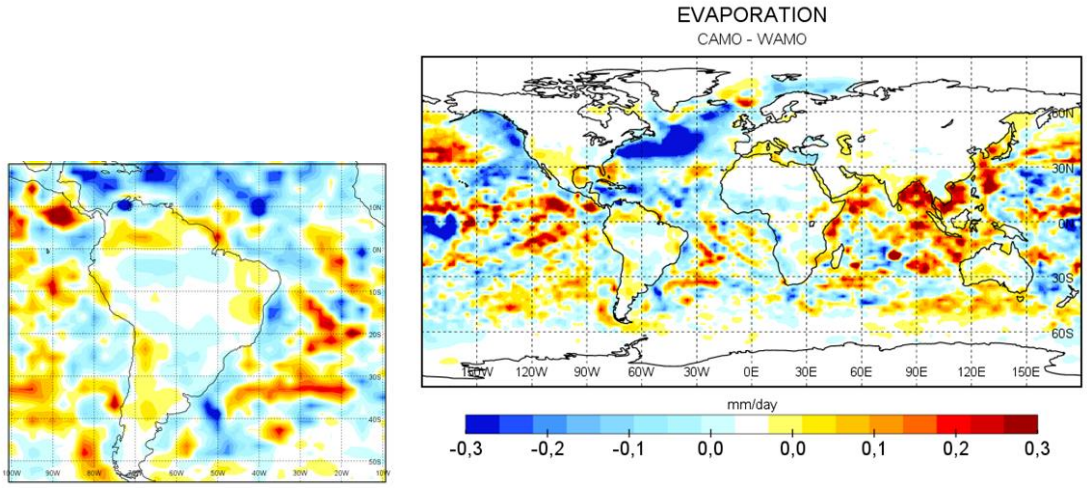

Figure A.6 - Distribution of Brazilian biomes projected by the Center for Weather Forecasting and Climate Studies Potential Vegetation Model version 2 (CPTEC-PVM2) for the the cold Atlantic Multidecadal Oscillation (CAMO) and the warm Atlantic Multidecadal Oscillation (WAMO) experiments. The color scale displays different biomes.

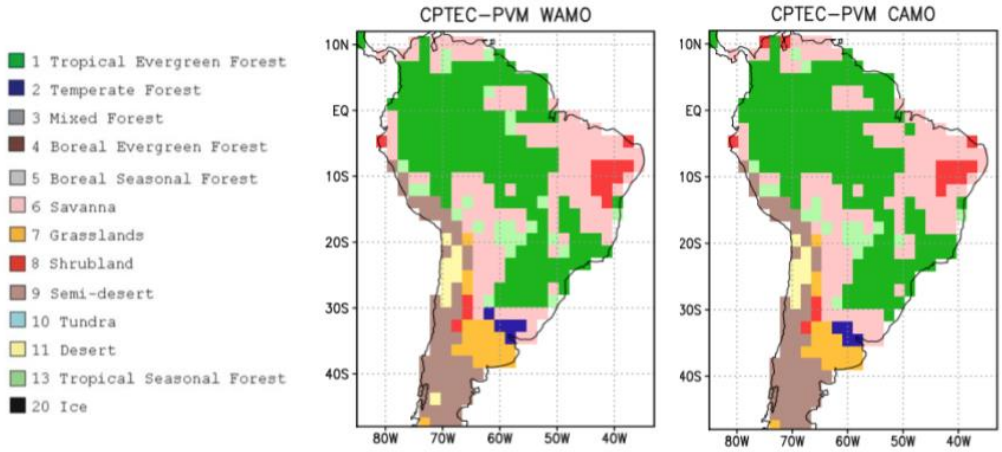

Table A.2 - Compilation of hydroclimate records with their respective references. The red (blue) dots represent drier (wetter) conditions; grey color dots represent neutral conditions.

	Article	Site name	Region	Lat	Lon	m.a.s.l.	Proxy	MCA	LIA
1	Wogau et al., 2022	Alchichica lake	Northern Serdan Oriental Basin	19.24° N	97.24° W		Lake sediment cores	🔴 ~930 and 1500	🔵 1500 - 1900 (dry interval centered at 1405, 1600 and 1870)
2	Obrist-Farner et al., 2022	lake Izabal	Central America, Caribbean Sea	15.24° N	89.16° W	~1.5 m	Lake sediment cores	🔵 from 1100-1400	🔴
3	Obrist-Farner et al., 2022	lake Petén Itzá	Central America, Caribbean Sea	16.56° N	89.55° W	~110 m	Lake sediment cores	🔴 800 -1400, increase in evaporation at Lake Petén Itzá that peaked at ~1320 CE	🔴
4	Asmerom et al., 2020	Yok Balum (YOKG), Belize	Central America, Caribbean Sea	16.20° N	89.06° W	366	δ13C Speleothem	🔴	🔵
5	Haug et al., 2001	Cariaco, Venezuela	Central America, Caribbean Sea	10.71° N	65.17 ° W		Ocean Sediment Titanium Conc.	Δ	Δ
6	Winter et al., 2017	Perdida Cave	Puerto Rico, Caribbean Sea	8.0°N	67.0°W	350–400	δ18O speleothem	proxy starts at 12th century with steady decrease to mid 15th century, then increase till 17th and later decrease early-18th	🔵 The most isotopically enriched intervals are centered in the late 16th century
7	Shanahan et al., 2009	LakeBosumtwi, W. Africa	West Africa	6.30°N	1.25 °W		Carbonate δ18O	🔵	🔴
8	Sachs et al., 2009	Washington Island	Central Pacific Ocean	4.43° N	160.25° W		TLE δD, salinity	🔵	🔴
9	Nelson and Sachs, 2016	Bainbridge Crater; El Junco Lake; Isabela lakes.	Galápagos lakes	1° S	90°W		salinity and δ2HWater	🔴	🔵
10	Wang et al., 2017	Paraiso (PAR01,PAR03)	Eastern Amazon	4.07 °S	55.45°W	60	δ18O / δ13C Speleothem	🔵🔴 PAR3	🔴 PAR1
11	Utida et al., 2019	Boqueirão Lake	Northeast Brazil	5.14°S	35.32°W		hydrogen isotope composition of the n-C28 alkanoic acid (δDwax)	🔴	🔵

continue

Table A.2 - Continuation.

	Article	Site name	Region	Lat	Lon	m.a.s.l.	Proxy	MCA	LIA
12	Utida et al., 2022	RN caves (Trapia, Furna Nova)	Northeast Brazil	5.56°S	37.62°W	70	δ18O speleothem composite	● although relativley wet it is drier then LIA	●
13	Apaéstegui et al., 2014	Palestina, Peru (PAL03,PAL04)	Eastern side of the Andes	5.92°S	77.35 °W	870	δ18O / δ13C Speleothem	●	●
14	Reuter et al., 2009	Cascayunga Cave, Peru	T.Andes	6.05° S	77.13° W	930	δ18O speleothem	No data	●
15	Polissar et al., 2006	Blanca, Venezuela	Venezuelan Andes	8.33°S	71.78°W	1620	Lake Sediment Multi-proxy PC	●	●
16	Bird et al., 2011	Pumacocha lake, Peru	T.Andes	10.70 °S	76.06 °W	4300	δ18Olw the intensity of monsoon precipitation upstream	●	●
17	Della Libera et al., 2022	Cuíca cave (PIM4 and PIM5)	SW Amazon region	11.40°S	60.38°W	310	d18O and d13C speleothems / degree of rainout / upstream plant transpiration and moisture recycling via forest changes upstream	●	●
18	Kanner et al., 2013	Huagapo cave	T.Andes	11.27°S	75.79°W	3550	δ18O speleothem	●	●
19	Azevedo et al., 2019	Mata Virgem Cave, Brazil (MV3) and Arapujá Lake	Cerrado region	11.37°S	47.29°W	365	δ18O and δ13C Speleothem and lacustrine record/pollen grain analyses	●● 925–1150 C.E. This humid period is followed by drier conditions during the 1150–1350 C.E.	●
20	Novello et al., 2012	Diva de Maura and Torinha cave	Bahia, northeastern South America	12.22°S	41.34° W	480	Speleothem δ18O	●●	●
21	Novello et al., 2018	São Bernardo and São Mateus caves, Brazil	Central Brazil	13.81°S	46.35°W	631	Speleothem δ18O	●	●

continue

Table A.2 - Conclusion.

	Article	Site name	Region	Lat	Lon	m.a.s.l.	Proxy	MCA	LIA
22	Thompson et al., 1986	Quelccaya, Peru	T.Andes	13.93°S	70.83° W	5670	δ18Oic	●	🌐 ● The 1500-1720 interval was the wettest in the 1000-year record, whereas the 1720-1860 interval was very dry
23	Novello et al., 2016	Pau d'Alho (ALHO6)	Central-West Brazil, Mato Grosso State	15.12°S	56.48°W	600	δ18O stalagmite / strength of monsoon precipitation	●	🌐
24	Wortham et al., 2017	Tamboril Cave	Central Brazil	16°S	47°W	700	δ18O, δ13C, 87Sr/86Sr speleothem	●	●
25	Apaéstegui et al., 2018	Umajalanta–Chiflonkhakha cave system/Boto	Eastern Bolivian Andes	18.12°S	65.77°W	2650	δ18O Speleothem / rainfall intensity upstream during the austral summer SAMS season	🌐●	🌐
26	Kock et al., 2019a	Cerro Tuzgle peatland, Argentina	Southern Central Andes/Argentina	24.09°S	66.24°W	4800	δ18Ocell	●	🌐
27	Vuille et al., 2012	Crystal cave	Southeastern Brazil	24.58°S	48.58°W	130	Speleothem calcite δ18O	●	🌐
28	Kock et al., 2019b	Lagunillas peatland, Chile	Southern Central Andes/Argentina	27.12°S	69.17°W	3770-4075	δ18Ocell	●	🌐
29	Perez et al., 2016	Core GeoB 13813-4	Uruguayan coast	34.44°S	53.33°S		river discharge	●	🌐

APPENDIX B

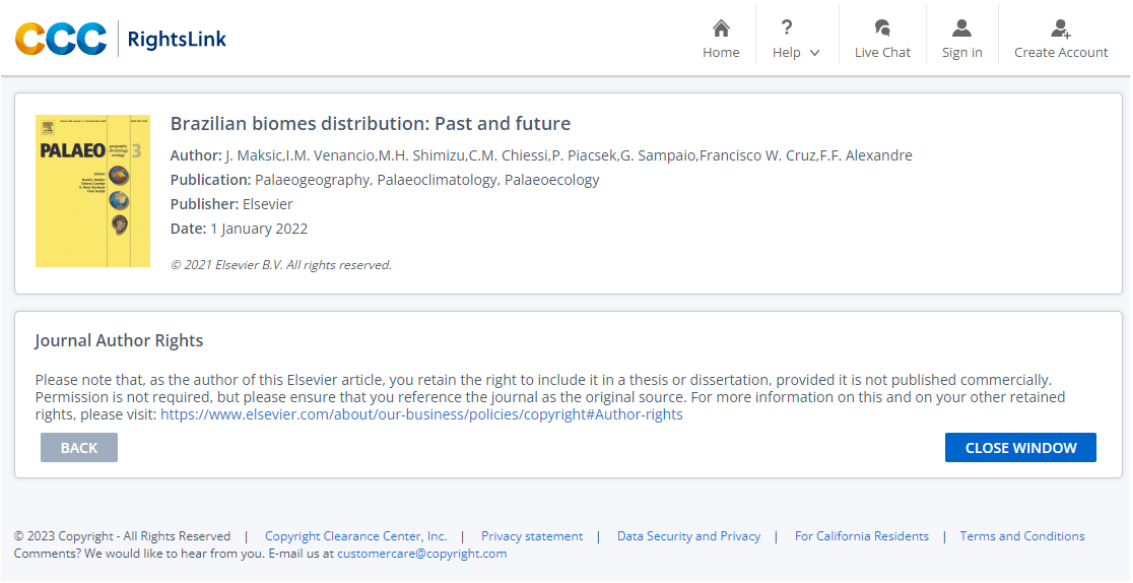

RightsLink

Home | Help | Live Chat | Sign in | Create Account

Brazilian biomes distribution: Past and future

Author: J. Maksic,I.M. Venancio,M.H. Shimizu,C.M. Chiessi,P. Piacsek,G. Sampaio,Francisco W. Cruz,F.F. Alexandre

Publication: Palaeogeography, Palaeoclimatology, Palaeoecology

Publisher: Elsevier

Date: 1 January 2022

© 2021 Elsevier B.V. All rights reserved.

Journal Author Rights

Please note that, as the author of this Elsevier article, you retain the right to include it in a thesis or dissertation, provided it is not published commercially. Permission is not required, but please ensure that you reference the journal as the original source. For more information on this and on your other retained rights, please visit: https://www.elsevier.com/about/our-business/policies/copyright#Author-rights

BACK | CLOSE WINDOW

© 2023 Copyright - All Rights Reserved | Copyright Clearance Center, Inc. | Privacy statement | Data Security and Privacy | For California Residents | Terms and Conditions
Comments? We would like to hear from you. E-mail us at customercare@copyright.com

This article was published in Palaeogeography, Palaeoclimatology, Palaeoecology, Volume 585, Maksic, J., Venancio, I.M., Shimizu, M.H., Chiessi, C.M., Piacsek, P., Sampaio, G., Cruz, F.W. and Alexandre, F.F., Brazilian biomes distribution: Past and future. Palaeogeography, Palaeoclimatology, Palaeoecology, 585, p.110717, 2022. https://doi.org/10.1016/j.palaeo.2021.110717

PANGAEA.
Data Publisher for Earth & Environmental Science

SEARCH SUBMIT HELP ABOUT CONTACT

Citation: **Maksic, Jelena; Venancio, Igor Martins; Shimizu, Marilia Harumi (2021):** Compilation of proxy data from paleoclimate archives of South America. *PANGAEA*, https://doi.org/10.1594/PANGAEA.927527

Always quote citation above when using data! You can download the citation in several formats below.

RIS Citation | BibTeX Citation | Copy Citation | Facebook | Twitter | 69 | 12

Abstract: Compilation of 149 published vegetation and hydroclimate records with their respective references. It is updated compilation of hydroclimate records from tropical South America made by Zhang et al. (2016). We considered all their records that cover the Last Glacial Maximum and added new ones, published since then, that showed vegetation, hydroclimate and environmental reconstructions. Original chronologies of all paleorecords were used. To evaluate the dating quality of the compiled records, we applied a chronological reliability index (CRI). In order to compare the results from the compilation with model simulations, we defined categories for precipitation and vegetation (biome) changes based on the original interpretations of the authors. In the case of precipitation, anomalies are expressed as the difference between LGM and present time, and the categories are "drier", "wetter" and "unclear". Also for vegetation anomalies are expressed as the difference between LGM and present time, and the categories are "change", "no change" and "unclear".

Keyword(s): biomes; Last Glacial Maximum; models; proxy; Vegetation

Related to: **Maksic, Jelena; Venancio, Igor Martins; Shimizu, Marilia Harumi; Chiessi, Cristiano Mazur; Piacsek, Patricia; Sampaio, Gilvan; Cruz, Francisco William; Alexandre, F F (2022):** Brazilian biomes distribution: Past and future. *Palaeogeography, Palaeoclimatology, Palaeoecology*, **585**, 110717, https://doi.org/10.1016/j.palaeo.2021.110717

License: Creative Commons Attribution 4.0 International (CC-BY-4.0)

Size: 102.7 kBytes

Download Data

Download dataset

This data was published by PANGAEA Maksic, Jelena; Venancio, Igor Martins; Shimizu, Marilia Harumi (2021): Compilation of proxy data from paleoclimate archives of South America. PANGAEA, https://doi.pangaea.de/10.1594/PANGAEA.927527

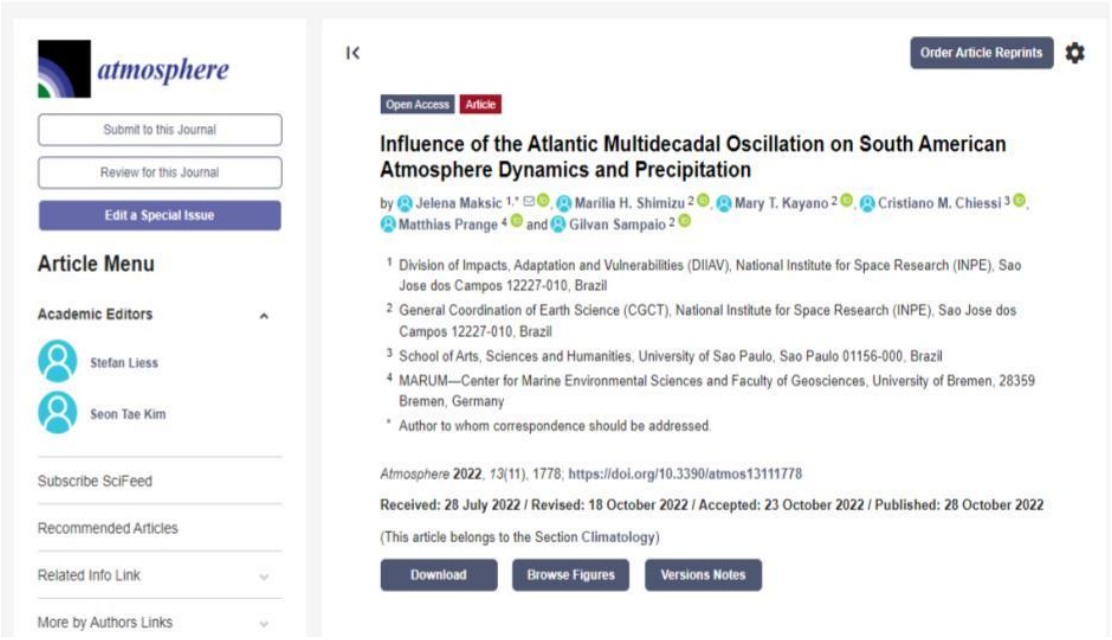

This article was published in Atmosphere, Volume 13(11), Maksic, J., Shimizu, M.H., Kayano, M.T., Chiessi, C.M., Prange, M. and Sampaio, G., Influence of the Atlantic Multidecadal Oscillation on South American Atmosphere Dynamics and Precipitation. 13(11), p.1778., 2022. **https://doi.org/10.3390/atmos13111778** (Copyright permissions are not needed since published by open access publisher and papers are not protected by copyright.)